UNCLASSIFIED

AD NUMBER

AD132168

LIMITATION CHANGES

TO:

Approved for public release; distribution is unlimited.

FROM:

**Distribution authorized to U.S. Gov't. agencies and their contractors;
Administrative/Operational Use; MAR 1957. Other requests shall be referred to Ballistic Research Lab., Aberdeen Proving Ground, MD.**

AUTHORITY

BRL ltr 22 Apr 1981

THIS PAGE IS UNCLASSIFIED

BRL
1005
Pt. 2
c.2A

[redacted]

UNCLASSIFIED

BRL
1005
Pt. 2

DEC NOV 1996
CIRCULATING COPY

000009

REPORT NO. 1005 PART II

MARCH 1957

UNCLASSIFIED

Per DA Form 1575
ltd 23 Jan 1978, Director, BRL
CA fife
The 8 Aug 1978

TECHNICAL LIBRARY
U. S. ARMY ORDNANCE
ABERDEEN PROVING GROUND, MD.
ORDBG-LM

PROCEEDINGS OF THE AERODYNAMICS RANGE SYMPOSIUM

JANUARY 1957 (U)

PROPERTY OF U.S. ARMY
STINFO BRANCH
BRL, APG, MD. 21005

[redacted]

FOR REFERENCE
[redacted] BE TAKEN FROM THE ROOM
EC 12W

Department of the Army Project No. 5B03-03-001
Ordnance Research and Development Project No. TB3-0108

BALLISTIC RESEARCH LABORATORIES

ABERDEEN PROVING GROUND, MARYLAND

[redacted] UNCLASSIFIED

[redacted]

UNCLASSIFIED

BALLISTIC RESEARCH LABORATORIES

REPORT NO. 1005 PART II

March 1957

PROCEEDINGS
OF THE
AERODYNAMICS RANGE SYMPOSIUM
JANUARY 1957

[redacted]

PROPERTY OF U.S. ARMY
STINFO BRANCH
BRL, APG, MD., 21005

TECHNICAL LIBRARY
U. S. ARMY ORDNANCE
ABERDEEN PROVING GROUND, MD.
ORDBG-LM

Department of the Army Project No. 5B03-03-001
Ordnance Research and Development Project No. TB3-0108

ABERDEEN PROVING GROUND, MARYLAND

UNCLASSIFIED

[redacted]

UNCLASSIFIED

TABLE OF CONTENTS*

PART II

* The list of conferees, agenda, and unclassified papers appear in Part I.

UNCLASSIFIED

INTENTIONALLY LEFT BLANK.

SIMULATION OF THE ATMOSPHERIC ENTRY OF BALLISTIC MISSILES II:13

(CONFIDENTIAL)

S. E. Neice and J. A. Carson
Ames Aeronautical Laboratory, NACA

It has been demonstrated theoretically that the aerodynamic heating and thermal stresses experienced by a ballistic missile entering the earth's atmosphere can be duplicated with a model launched from a hypervelocity gun upstream through a specially-designed supersonic nozzle. The demonstration, summarized in this paper, requires the model and missile to be geometrically similar and made of the same material as well as to have the same speed and Reynolds number at corresponding points in their trajectories. The hypervelocity gun provides the model's initial speed, while the supersonic nozzle is designed to provide, on a much smaller scale, the density variation present in the atmosphere. This combination of gun and supersonic nozzle is therefore termed an "Atmospheric Entry Simulator".

In order to check the basic simulation theory, provide experience applicable to the design and operation of a larger facility, and to conduct preliminary tests on small models of ballistic missiles, a small-scale atmospheric entry simulator has been built and operated at the Ames Aeronautical Laboratory. The experience gained in the operation of the equipment is discussed and results of preliminary tests of simple missile shapes are presented.

SOME PROBLEMS ASSOCIATED WITH THE DETERMINATION, FROM RANGE FIRINGS, OF DYNAMIC STABILITY OF BALLISTIC MISSILE RE-ENTRY SHAPES II: 37

(CONFIDENTIAL)

L. C. MacAllister
Ballistic Research Laboratories

In the past, free flight ranges have been useful in the determination of the dynamic stability of bodies of revolution and of symmetric missiles. Recently a considerable amount of work has been devoted to firings of models of war heads. The conditions under which the models are fired and the aerodynamic properties of the shapes make the determination of the dynamic stability of the models quite difficult. The problems that arise and some possible solutions are discussed.

UNCLASSIFIED

UNCLASSIFIED

[redacted]

A CORRELATION OF FREE-FLIGHT TRANSITION MEASUREMENTS ON VARIOUS BLUNT NOSE SHAPES BY USE OF THE MOMENTUM-THICKNESS REYNOLDS NUMBER

I:23

W. R. Witt, Jr. and J. Persh
U. S. Naval Ordnance Laboratory

A systematic series of blunt nose shapes has been fired in the Pressurized Ballistics Range for boundary-layer transition studies. The transition of the boundary-layer flow from laminar to turbulent is determined directly from the shadowgraph plates. The nose shapes have all been fired near a Mach number of 3 and the Reynolds number per foot has been varied by changing the pressure (density in the firing range).

The Reynolds number based on momentum thickness, Re_θ, at the observed transition location, was calculated using the laminar boundary-layer calculation method given by Cohen and Reshotko in "The Compressible Laminar Boundary Layer with Heat Transfer and Arbitrary Pressure Gradient" (NACA TN 3326). In general, the results indicate that transition occurs at values of Re_θ which are of the same order of magnitude as the values of minimum critical Reynolds number usually associated with incompressible flow.

ADVANCES IN THE DYNAMIC ANALYSIS OF RANGE DATA

I:45

C. H. Murphy
Ballistic Research Laboratories

The range technique has been usually restricted to dynamic analysis of the motion of thrustless symmetric missiles acted on by linear aerodynamic forces. In recent years all three of these restrictions have been relaxed.

First, a gun-boosted burning rocket program fired on the Transonic Range is described and the relatively minor alterations to the data analysis procedure are indicated. Next the more difficult problem of a finned missile with bent fins and spin rate varying through resonance is discussed. Finally, the successful treatment of cubic nonlinearities in static and Magnus moments and their associated forces is described.

UNCLASSIFIED

SURVEY, CALIBRATION, AND REDUCTION TECHNIQUES USED AT THE THOMPSON AEROBALLISTICS LABORATORY I: 85

W. H. Allan and E. L. Dunn
U. S. Naval Ordnance Test Station

The cameras of the Thompson Aeroballistics Laboratory are calibrated once a year by photographing reference markers in the field of view of each camera. Three wires, anchored to towers at each end of the range, are suspended in space near the range line. The reference markers are 1/8-inch plastic beads located every two ft. along the wire. This paper describes the techniques used to measure the coordinates of the cameras and the plastic beads; the mathematical treatment of these coordinates to furnish calibration equations for each camera; the use of the equations in solving for orientation and location of the missile in space; the results obtained through this system; and a discussion of the limitations and advantages of this system.

WAKE VISUALIZATION STUDIES IN THE AEROBALLISTICS RANGE I: 127

G. V. Bull and C. B. Jeffery
Canadian Armament Research and
Development Establishment

By the interaction of hydrochloric acid and ammonium hydroxide vapours, a plane sheet of laminar smoke filaments can be produced in the range along the flight trajectory. Models developing lift due to incidence were fired through these planar sheets. Spark and fastax photography was used to record the development of the wake profiles in the plane of the smoke. Wake distortions and vortex formations have been studied for several types of bodies; for a cruciform arrangement of rectangular panels of aspect ratio 1.9 on a cylindrical body, the wake distortion as determined from these tests have been compared with computations based on the assumptions of linear theory.

THE CONTROLLED-TEMPERATURE-PRESSURE RANGE I:149

F. D. Bennett
Ballistic Research Laboratories

A survey is given of the research and development program which has culminated in operation of the Controlled-Temperature-Pressure Range (CTPR) for production of flows up to Mach 11. Methods of control of temperature and pressure in the 45' working section are described. The instrumentation necessary for

(1) measurement of projectile drag coefficient and (2) measurement of density throughout the field of flow is discussed in some detail. The 10" Mach-Zehnder interferometer is a special feature. Various research problems encountered in the development of light sources, projectile launchers and data handling schemes are briefly touched upon.

At low supersonic Mach numbers a problem requiring the full field of the 10" Mach-Zehnder interferometer has recently been completed. Here a study of phenomena in the distant N-wave about a small sphere has led to a new and simple experimental criterion for N-wave flow and to information about convergence to N-wave flow with radial distance from the projectile.

TWO AEROBALLISTIC RANGE TOPICS: I:183

J. D. Nicolaides
Bureau of Ordnance

(1) MASS ASYMMETRY

with

J. E. Long, U. S. Naval Ordnance Laboratory
Gene Parrish, Bureau of Ordnance

A simple approximate theory for the free flight motion of ballistic missiles having mass asymmetry is given and proofed by experimental firings in the NOL Pressurized Aeroballistic Range.

(2) DYNAMIC STABILITY

The Epicyclic Theory for the flight dynamics of ballistic missiles has yielded various "Dynamic Stability Criteria" which are often used to evaluate missile performance. Recent misleading uses of the theory and criteria in appraising missile performance require a simple restatement of the theory, its assumptions and its use.

The parameters of Nutation Half-Life, Precession Half-Life and Total Motion Half-Life are suggested as better criteria for missile dynamics than those classically based on the Linear Theory.

Also a summary of important Nonlinear Cases of ballistic missile flight performance is given.

DESIGN AND INITIAL TESTS OF THE NOL SHOCK GUN (CONFIDENTIAL)

II: 61

V. C. D. Dawson
U. S. Naval Ordnance Laboratory

The design and initial tests of the NOL Shock Gun are described. The operation of this gun, which was conceived by Dr. A. E. Seigel and Dr. Z. I. Slawsky, is based upon a new principle and missiles weighing two grams have been launched from a 0.50-caliber smoothbore gun at velocities in excess of 13,000 feet per second.

AN APPLICATION OF AEROBALLISTICS RANGE TECHNIQUES

I:219

G. H. Tidy and M. E. Thomas
Canadian Armament Research and
Development Establishment

A series of flat plate wings of triangular planforms has been fired at Mach numbers 1.5 and 2 and their trajectories have been measured.

Preliminary manual reduction of the data is presented and the derived values of some aerodynamic coefficients are compared with NACA wind tunnel measurements. The possibility of more complete analysis and of application of the range technique to airplane configurations are considered.

SABOTS USED AT THE THOMPSON AEROBALLISTICS LABORATORY

I: 241

W. H. Allan
U. S. Naval Ordnance Test Station

A review of sabots used at the Thompson Aeroballistics Laboratory from the beginning of operations to the present. The discussion will cover spinner and finner sabots used in guns ranging from 40mm to 8-inch bore diameter. Follow-thru, breakapart, slug styrofoam, and slow-spin smooth bore sabots will be discussed along with the use of the sabot retarder.

UNCLASSIFIED

RESEARCH INVESTIGATIONS IN THE AMES SUPERSONIC FREE-FLIGHT FACILITIES

II: 81

(CONFIDENTIAL)

T. N. Canning
Ames Aeronautical Laboratory, NACA

The features which distinguish the Ames Supersonic Free-Flight Wind Tunnel from other ballistic-range facilities will be discussed and evaluated. The capacity of the facility for a variety of aerodynamic studies will be illustrated with three examples of programs conducted in the past. The first such example is the measurement of the skin-friction of turbulent boundary layers at Mach numbers up to 7 at Reynolds numbers around 8 million. The critical experimental techniques for these tests will be discussed.

The second test involved measuring the static longitudinal and directional characteristics as well as the damping in pitch and yaw of an airplane-like model. Some difficulties in tests of this sort will be noted.

The third field of research to be discussed is the study of boundary-layer transition on bodies of revolution at Mach numbers up to 9. The importance of this problem will be noted and the techniques whereby transition is detected will be described.

AEROBALLISTIC RANGE MEASUREMENTS OF THE PERFORMANCE AND STABILITY OF A SUPERSONIC FIGHTER AIRCRAFT

II:101

(CONFIDENTIAL)

H. R. Warren*, R. J. Templin**, and B. Cheers
Canadian Armament Research and
Development Establishment

This paper describes a method being developed for measuring aircraft performance and stability characteristics in free flight. Tests have been made firing into the Aeroballistics Ranges small scale models of a current delta wing fighter at a supersonic Mach number and approximately 1/10 its combat Reynolds number. Velocity screens, schlieren and yaw card measurements are used to obtain histories of the models speed, altitude and later motion during flight. From the analysis of these records information is obtained about the aircraft drag, lift, lateral and longitudinal aerodynamic derivatives.

* DeHavilland of Canada, Limited

** National Aeronautical Establishment

UNCLASSIFIED

UNCLASSIFIED

MODEL LAUNCHING TECHNIQUES AND OTHER ITEMS RELATED TO RANGE FIRINGS

J. E. Long
U. S. Naval Ordnance Laboratory

A discussion of the variety of methods used to launch scaled models in the free-flight precision ranges at NOL is given. These methods include such items as: (1) launching finned missiles from rifled guns; (2) launching subcaliber spinning models from oversized sabots; (3) launching spheres as small as 1/32 inch in diameter for drag; and (4) launching model aircraft.

Under related items the discussion will be centered about the following techniques: (1) firing models with a jet exhausting from the model base; (2) investigating the arming of fuzes by X-raying the recovered round; (3) firing spinning models with hot and cold plastics rotating bands; (4) development of the spin sonde; and (5) firing models from powder guns at 10,000 ft/sec.

UNCLASSIFIED

SIMULATION OF THE ATMOSPHERIC ENTRY OF BALLISTIC MISSILES

Stanford E. Neice

James A. Carson

National Advisory Committee for Aeronautics
Ames Aeronautical Laboratory
Moffett Field, California

INTENTIONALLY LEFT BLANK.

UNCLASSIFIED

NOTATION

A	reference area for drag evaluation
C_D	drag coefficient
C_f'	equivalent skin-friction coefficient
m	mass of missile or model
Q	total convective heat transfer
S	surface area
V	velocity
V_e	velocity at entrance to earth's atmosphere or simulator
y	altitude
β	constant in the altitude density relation (fig. 1)
θ_e	angle of flight path of missile with respect to horizontal at entrance to earth's atmosphere.
ρ	air density
ρ_o	reference air density (simulator reservoir or earth's surface)

UNCLASSIFIED

SIMULATION OF THE ATMOSPHERIC ENTRY OF BALLISTIC MISSILES

by

Stanford E. Neice* and James A. Carson*

National Advisory Committee for Aeronautics
Ames Aeronautical Laboratory
Moffett Field, California

INTRODUCTION

The aerodynamic heating associated with the atmospheric entry of ballistic missiles poses problems of such importance that the success or failure of a missile may well depend upon their solution. The solution to these problems requires an understanding of several complicated phenomena. The construction of a long-range ballistic missile, for example, will involve structural problems resulting from the thermal stresses associated with aerodynamic heating as well as problems which may result from actual melting or burning of the surface. The ultimate solution to these problems will be obtained from full-scale flight tests, but such tests are both time consuming and costly. It is appropriate, therefore, to attempt a method for simulating the heating and resultant thermal stresses with the use of relatively simple equipment on the ground. Thus we have been led to the concept of an atmospheric entry simulator in an effort to bridge the gap between detailed aerodynamic testing and flight testing. Basically, the method consists in propelling a missile model through a small scaled atmosphere, observing the model throughout its flight as well as its condition at the end of flight. Such apparatus also has the possibility of revealing unexpected problems as well as aiding in their solution.

A small-scale atmospheric entry simulator has been constructed and put into operation at the Ames Aeronautical Laboratory of the NACA. The design and operation of this facility as well as a presentation and discussion of the results of initial tests, form the subject of this paper.

---

*Aeronautical Research Engineer

UNCLASSIFIED

THEORETICAL CONSIDERATIONS

Before discussing the facility, it might be well to consider some theoretical aspects of the problem to establish how simulation can be accomplished. In reference 1 the motion and heating of missiles entering the atmosphere were studied, and expressions were developed for the determination of the altitude variation of velocity, total heat transfer by convection, and rates of convective heat transfer: These theoretical results were used in a subsequent study (ref. 2) to show that the aerodynamic heating and thermal stresses experienced by a ballistic missile during atmospheric entry could be duplicated with a model launched upstream through a specially designed supersonic nozzle. A basic feature of the analysis, which makes it possible to accomplish simulation in such a facility, is that the motion of a ballistic missile can usually be determined without consideration of gravity. Without going further into the prior assumptions and development, the basis for simulation is demonstrated in figure 1.

For convenience of analysis, it was decided to use an isothermal atmosphere, which closely approximates the earth's atmosphere from the surface to about 200,000 feet. Thus we have the exponential altitude-density relation as shown. It follows from reference 1 that the heat absorbed per unit mass by a missile entering the atmosphere can be expressed in the form shown. If we wish to duplicate this quantity in model tests the various factors in the equation must remain the same, Thus

(a) The same entrance velocity, V_e, for both model and missile is required.

(b) Geometric similarity between missile and model is required, with the resultant duplication of S/A, the ratio of surface to cross-sectional area.

(c) The same Reynolds number for both model and missile is required, which results in the duplication of the modified

UNCLASSIFIED

UNCLASSIFIED

skin friction coefficient, C_f', and in conjunction with the previous requirement of geometric similarity, duplicates the total drag coefficient, C_D.

(d) The same value of βy is required, which means that the density ratio at corresponding points in the atmosphere and the simulation facility must be the same.

(e) The same value of $C_D \rho_o A/\beta m \sin \theta_e$ is required, which means as detailed in reference 2, that the velocity at corresponding points in the atmosphere and simulator must be the same.

With these conditions established, we can see that the total convective heat transfer per unit mass will be duplicated. It has also been shown in reference 2 that for any fixed ratios of model to missile size, the requirements for similitude determine the test chamber length and reservoir density for the portion of the atmosphere to be simulated.

Duplication of the total convective heat transfer per unit mass, as we have done here, causes the heat-transfer rates for the model to be higher in proportion to the ratio of the missile to model size. For a geometrically similar model, however, the shell thickness is reduced in proportion to the scale factor; hence, the product of heat-transfer rate and shell thickness is the same for both model and missile. Thermal stresses, which are proportional to this product, will be the same for model and missile, provided, of course, that identical materials are used. A more rigorous demonstration of the similitude for thermal stress is presented in reference 2. This demonstration requires a rather lengthy analysis, details of which can best be obtained from reference to the paper itself.

UNCLASSIFIED

APPARATUS AND TEST PROCEDURE

Small-Scale Atmospheric Entry Simulator

In order to construct a practical atmospheric entry simulator we first had to provide a model with the correct initial high velocity required for simulation. For this purpose we used a particular type of hypervelocity gun, the details of which will be discussed later. Next we had to provide a test chamber which would simulate the lower portion of the atmosphere. For this purpose it was found that the density variations present in a portion of the atmosphere could be simulated with the use of a specially designed supersonic nozzle. To elaborate this point, it was shown, in reference 1, that the major part of the aerodynamic heating of a ballistic missile entering the atmosphere occurs within a 100,000-foot altitude range. The corresponding density limits could be obtained between the reservoir and exit section of a Mach number 5 supersonic nozzle. The appropriate exponential density variation between reservoir and exit section could be obtained by proper nozzle geometry. Unlike atmospheric air, however, the air in the simulator is in motion and actually provides us with an effective increase in entrance velocity, V_e, of about 2300 feet per second. Using relative velocities in this manner is permissible to the accuracy of the simulation.

On the basis of the foregoing considerations, a small-scale atmospheric entry simulator was constructed and put into operation at the Ames Aeronautical Laboratory. A schematic diagram of this facility is shown in figure 2 and consists of four main parts: the pressure tank, test section, vacuum tank, and the helium gun which launches a .22 caliber model. The test section is about 8-1/2 feet long and duplicates a 100,000-foot segment of the atmosphere. Operating pressures in the pressure reservoir vary from about 200 to 500 pounds per square inch depending upon the desired altitude range to be simulated.

Testing is performed in the following manner. A copper diaphragm is placed between the high-pressure reservoir and the small end of the test section, and the connection is secured. The model and shear disk

are placed in position at the large coupling in the helium gun. The vacuum tank is then evacuated to a pressure of about two millimeters of mercury - the vacuum also extending through the test section and the forward half of the helium gun. When the evacuation is accomplished, the helium gun is loaded, the high-pressure tank is pressurized to the desired amount, and we are ready to test.

The diaphragm between the high-pressure reservoir and the test section is ruptured. This results in the formation of a strong shock wave which discharges through the test chamber into the vacuum tank and establishes supersonic flow in the test chamber. After allowing a suitable time for this flow to stabilize, generally about 150 milliseconds, the helium gun is fired and the model is propelled upstream through the test section. As the model proceeds through the test section, a time-distance history is deduced from electronic counters which operate from the signals from the photobeam stations (fig. 2). From this history, a velocity record can be obtained. The photobeam signal also operates through a time delay circuit to take a spark shadowgraph of the model at a point downstream of each photobeam station. The model velocity will be nearly zero about the time it reaches the upstream end of the test section. The model is then carried downstream and can be recovered in the vacuum tank.

[redacted]

Helium Gun

An interesting feature of the atmospheric entry simulator, which merits more explanation, is the model launcher or, as we have termed it, the helium gun. This apparatus is illustrated in more detail in figure 3 which shows the gun as it is ready to be fired. As shown in the figure, the gun consists of two main parts: a .22 caliber launch barrel (in housing) and a 20 millimeter pump barrel which are connected in such a way as to enable the placement of the model and shear disk at the barrel coupling. The shear disk provides a pressure seal between the two chambers. At the muzzle end of the .22 caliber barrel, baffle plates are placed to reduce the action of expanding gases on the model immediately after launching. A vacuum manifold is incorporated ahead of the baffles to keep the .22 caliber barrel at as low a pressure as possible prior to firing. The blast cone functions to protect the gun from the shock wave produced when the copper diaphragm between the high-pressure reservoir and the test section is ruptured.

In the firing condition shown here, the .22 caliber barrel is at a partial vacuum; the 20 millimeter barrel is sealed from the .22 caliber barrel by the shear disk; the powder charge is in place; and the breech block secures a seal at the breech end. The pump barrel is then filled with helium under pressure.

The launching action is as follows: The ignition of the powder charge creates a strong shock wave which travels down the pump barrel through the helium and reflects from the end of the barrel. This forms a small volume of helium gas at a high pressure and temperature. The sudden increase in pressure at the coupling ruptures the shear disk and propels the model down the launch barrel and subsequently into the test section.

For models whose weights lie between 0.06 and 0.17 gram, an initial helium pressure of about 920 pounds per square inch gage and a powder charge of 32-1/2 grams of Hercules "Unique" pistol powder was found to

[redacted]

produce the highest velocities. It might be mentioned that the magnitude of the helium pressure is not extremely critical, a variation of 50 pounds per square inch producing a loss of only a few hundred feet per second in the muzzle velocity of the model. Increasing the powder charge to 33 grams, however, was found to cause detonation with an attendant sharp rise in pressure throughout the 20 millimeter barrel. Under the operating conditions shown here, the highest pressure in the 20 millimeter barrel is about 70,000 pounds per square inch at the breech.

Performance of the gun, under optimum firing conditions of helium pressure and powder charge was evaluated by firing a series of nylon cylinders into a vacuum. The experimental results are presented in figure 4 which shows the observed effect of model weight on muzzle velocity, and makes a comparison with theoretical predictions obtained from shock tube considerations. Velocities of about 17,200 feet per second were obtained with models weighing 0.06 gram. Further reduction in weight resulted in failure of the model to withstand the launching pressures. Increasing model weight from 0.06 gram is seen to result in a velocity decrement in excess of the predicted value. It is felt that the experimental decrement could be decreased by increasing the length of the pump barrel.

The small-scale atmospheric entry simulator, as it presently exists, is shown in figures 5,6, and 7. In figure 5 we see the high-pressure reservoir and test chamber. Figure 6 shows a close-up view of the test chamber. Air flow is from left to right while the model is fired upstream, from right to left. The photobeam light sources on the side of the chamber can also be seen. The shadowgraph stations, operating in the vertical plane, are placed between the photobeam stations; the spark sources on top of the chamber and the film holders below. The third photo station from the left has been modified to take reflected light pictures of the model as it traverses the test chamber. In figure 7 we see the helium gun or model launcher, as it is attached to the vacuum tank. The test chamber and high-pressure reservoir are on the opposite side of the vacuum tank. From right to left we see the 20-millimeter pressure barrel, the

[redacted]

high-pressure coupling, and the 22-caliber launch barrel which is contained in a housing.

[redacted]

[redacted]

Models

Cylindrical models were chosen for initial tests in the simulator. Such models are easy to construct and would produce results indicative of those for a practical vehicle. Several launchings have been made of this particular shaped model and certain preliminary results can be considered. A sketch of the model shape is shown in figure 8. The model was constructed of nylon, with a 0.007-inch copper piece cemented to the forward circular face as shown in figure 8. The 0.010-inch, 45° chamfer was incorporated to prevent contact between the edge of the copper face and the inside of the launch barrel.

[redacted]

RESULTS AND DISCUSSION

Results obtained can best be shown by reference to one of the typical tests. In this particular test, the model was launched at a velocity of 14,300 feet per second, relative to the airstream at the entrance to the test section. The reservoir pressure at the time of launching was 198 pounds per square inch absolute. Using the methods of references 1 and 2, the dimensions of the simulated missile were determined and the variations of velocity with altitude were calculated for an atmospheric entrance velocity of 14,300 feet per second. The theoretical velocities for the simulated missile along with the experimental velocities obtained in the simulator are plotted according to the simulated altitude and presented in figure 9. As indicated in figure 9, the simulated missile has a diameter of 2.5 feet and weighs about 750 pounds. From reference 3, in which the optimum performance characteristics of ballistic missiles are evaluated, this missile, when fired at an initial exit angle of about 40° to the horizontal, should have a total range of about 1500 miles. What we have actually simulated, therefore, is an intermediate range ballistic missile. The thickness of the copper face on this simulated missile would be 1 inch and would comprise the main heat absorbing medium. The model we have used here has the copper face cemented to a nylon cylinder. which is a relatively nonconducting substance, and which should, therefore, absorb a relatively small amount of heat. The altitude range which the facility simulated is from about 60,000 to 160,000 feet as indicated in figure 9. Although the lower 60,000 feet of the trajectory is eliminated, it is apparent that more than half the velocity decrement, and consequently the large majority of the energy decrement is accounted for in the chosen range. Since this energy decrement is proportional to the total heat absorbed, we feel confident that we are accomplishing the desired simulation.

Spark shadowgraphs were obtained throughout the model's trajectory. Representative ones are shown in figure 10. Starting from the top we

see the model near the beginning of its entry. The simulated altitude is about 150,000 feet and its velocity is about 14,000 feet per second.

In the second photograph we see the model at a simulated altitude of 90,000 feet, traveling with a velocity of about 10,300 feet per second. According to the theory of reference 1, this portion of the trajectory is where the maximum average convective heat-transfer rate occurs with the accompanying maximum thermal stresses. The model in this photograph appears to be distorted in the vicinity of the front face. Much of this is optical distortion. Recovered models gave evidence of no permanent distortion of the amount indicated here.

The lower picture shows the model at a simulated altitude of about 75,000 feet traveling at a velocity of 7,000 feet per second. According to reference 1, the altitude of maximum deceleration occurs at 84,000 feet at a velocity of 8,700 feet per second. The model has passed this point and is still intact. Some information on the condition of the front face may be deduced from the shock pattern. The irregular appearance of the shock from the edge of the front face may be due in part to separation at that point. Such separation could be caused by some distortion of the model due to the rapid deceleration or by roughness caused by actual burning at the edge. Computations based on the methods presented in reference 4 indicate the heat transfer to be highest at the edge of the cylindrical face.

Figure 11 is a streak photograph which shows the illumination produced by the model as it passes through a simulated altitude of about 115,000 feet at a velocity of about 12,500 feet per second. The bright central streak is the path taken by the model, while the remaining illumination is produced by reflection from the inside walls of the chamber.

Much evidence can be obtained by observing the condition of recovered models. As mentioned previously, conditions are such that the model velocity goes to zero at the upstream end of the test section. The model is then carried downstream into the vacuum tank where it is recovered.

The resultant damage to models impacting in the vacuum tank often prevents any successful observation. Such was the case for the particular model in the test just described. A series of such tests were, however, conducted under identical test conditions. Recovered models all showed a large degree of similarity with regard to surface condition. Figure 12 is a photomicrograph of a copper face of a model before and after flight through the simulator. With regard to the model prior to firing, we can clearly see small concentric machine marks as well as some small scratches and irregularities. The surface condition is considerably altered by traverse through the simulator. The most striking feature about the surface is, of course, the several small craters. There is some indication that these craters are formed by impact with impurities in the airstream which range in diameter from about 0.008 to 0.0001 inch.

Aside from the surface pitting, other interesting observations can be made. In particular we can see that only slight evidence exists of the concentric machine marks which were so prominent in the unfired model. Evidently a portion of the outer surface of the model has been either fused or burned in the traverse through the simulator. Another feature is the coloring of the copper face at the outer edge. This coloring is identical with that obtained on a rapidly cooled copper sheet where a portion of the sheet had been heated to a temperature on the order of 1000° to 1500°F while adjacent areas were relatively cooler. It will be recalled that convective heat transfer is, according to theory, greatest at the outer edge of a cylindrical face.

There is, of course, one gross, but important, implication of these tests: the missile simulated could probably survive the heating associated with its entry into the earth's atmosphere.

[redacted]

CONCLUDING REMARKS

The results which have been presented and discussed represent the initial attempts to simulate the atmospheric entry of a ballistic missile. In conclusion, it might be well to indicate the direction of our future plans.

Plans are already proceeding to build a larger facility, for which the present apparatus is a pilot model. The new simulator will accommodate a model of larger size (by a factor of about 4) and more complex shape.

Entrance velocities should be much higher. To accomplish this, an improved version of the helium gun has been constructed and will shortly undergo initial firing tests. If results are realized in the same proportion to theoretical indications as they were for the present gun, we might anticipate velocities in excess of 20,000 feet per second from this relatively simple and easily handled device. This new gun will be put into operation with the present small-scale facility in a few months.

At stations near the "altitude" of maximum heating rates, fogging of the shadowgraph films has been noticed. This is hardly surprising, in view of the incadescence evidenced in figure 11. It remains to determine the characteristics and origin of the light - whether it results from the heating of the copper face, the ionization of the air around the model, or both. To this end, spectroscopic analysis of the emitted light has been undertaken. The duration of light into the spectroscope is too short to obtain a satisfactory spectrum with the present apparatus. Further tests will be performed with an improved spectroscopic system.

[redacted]

[redacted]

REFERENCES

1. Allen, H. Julian, and Eggers, A. J., Jr.: A Study of the Motion and Aerodynamic Heating of Missiles Entering the Earth's Atmosphere at High Supersonic Speeds. NACA RM A53D28, 1953.

2. Eggers, A. J., Jr.: A Method for Simulating the Atmospheric Entry of Long-Range Ballistic Missiles. NACA RM A55I15, 1955.

3. Eggers, A. J., Jr., Allen, H. Julian, and Neice, Stanford E.: A Comparative Analysis of the Performance of Long-Range Hypervelocity Vehicles. NACA RM A54L10, 1955.

4. Stine, Howard A., and Wanlass, Kent: Theoretical and Experimental Investigation of Aerodynamic-Heating and Isothermal Heat-Transfer Parameters on a Hemispherical Nose With Laminar Boundary Layer at Supersonic Mach Numbers. NACA TN 3344, 1954.

[redacted]

ALTITUDE-DENSITY RELATION: $\frac{\rho}{\rho_o} = e^{-\beta y}$

HEAT ABSORBED PER UNIT MASS AT ALTITUDE, y

$$\frac{Q}{m} = \frac{V_E^2}{4}\frac{C_f' S}{C_D A}\left[1 - e^{\frac{C_D \rho_o A}{\beta m \sin\theta_e} e^{-\beta y}}\right]$$

FOR SIMILITUDE–

SAME ENTRANCE VELOCITY, V_E
GEOMETRIC SIMILARITY–SAME S/A
SAME REYNOLDS NUMBER–SAME C_f', C_D
SAME VALUE OF βy
SAME VALUE OF $\frac{C_D \rho_o A}{\beta m \sin\theta_e}$

Figure 1.- Theoretical basis for simulation.

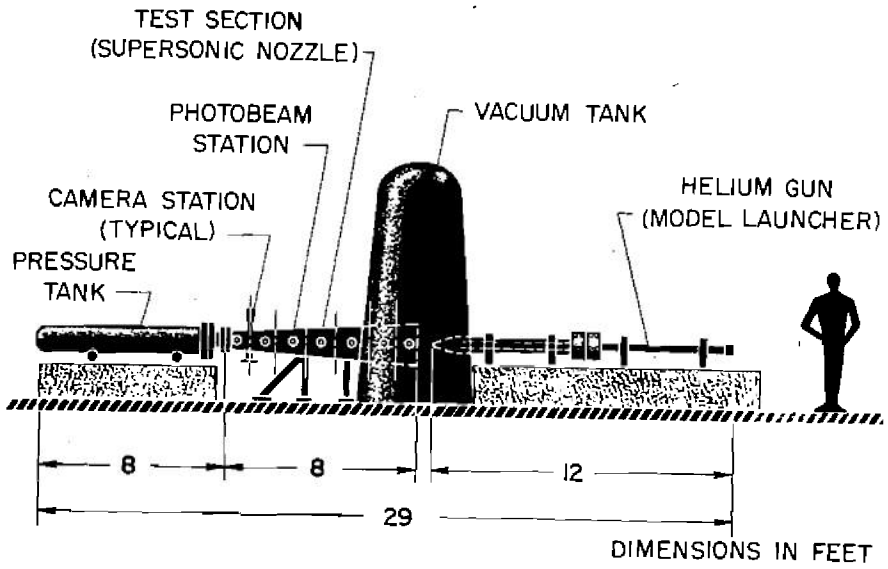

Figure 2.- Schematic diagram of the small-scale atmospheric entry simulator.

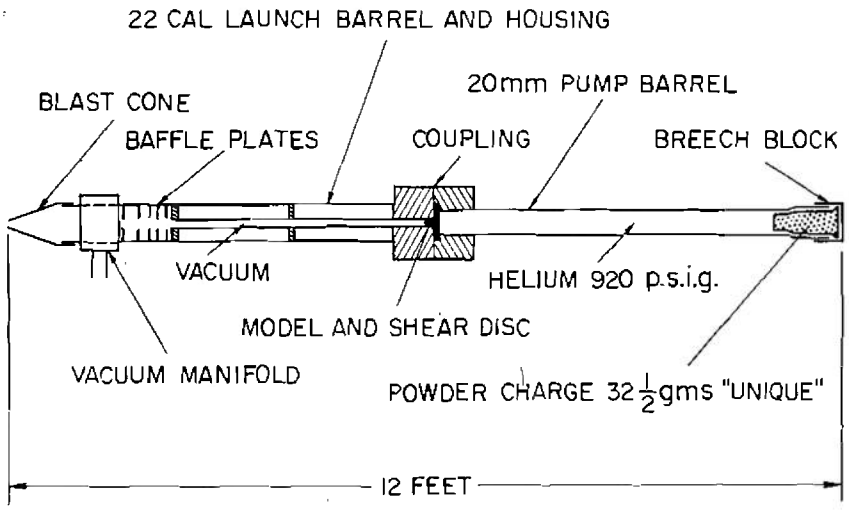

Figure 3.- Schematic diagram of the helium gun used to launch models.

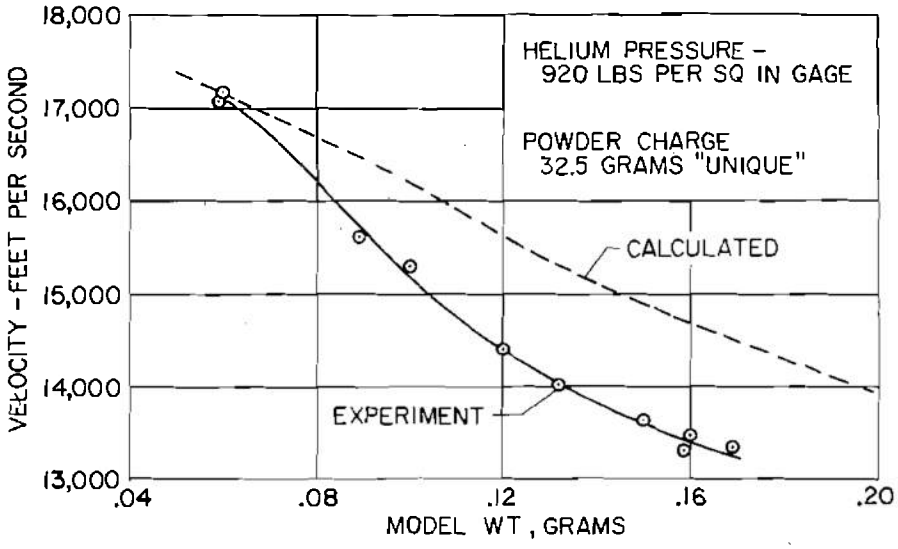

Figure 4.- Performance of the helium gun in vacuum.

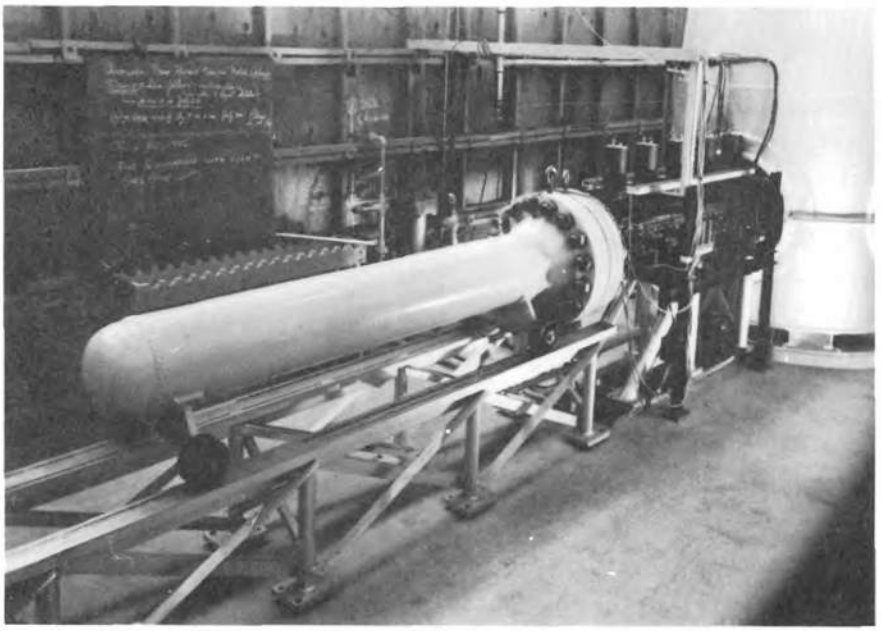

Figure 5.- Small-scale atmospheric entry simulator: high pressure reservoir and test chamber.

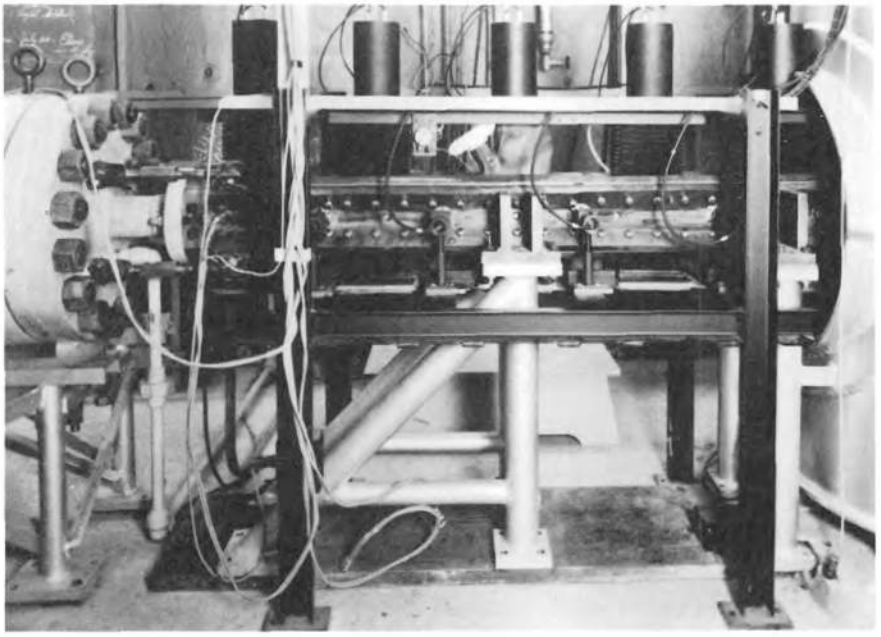

Figure 6.- Small-scale atmospheric entry simulator: test chamber.

Figure 7.- Small-scale atmospheric entry simulator: helium gun.

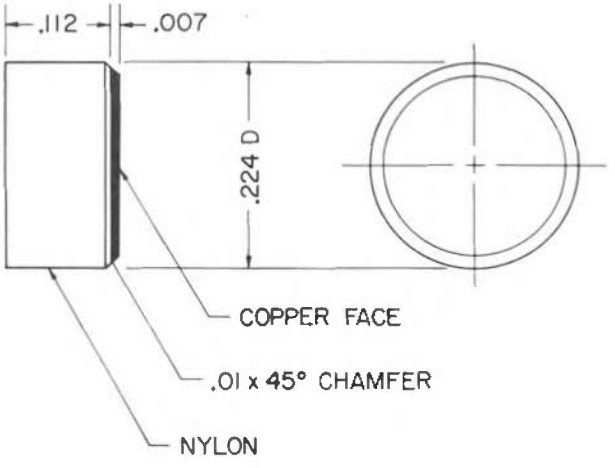

Figure 8.- Copper-faced models tested in small scale atmospheric entry simulator.

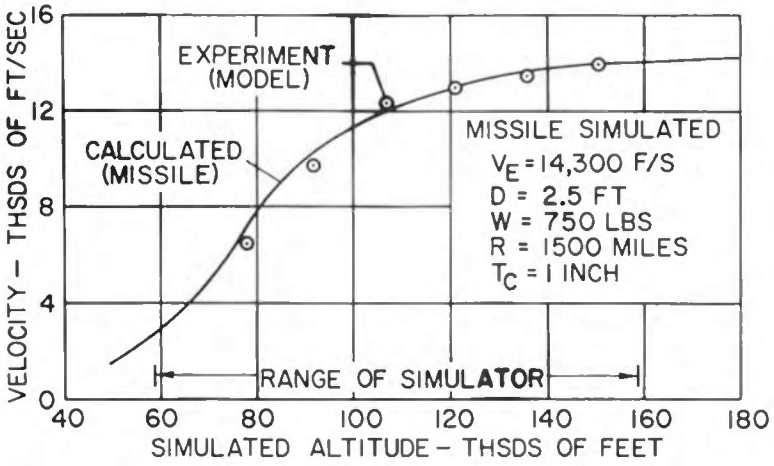

Figure 9.- Velocity of copper-faced models and comparison with theoretical predictions.

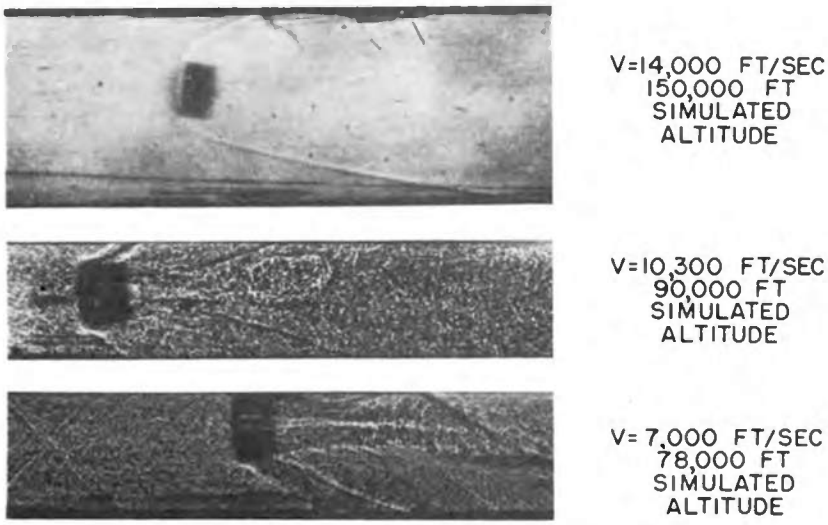

Figure 10.- Copper-faced models in flight through small-scale atmospheric entry simulator.

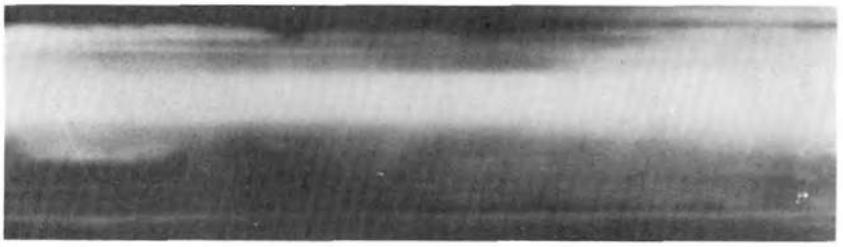

VELOCITY, 12,500 FEET PER SECOND
SIMULATED ALTITUDE, 115,000 FEET

Figure 11.- Illumination caused by models during test.

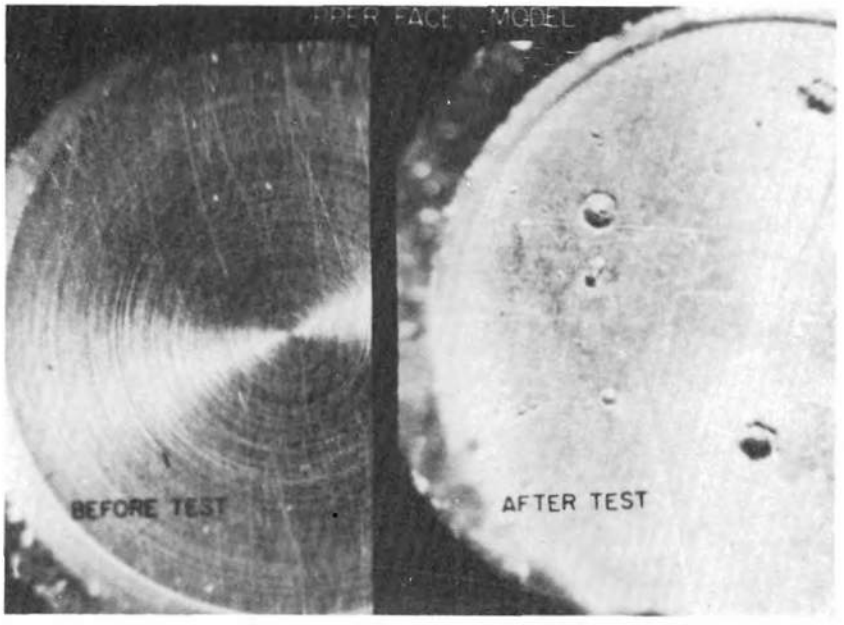

Figure 12.- Copper face of models before and after tests.

INTENTIONALLY LEFT BLANK.

SOME PROBLEMS ASSOCIATED WITH THE DETERMINATION, FROM RANGE FIRINGS, OF DYNAMIC STABILITY OF BALLISTIC MISSILE RE-ENTRY SHAPES

L. C. MacAllister

Ballistic Research Laboratories
Aberdeen Proving Ground, Maryland

INTENTIONALLY LEFT BLANK.

SYMBOLS

$C_D = \dfrac{\text{Drag}}{\bar{q}\ S}$

$C_{L_\alpha} = \dfrac{\text{Lift}}{\bar{q}\, S\alpha}$

$C_{M_\alpha} = \dfrac{\text{Righting Moment}}{\bar{q}\ S\ d\ \alpha}$

$C_{M_q} = \dfrac{\text{Damping Moment}}{\bar{q}\ S\ d\ \left(\frac{qd}{2V}\right)}$

$C_{M_{\dot{\alpha}}} = \dfrac{\text{Damping Moment}}{\bar{q}\ S\ d\ \left(\frac{\dot{\alpha}d}{2V}\right)}$

α = Angle of yaw

q = Angular velocity

$\bar{q}$ = Dynamic pressure

S = Characteristic Area $\left(\frac{\pi d^2}{4}\right)$

d = Characteristic dimension (diameter)

M = Mach number

[redacted]

SOME PROBLEMS ASSOCIATED WITH THE DETERMINATION, FROM RANGE FIRINGS, OF DYNAMIC STABILITY OF BALLISTIC MISSILE RE-ENTRY SHAPES

L. C. MacAllister
Ballistic Research Laboratories

INTRODUCTION

One of the perennial problems in projectile or free missile design is dynamic stability. Practically, the ability to damp out a transient yaw oscillation has two aspects: one, associated with the conditions imposed by the trajectory of the missile; the second, associated with the aerodynamic properties of the missile itself. The stabilizing, or destabilizing, effects of the trajectory conditions must be evaluated from a knowledge of variations in the velocity and density conditions along the trajectory. The inherent aerodynamic damping of the missile can be determined separately. If the trajectory conditions are destabilizing, it is desirable for the aerodynamic damping of the missile to be sufficient to overcome them.

One of the better test means for determining the natural damping of projectiles has been the precision enclosed range. Considerable work has been done over the years on Ordnance shell and, more recently, on missiles with wings and fins. Since current nose-cone designs for ballistic missiles involve bodies of revolution, and frequently look like blunt bullets, it is not surprising that ranges became involved in trying to determine the dynamic stability of some nose-cone designs. In view of their similarity to shell, no unsurmountable problems should occur in determining their properties. Some problems could be foreseen, however, and over the period of the last two years it has become quite evident that these problems are quite serious. A discussion of these problems is the subject of the present paper.

A brief digression from the main theme will be made to outline the current potential of the precision range facilities at the Exterior Ballistics Laboratory.

[redacted]

[redacted]

EXTERIOR BALLISTICS LABORATORY RANGES

There are two atmospheric ranges, one 300 feet long and the other about 800 feet long[1]; and also a controlled temperature and pressure range which is described elsewhere[2]. Generally, drag, static stability, lift derivative and dynamic stability can be obtained in the atmospheric ranges with models from less than one inch in diameter to as large as six inches in diameter (or maximum wing span) at Mach numbers from about 0.5 to 4 or better[3]. Flow field shadowgraphs are also obtained. By using the smaller controlled temperature pressure range, models on the order of a half-inch in diameter can be launched at various Reynolds and Mach numbers. With special atmospheres or extremely low temperatures, or both, Mach numbers as high as eleven can currently be reached[3] and it is hoped that soon the upper limit will be pushed to Mach twenty. At present, only drag, shadowgraphic flow patterns and interferograms can be obtained consistently in this range. It is possible, with some models, to obtain static stability information also, but the station spacing is such that this is very difficult to obtain with nose-cone models.

Some data taken from both atmospheric and controlled temperature and pressure ranges are shown in Figure 1. These are drag data for a series of AVCO shapes. The lower Mach number portion has been determined by firings of 1.4-inch diameter models in air at normal condition; the upper Mach number regions, by firings of 0.6-inch diameter models in nitrogen at about 86° Kelvin. The lack of data overlap for these two firings prevents a good comparison of the consistency of the data from the two sources. The top curve is of particular interest, since the character of the flow over the model for Mach numbers less than 4.6 was different from that for higher speeds. The flow was not attached to the Model's afterbody at low speeds and was attached at high Mach numbers. This flow phenomenon is shown in Figure 2.

[redacted]

DRAG COEFFICIENT vs MACH NUMBER

AVCO SHAPES

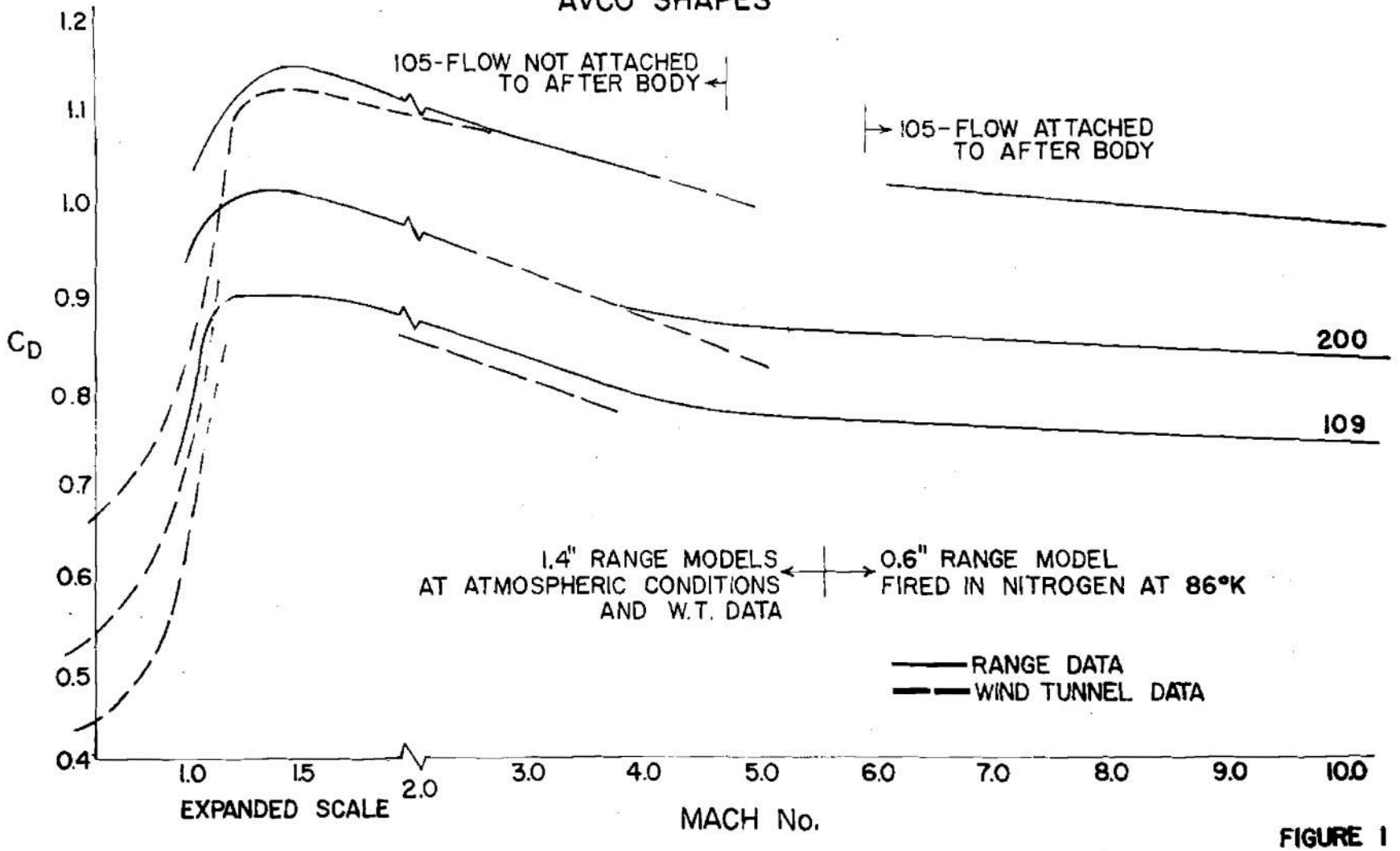

FIGURE 1

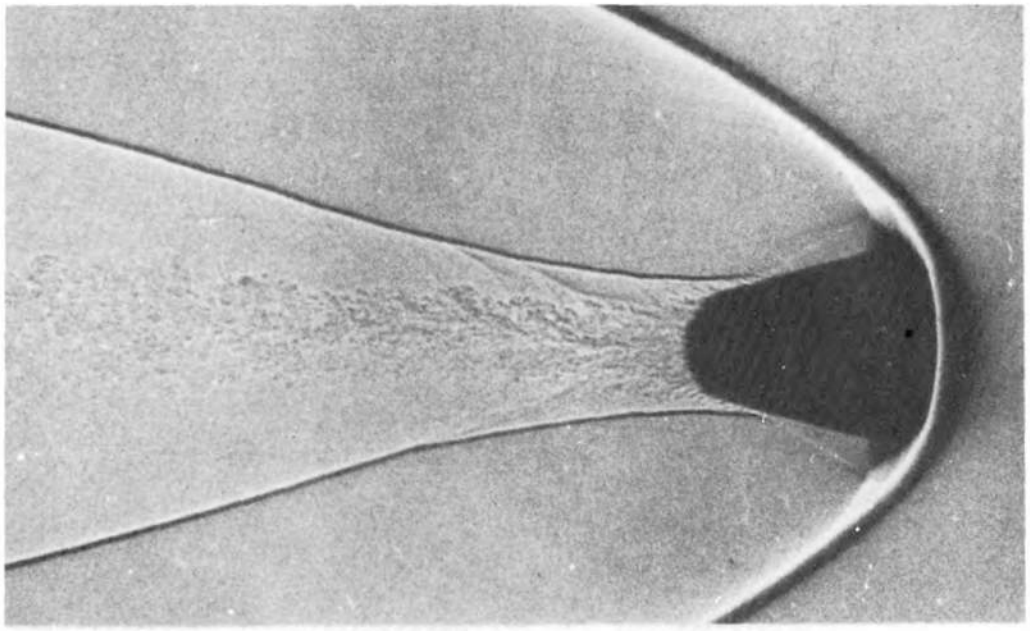

AVCO SHAPE 105 MODEL M≐4.6

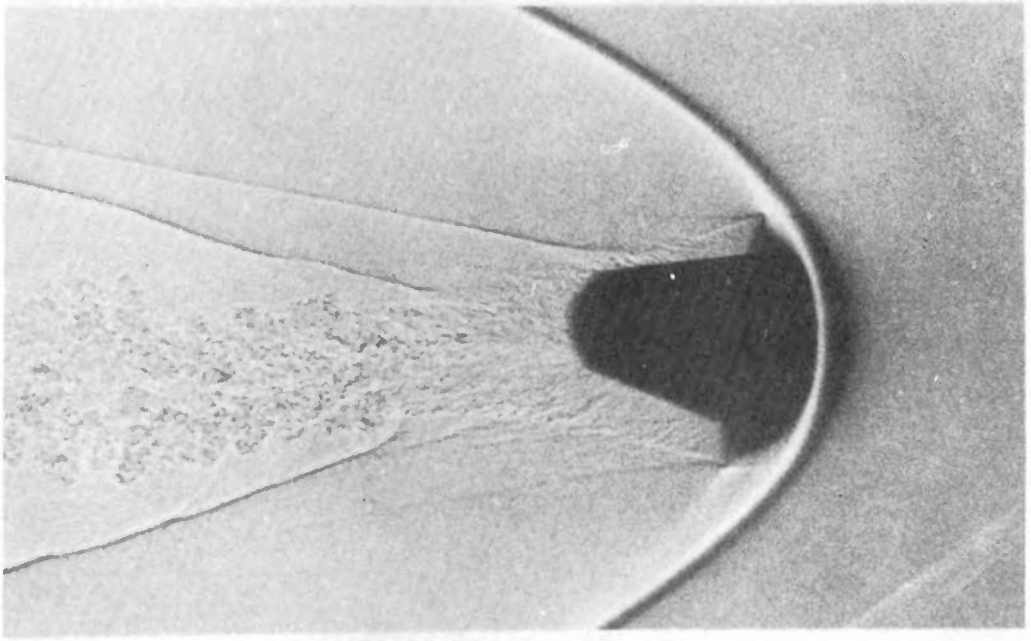

AVCO SHAPE 105 MODEL M≐4

FIGURE 2

DETERMINATION OF DAMPING

A description of the range method of determining the dynamic stability of a model[4, 5, 6] is perhaps in order before a discussion of the problems. Figure 3 shows the necessary data that must be determined in order to evaluate the damping derivatives with a single shot.

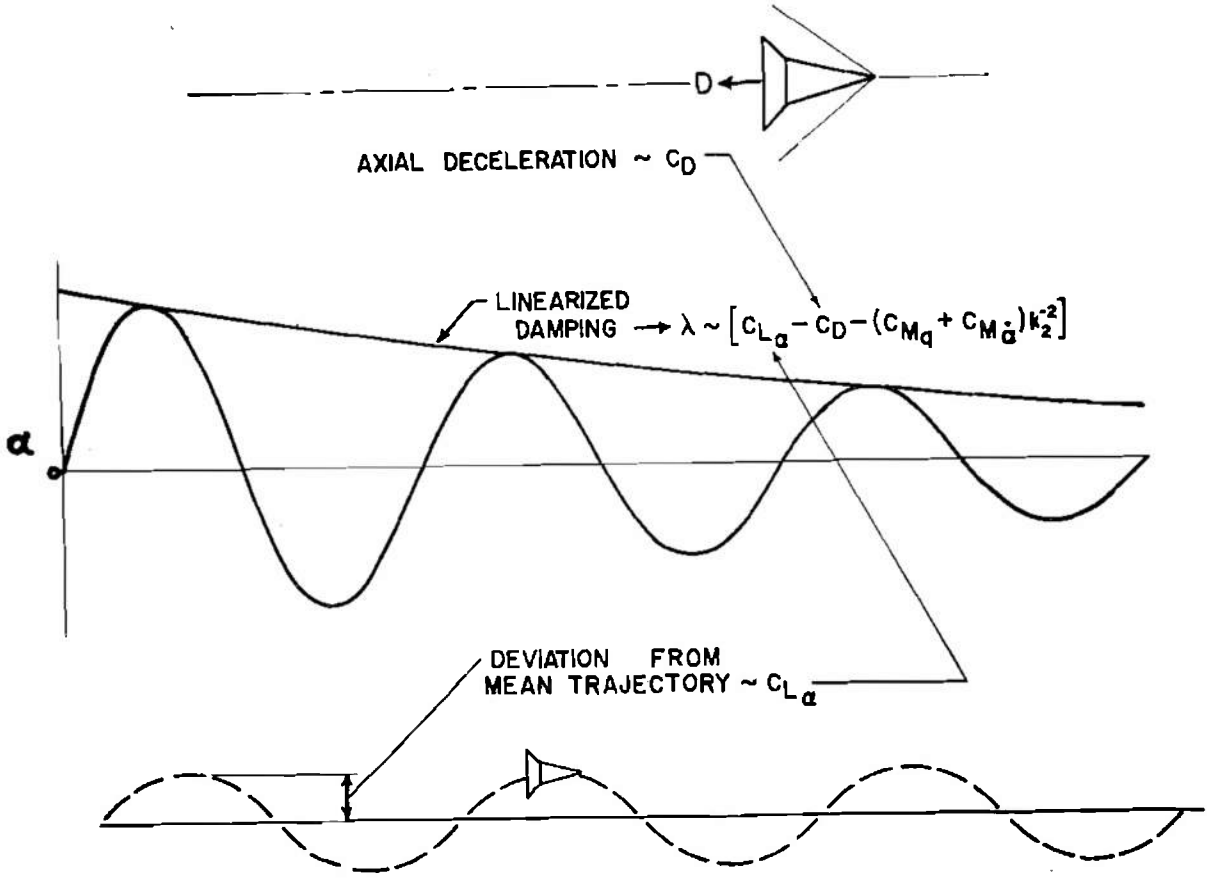

DETERMINATION OF DAMPING DERIVATIVES

FIGURE 3

These data are: the axial deceleration, leading to the drag; the overall variation of the yaw, leading to the total damping of the model; and the transverse excursions of the center of mass of the model, leading to a determination of the lift derivative. Determination of the drag is, in itself, no problem; although it must be admitted that high drag, in part, contributes to some of the problems in determining the dynamic stability. Range determinations of the actual drag of a model are generally so good that for the purpose of future discussions the drag coefficient may be considered easily determinable and without error. The effect of the drag on the dynamic stability of a model is always destabilizing for most of the nose-cone shapes fired at BRL the drag was large.

The effect of the lift derivative, C_{L_α}, is stabilizing for most ordinary configurations. Nose-cone shapes, however, have produced

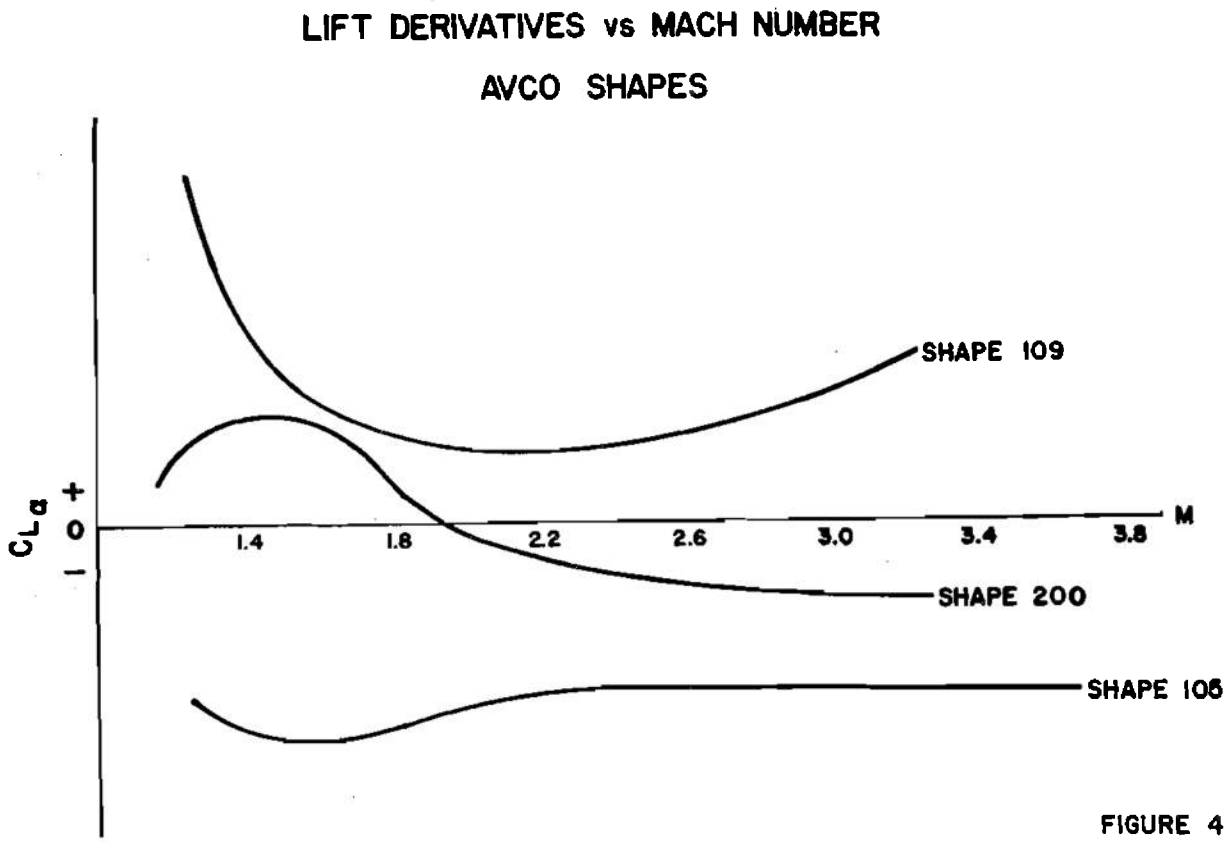

FIGURE 4

destabilizing negative values of C_{L_α}. Figure 4 shows the data on three AVCO shapes: one has a negative C_{L_α} over the entire range of Mach numbers; another, a positive C_{L_α}; and the third, a C_{L_α} which changes sign.

The effect of the damping derivatives, $C_{M_q} + C_{M_{\dot{\alpha}}}$, on the dynamic stability is generally stabilizing at high Mach numbers but is frequently destabilizing near sonic speeds. This effect has appeared to hold for the extremes, in bluntness, of the shapes tested here. This is shown in Figure 5. Although the existent data are sparse, and the curves shown may not be final, the trends seem quite clear.

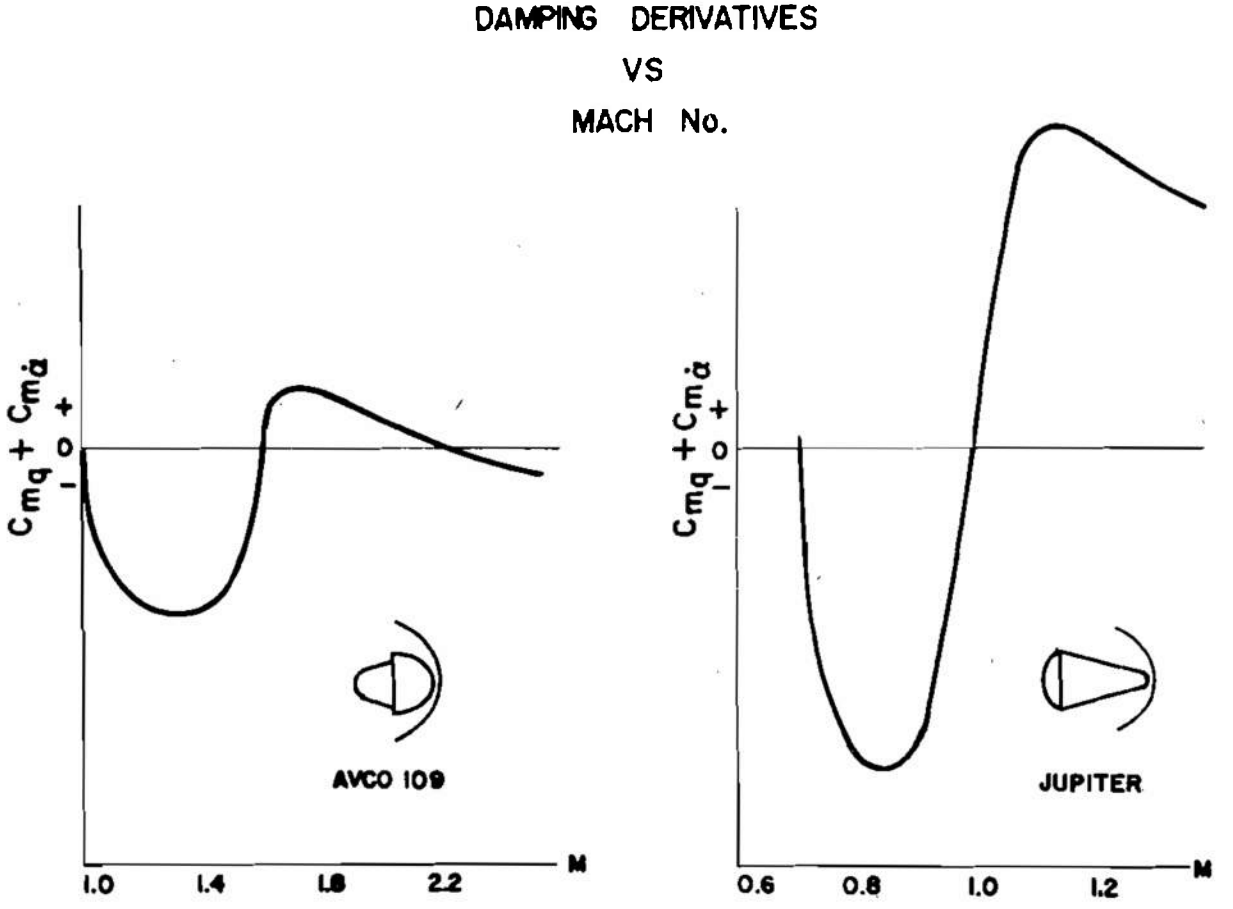

FIGURE 5

PROBLEMS AND REMEDIES

The major problems in determining the dynamic stability of nose-cone models arise from three causes. First is the difficulty encountered in measuring the spark photographs; second, the high deceleration in flight through the range; and third, the existence of nonlinear forces and moments.

Accurate measurement of the photographs of nose-cones is particularly difficult at high Mach numbers. The optical distortion due to the heavy shock front, which is essentially wrapped around the body, obscures the physical outlines of the model (Fig. 6).

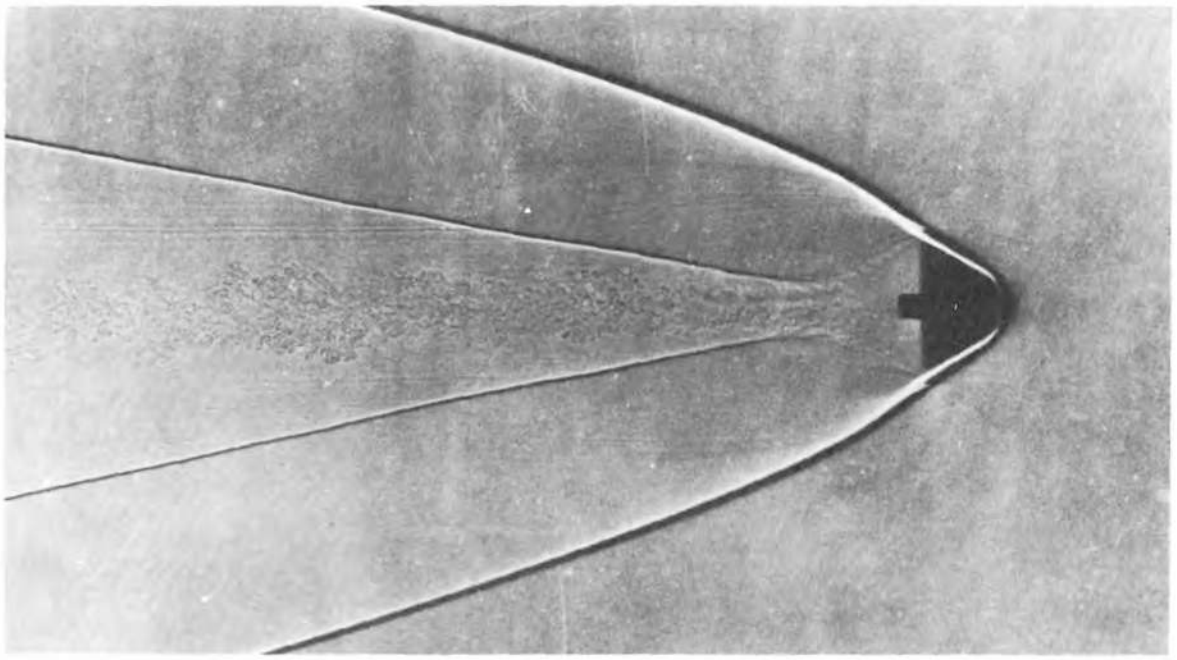

20mm RAMO-WOOLDRIDGE 30° SEMI-ANGLE MODEL M=5

FIGURE 6

TECHNICAL LIBRARY
U. S. ARMY ORDNANCE
ABERDEEN PROVING GROUND, MD.
ORDBG-LM

The extremely high deceleration of nose-cones is due to their high drag and to their poor ballistic coefficients. It is a practical impossibility to design models of this type with good ballistic coefficients (large mass per unit frontal area, for a given drag). As a result, these models traverse a rather large Mach number interval in a range test (Fig. 7). Admittedly, the case shown is an extreme one, for this model would traverse a Mach number band from 6 to 2 within a single flight through the range instrumentation.

The existence of nonlinear variation with yaw level, of some of the aerodynamic forces and moments, is particularly troublesome near transonic speeds. This certainly is not surprising, for even quite conventional projectiles exhibited definite nonlinearities of their aerodynamic properties in the transonic region. Figure 8, for instance, shows the damping properties of a standard 20-mm shell. As can be seen, there is a definite variation with yaw level. It must then be expected that nose-cone models will be as bad or worse.

What can be done about these difficulties? Some of them can only be alleviated. Consider the problem of improving the accuracy of measurement for these particular shapes. This can be disposed of easily. The measurability can be improved by modifications of the geometry of the model that do not effect its aerodynamic properties, or by reducing the optical distortion, or both. Figure 9 shows pictures of two shapes, one of which has a long tail sting for measurement purposes. This modification complicates the launching of the model somewhat but gives a very good base point from which to measure. Two shadowgraphs taken in the Controlled-Temperature-Pressure Range are shown in Figure 10: one is a normal shadowgraph utilizing a conical light source; the other is a focused, parallel-light shadowgraph. Clearly, a major part of the distortion at the front of the body has been eliminated in the latter case.

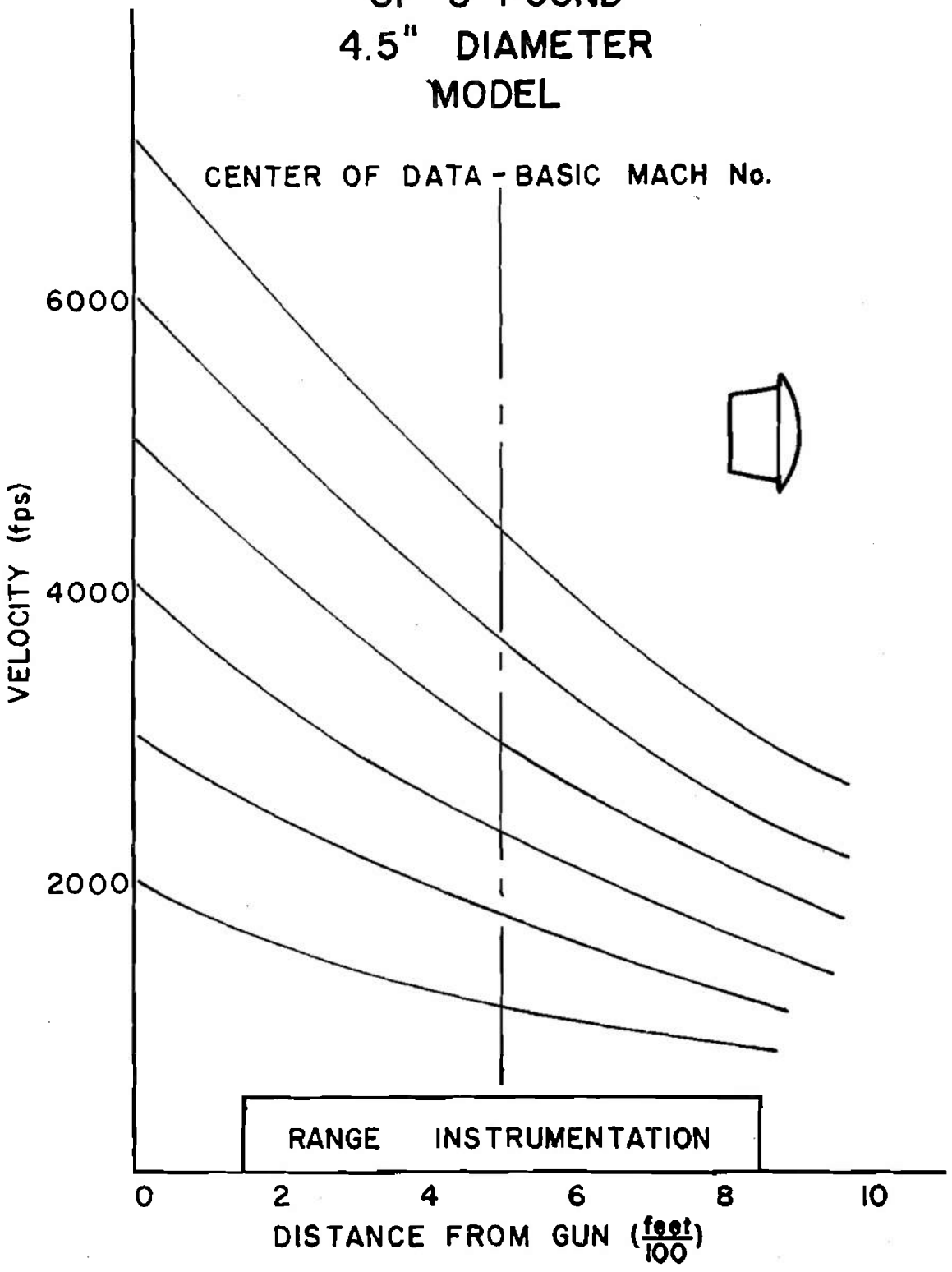
VELOCITY FALLOFF
OF 5 POUND
4.5" DIAMETER
MODEL
CENTER OF DATA - BASIC MACH No.
6000
4000
2000
VELOCITY (fps)
RANGE INSTRUMENTATION
0
2
4
6
8
10
DISTANCE FROM GUN (feet/100)

FIGURE 7

NUTATIONAL DAMPING RATE
VS
EFFECTIVE YAW SQUARED

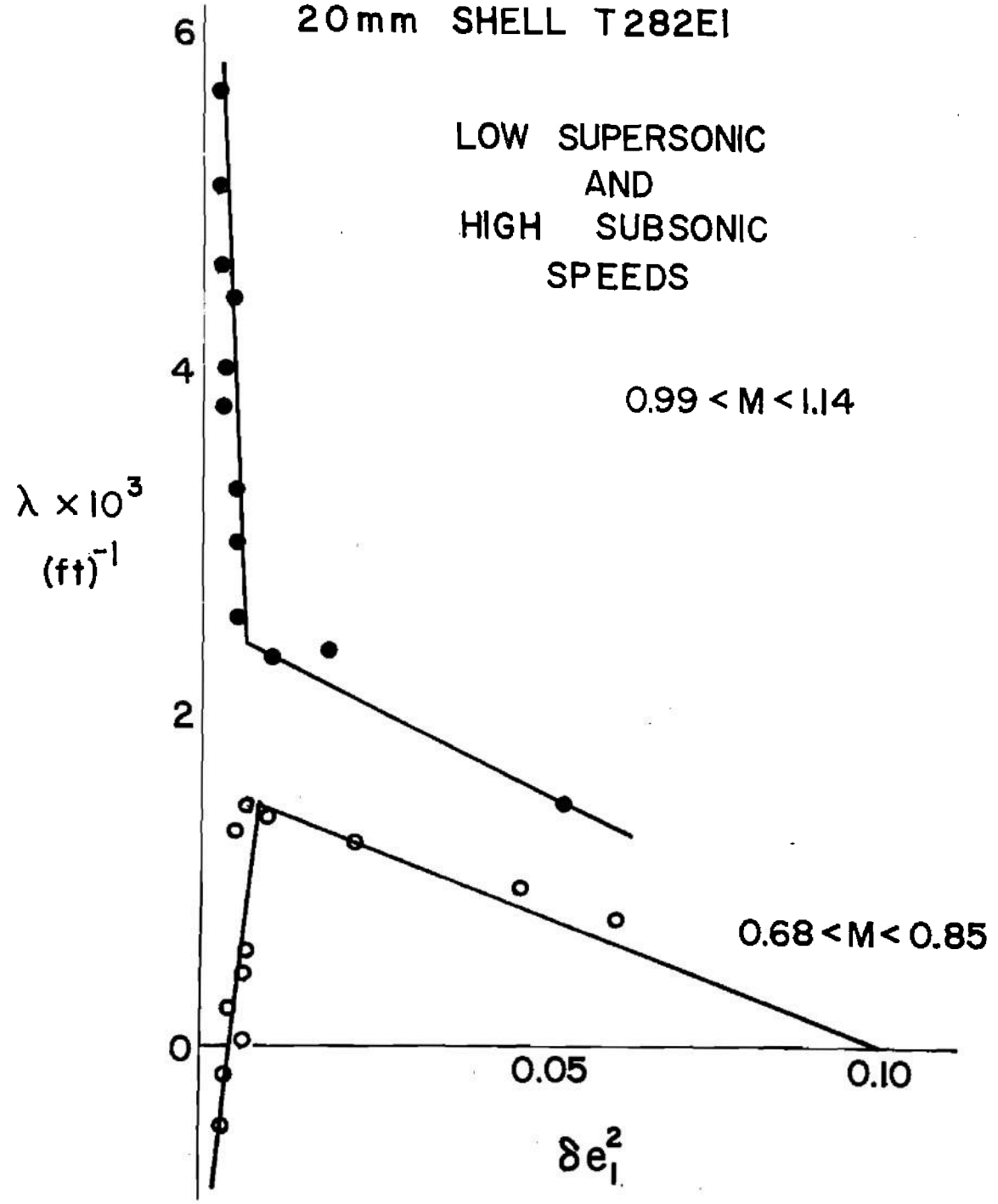

FIGURE 8

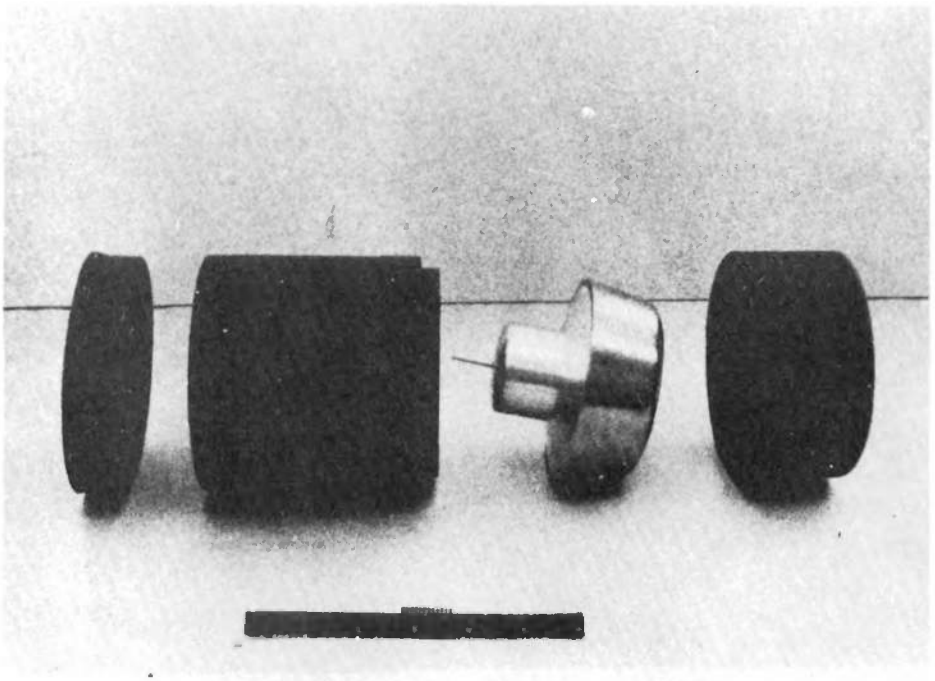

4.5 INCH AVCO SHAPE 801 AND SABOT

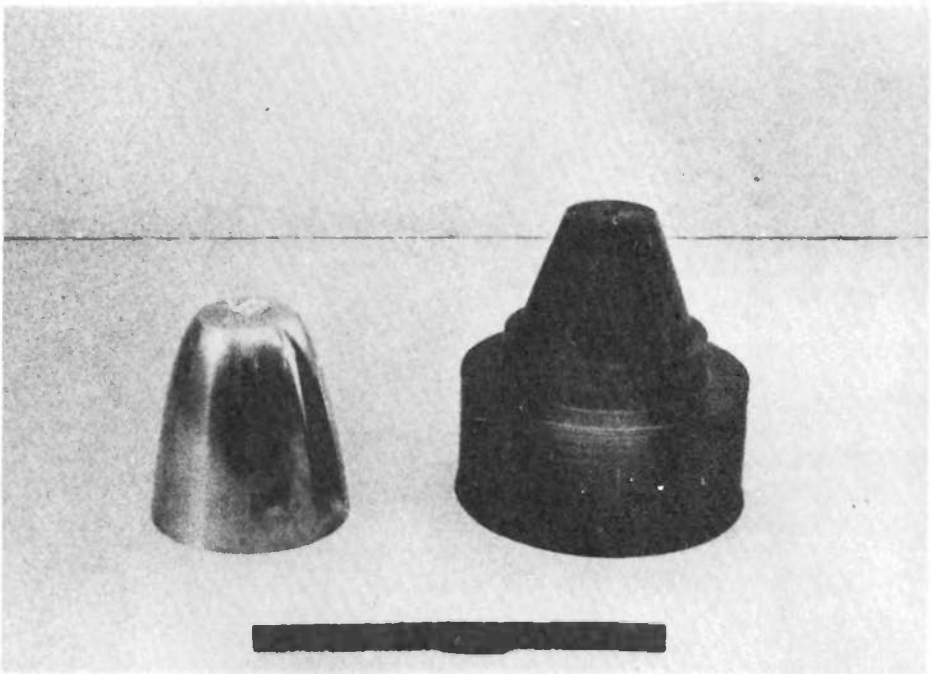

3.5 INCH GE SHAPE E4 AND SABOT

FIGURE 9

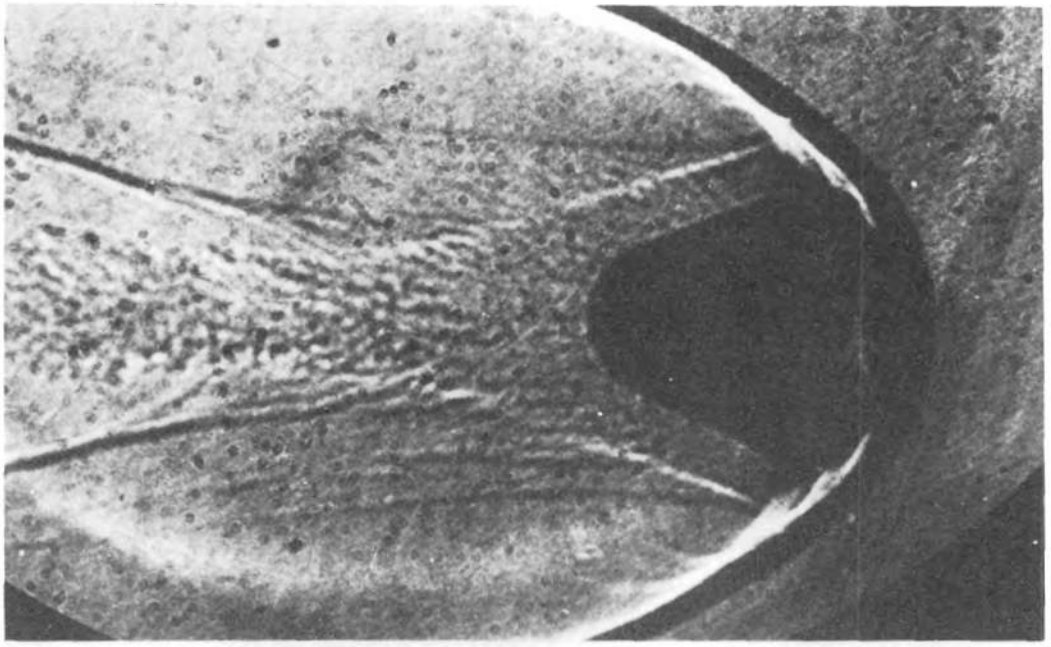

STANDARD SHADOWGRAPH M = 9.0

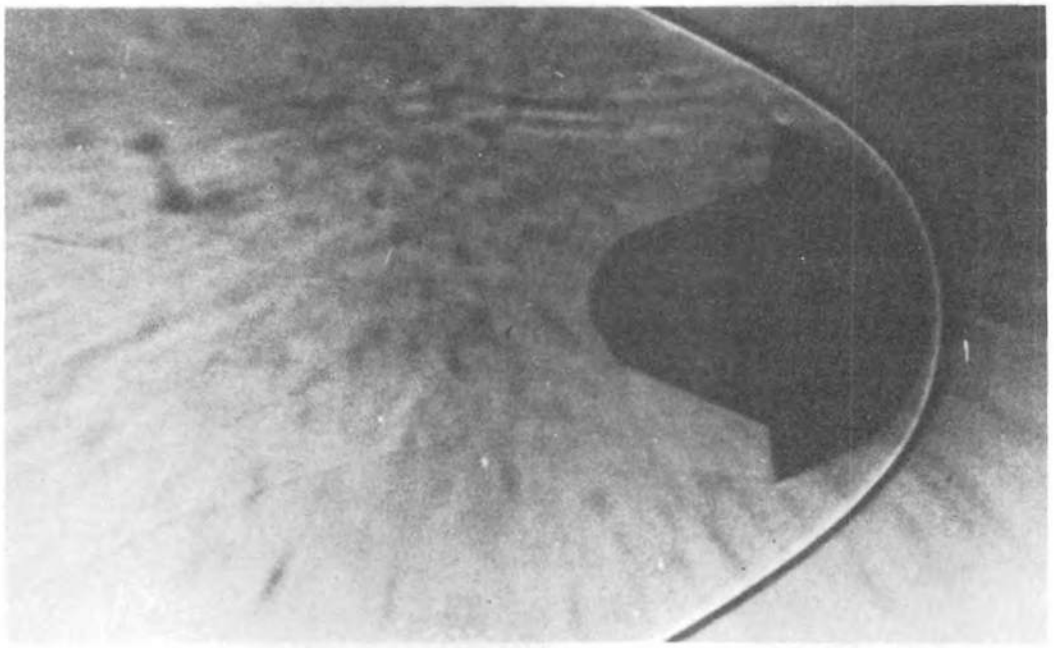

FOCUSED SHADOWGRAPH M=9.9

AVCO SHAPE 200 MODEL

FIGURE 10

The task of reconverting all our recording stations to the focused type is formidable, as would be the corresponding increase in the upkeep that would be necessary. This solution is not impossible, however, nor even impractical.

The retardation problem or the fact that the model traverses a wide Mach number band in the range is a more difficult problem. Contractors are already making extensive use of Tungsten alloys to give their models a high sectional density. Ranges with pressure control can, of course, reduce the test chamber density so that the model slows down less. But this partially begs the issue since the models' characteristic oscillations and damping lengths also increase. It takes correspondingly longer range to determine these parameters to an equal degree of accuracy. Basically, it must be remembered that in order to determine the static stability of a model in a range test it must go through enough of its motion in yaw, for a curve fitting process to determine a reasonable cycle; and in order to determine its damping properties it must go through enough cycles so that the change of amplitude is definite with respect to the errors of measurement. The observed damping, of course, is dependent on the mass and aerodynamic properties of the model also.

There are three basic directions in which we can go to solve the retardation problem; presuming, of course, that the model has already been designed to include the heaviest practical metals. First, we can fire bigger models, since the drag is a function of the area of the model, which increases as the diameter squared; while the mass of the model increases as the diameter cubed. A given design in a 6-inch diameter model will lose about half as much velocity in a range test as will a 3-inch diameter model. We are currently increasing our maximum test size to eight inches in diameter. As a rule, however, the big, heavy models can not be fired at as high speeds as the smaller, lighter ones.

The same inherent reason of relatively larger cross sectional density applies here also, since this affects the gun's ability to push the model as well as the air's ability to slow it down. Also, current high velocity gun designs are usually in the smaller calibers. This implies that, perhaps, instead of using one model size throughout an experiment one should use smaller, lighter models for high Mach number tests where Mach number effects on the aerodynamic properties are, as a rule, small and the bigger heavier models at transonic speeds where the variation in aerodynamic properties is much larger. This answer complicates the test somewhat but probably should be applied more often than it is. Figure 11 shows the damping derivatives for a Ramo-Wooldridge shape fired in two different model sizes, 1-1/2 inches in diameter and 6 inches[3] in diameter. The portion of the data curve that was covered by each

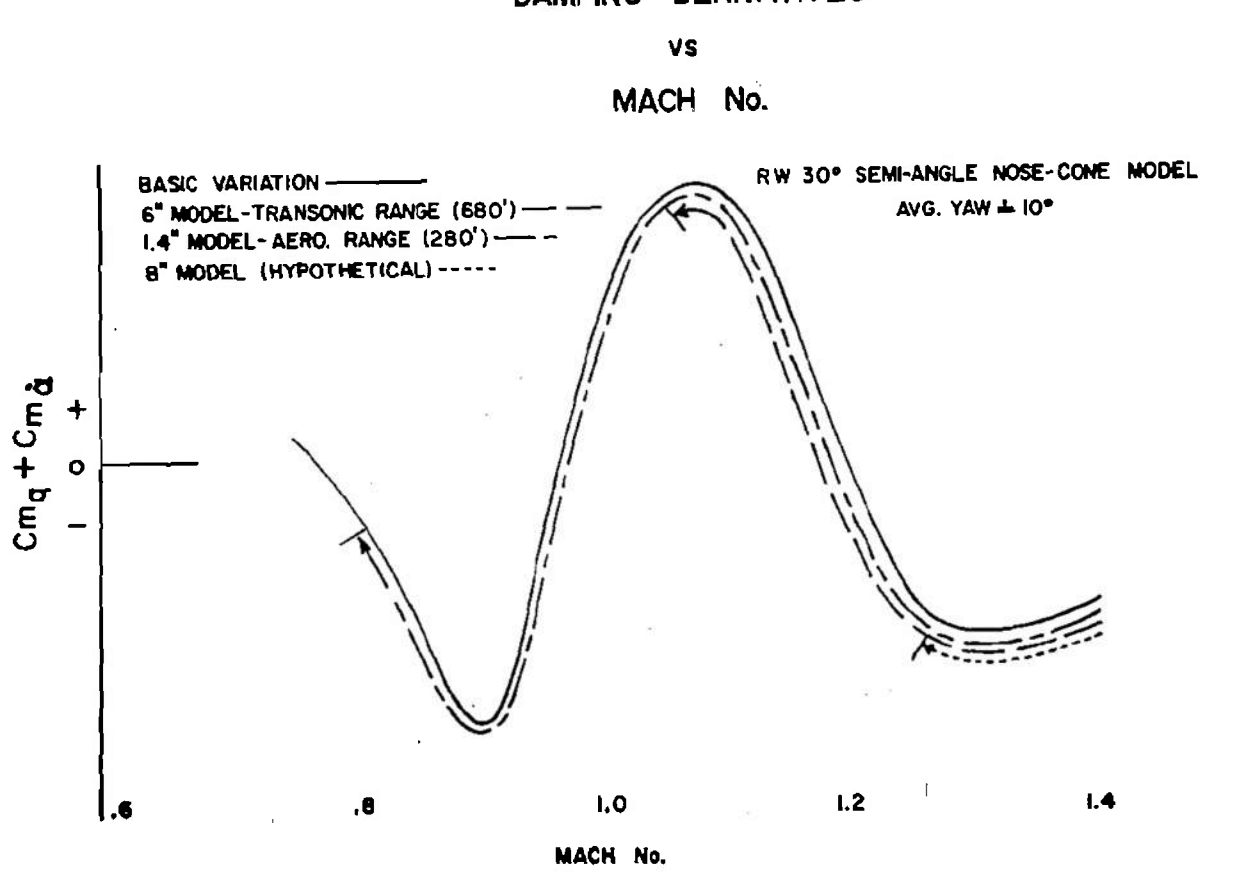

FIGURE 11

model in a given range flight is designated. It is clear that with variations of this type, the Mach number band covered by a single test model must be restricted if more than just qualitative information is desired. The practical Mach number range that would be covered by the heaviest eight inch model, is shown for comparison.

A second method for solving the problem is to fire models that are spin stabilized. This solution would, however, increase the size of a given program and would present other difficulties if the aerodynamics were too nonlinear. Most nose-cone models we have dealt with could have been two to three times as heavy if the full scale center of mass position had not been part of the model design criterion. A maximum weight model would certainly be unstable in the ordinary sense but could be tested by giving it enough spin to be gyroscopically stable. One would then have to perform enough testing to extrapolate the results to the correct center of mass position. This avenue of approach is currently being investigated.

A third possibility is to increase the density of the data for the curve fitting process. If we normally have ten stations over a hundred feet, and this distance involves too great a change of Mach number, we might do better to concentrate the ten stations in fifty feet. Clearly you cannot gain an equal return in this process since you are observing a shorter part of the model's trajectory, but some gain in precision is possible in a given interval by increasing the density of observation. Figure 12 shows the yawing motion of a typical 3.5-inch model in the last part of the range, and a Mach number interval of 0.3. The data points for the basic range spacing are shown in black. Present instrumentation is providing us with double points at some stations. This means that the station operates twice and gives us two pictures of the model. The model traverses about two feet between pictures. These points are shown as the open triangles on the graph. In addition, we are developing stations that may be placed in between the current units to provide a basic ten-foot interval rather than the present

twenty-foot one. These stations are designated by the open circles. Employing all of these new station modifications concurrently, which might be difficult, we would obtain about 56 observations in a 230-foot interval. Usually the Mach number change would be small enough in this distance for even the lighter nose-cone models.

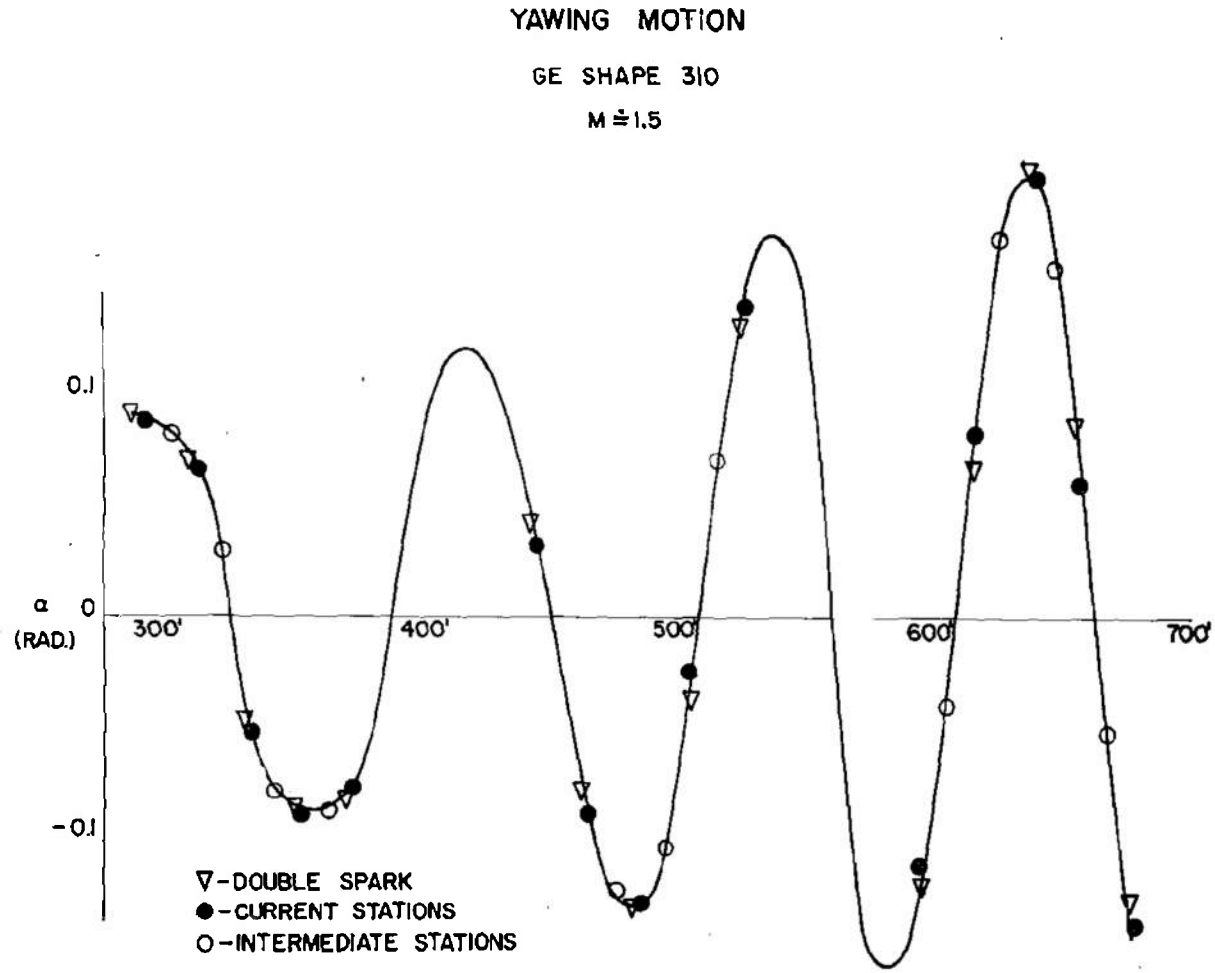

FIGURE 12

It is clear that this would be of considerable help in making the curve fitting process more definite. A shadowgraph taken at one of the double stations is given in Figure 13. Because of the geometry of the double spark arrangement, one shadow appears high on the plate and the other low, rather than in line as one might expect.

This added density of data would also be useful in attacking the problem of nonlinear variation of the aerodynamic properties. A method of processing the output values from the range reduction process, to allow for slight nonlinearities, is given in reference 7. An alternative method is to process the range data on an Analog Computer. Some success has been achieved with this procedure on similar problems[8]. To exploit the analog data reduction procedure denser data distribution would be essential.

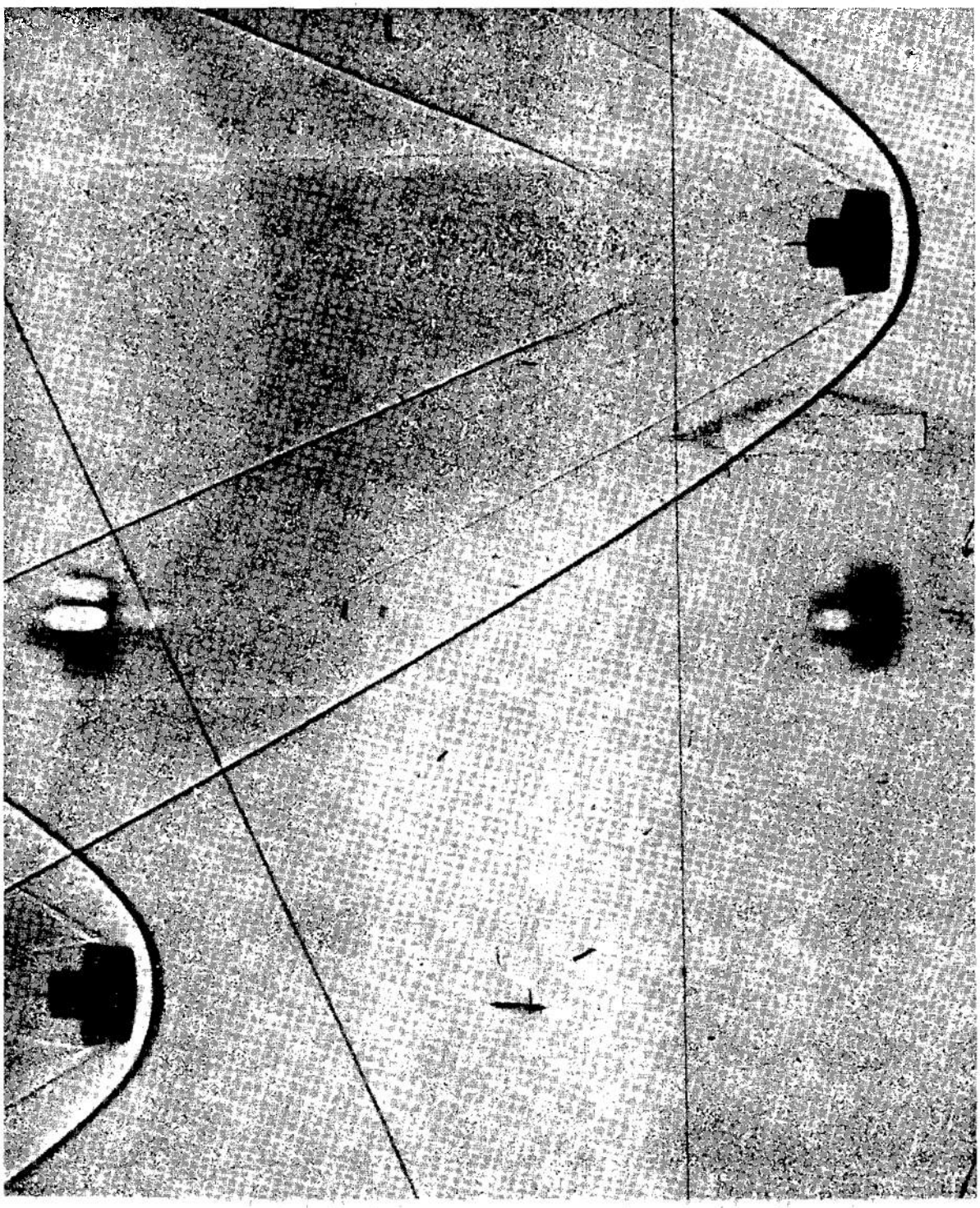

DOUBLE SPARK SHADOWGRAPH AVCO SHAPE 801 MODEL M=2.3

FIGURE 13

[redacted]

SUMMARY

Free flight ranges have been used extensively to determine the dynamic stability of spin stabilized bodies of revolution, namely shell, and some fin stabilized missiles. Recently the ranges have been involved in determining the dynamic stability of some nose-cone shapes, which are statically stable bodies of revolution. These models are generally short, blunt, and have unusual mass distribution. Because of their shapes, high drag, and probable nonlinearity of their aerodynamics, these models produce problems in range testing for dynamic stability. The solutions of these problems may require considerable improvement in instrumental and processing techniques. Most of the problems appear, however, to be solvable at the present state of the art.

[redacted]

[redacted]

REFERENCES

1. Rogers, W. K., The Transonic Free Flight Range, BRL Report 849 (Feb. 1953).

2. Bennett, F. D., The Controlled-Temperature-Pressure Range, BRL Report 1005 Part I (March 1957).

3. MacAllister, L. C., The Type of Data Obtainable in the Test Facilities of the Exterior Ballistics Laboratory. Transactions of the First Technical Symposium on Ballistic Missiles, June 56 Vol. IV, WDD, ARC and R-W Corp.

4. Murphy, C. H., Data Reduction for Free Flight Spark Ranges, BRL Report 900 (Feb. 1954).

5. Nicolaides, J. D., MacAllister, L. C., A Review of Aeroballistic Range Research on Winged And/or Finned Missiles Ballistic Tech Note No. 5 BuOrd, Dept. of the Navy, 1955.

6. Murphy, C. H., On the Stability Criteria of the Kelley, McShane Linearized Theory of Yawing Motion, BRL Report 853 (1952).

7. Murphy, C. H., The Measurement of Nonlinear Forces and Moments by Means of Free Flight Tests, BRL Report 974 (April 1956).

8. Schmidt, J. M., A Study of the Resonating Yawing Motion of Asymmetrical Missiles by Means of Analog Computer Simulation, BRL Report 922 (Nov 54).

[redacted]

DESIGN AND INITIAL TESTS OF THE NOL SHOCK GUN

V. C. D. Dawson

U. S. Naval Ordnance Laboratory
White Oak, Silver Spring, Maryland

INTENTIONALLY LEFT BLANK.

DESIGN AND INITIAL TESTS OF THE NOL SHOCK GUN

V. C. D. Dawson
U. S. Naval Ordnance Laboratory
White Oak, Silver Spring, Maryland

I. Early History of High Velocity Launchers

For the past ten years numerous scientific groups have been engaged in the development of high-speed launchers which can be used to propel missiles or models at speeds in excess of 10,000 fps. The basic principle of all high-speed gas guns can be demonstrated as follows:

1. The kinetic energy of the projectile is equal to the work done by the propellant gases during bore travel.

$$\frac{MV_m^2}{2} = \bar{p}AL$$

where M = mass of projectile

V_m = muzzle velocity

$\bar{p}$ = average pressure of the propellant gases over the length of travel

A = bore area

L = length of travel

For a fixed gun system with a given barrel length, bore area and missile weight, the velocity can only be increased by increasing the average pressure exerted by the propellant.

2. The equation for the base of projectile pressure in the case of a gun having a preburned propellant is*

$$p = p_o \left\{ 1 - \frac{V}{\frac{2}{\gamma-1} a_o} \right\}^{\frac{2\gamma}{\gamma-1}}$$

where p = base of projectile pressure

p_o = initial chamber pressure

V = velocity at any point in the bore

a_o = sound speed of the gas in the chamber initially, that is, at pressure p_o, temperature T_o

γ = specific heat ratio

This equation shows that if a_o is infinite the base of projectile pressure is always p_o and the maximum possible velocity is thereby obtained. The average base of projectile pressure is greater the higher the initial sound speed of the propellant gas. Therefore the muzzle velocity can be increased by employing a gas with a high sound speed. Since the sound

---

*This equation applies to the case where no chambrage exists; that is, the chamber of the gun has the same diameter as the bore. When the chamber diameter is larger than the bore, there will be a chambrage correction but the over-all effect of propellant sound speed is still the same.

speed is proportional to the square root of the temperature and inversely proportional to the square root of the molecular weight, a gas having a high initial temperature and/or a low molecular weight should be used as a propellant.

In general there have been two lines of experimental endeavor to obtain a low molecular weight, high temperature gas. The first method is to use a low molecular weight gas such as hydrogen or helium which is adiabatically compressed and heated by the single stroke of a piston. This system was originally developed by the New Mexico School of Mines and has since been modified and improved by the Ames Aeronautical Laboratory of NACA, Moffett Field, California, Ballistic Research Laboratories of Aberdeen Proving Ground, Maryland, and the Naval Research Laboratory of Washington, D. C. A 0.50-caliber hydrogen gun, 200 calibers in length, has fired a 1.25-gm missile at speeds up to 15,000 fps.

The second method that is employed is to use chemical energy to heat helium without having the chemical reaction products add too much to the molecular weight of the gas. This method was developed at the Naval Ordnance Laboratory where firings were initially made in a 0.50-caliber gun, 100 calibers in length, using a mixture of helium, hydrogen,

[redacted]

and oxygen; the hydrogen-oxygen reaction being used to supply the chemical energy. The 0.50-caliber tests indicated that a 1.25-gm missile could be fired at speeds up to 12,000 fps. On the basis of these experiments a 40-mm gun, 100 calibers in length, was designed, tested, and put in operation. This gun has propelled a 40-gm missile at 12,000 fps.

Each of the methods described above has advantages and disadvantages. In general, the hydrogen gun can fire a missile at a higher velocity than the NOL Gun but the compression ratios necessary to do so make the chamber size appear impractically large for a gun larger than 20 mm. It is for this reason that the Naval Ordnance Laboratory has adopted the helium-hydrogen-oxygen system since scaling is not difficult. At the present time, a 4" gun is in the design stage for use in a 1000-foot pressurized hyperballistics range.

II. Shock Gun Principle

The shock gun scheme has been conceived at the Naval Ordnance Laboratory* as a method of providing a gas with

---

*NAVORD Report 4345, "A Hypervelocity Gun Using a Shock-Compressed Steam-Heated Propellant", by A. E. Seigel and Z. I. Slawsky, July 1956

[redacted]

[redacted]

a higher sound speed than is now possible. The basic principle involved is the use of the chemical reaction presently employed together with the advantages of heating by compression. As such, it is, in a sense, a combination of the two methods previously described except that compression is produced by a shockwave rather than a piston.

Figure 1 represents a schematic diagram of the Shock Gun. It consists of a barrel and two propellant chambers, the forward one being called the gun chamber and the rear one the shock chamber. The gun chamber is closed at the forward end by a diaphragm and the two chambers are sealed from one another by a second diaphragm. These diaphragms are so constructed that at a given pressure they fold radially from the center with no parts of the diaphragm being propelled by the gas.

The conceived method of operation is as follows: the gun chamber is loaded with a standard mixture of 8 parts helium, 3 parts hydrogen and 1 part oxygen to an initial pressure of 850 psi. The shock chamber is loaded with the same mixture to an initial pressure of 7500 psi. The gun chamber mixture is then ignited raising the pressure to 7500 psi and the temperature to 2700°K. The sound speed will be about 7000 fps. Since the diaphragms are designed

[redacted]

to withstand higher pressures than this, the gun chamber is essentially in a hangfire condition. After a delay of a few milliseconds during which the gun chamber reaction is occurring the shock chamber mixture is ignited raising the pressure to 45,000 psi and the temperature to 2700°K. This pressure is sufficient to rupture the chamber diaphragm. In so doing a shock S_1, as shown in Figure 1.D, is propagated in the gun chamber by the rapidly expanding gases of the shock chamber. This raises the pressure and temperature of the gas in the gun chamber. At the forward end of the gun chamber, the shock is reflected thereby further raising the temperature and pressure of the gun chamber gas. At this final pressure the forward diaphragm opens and the missile is propelled by the gas at the forward end of the gun chamber. Under the conditions assumed, namely, 45,000 psi in the shock chamber, 7500 psi in the gun chamber and complete shock reflection, this gas will have a final pressure of 55,000 psi and a sound speed of 10,000 fps. Such a gas can propel a 1.25-gm missile at velocities of 15,000 to 16,000 fps in a 0.50-caliber gun, 100 calibers long.

You will note that a compression ratio of 6 has been assumed in these calculations. This brings up the question of scaling. It is believed possible to design a 40-mm shock

gun having a barrel 200 calibers long with an over-all gun length of no more than 40 to 50 feet. Such a gun would fire a 40-gm missile at 16,000 fps.

III. Construction and Instrumentation of the Experimental Shock Gun

Figure 2 indicates the gun that was constructed to test the theoretical results. An existing 0.50-caliber gun was attached to an adapter to provide the gun shown. It consists of a 0.50-caliber barrel, 60 inches long; a 1.2-inch gun chamber, 26 inches long, and a 2.75-inch shock chamber, 12 inches long. The gun chamber is ignited by a standard type primer which is located 2 inches from the rear of the chamber and fires radially through the side wall of the adapter. The shock chamber is ignited using two or three primers firing longitudinally in the chamber. The firing system is so arranged that the gun chamber is ignited first and then after a fixed delay, which can be varied shot to shot from 0.1 to 10 milliseconds, the shock chamber is actuated.

Pressures are recorded using piston type strain gages, one of which is located in the gun chamber at the same position as the primer but rotated 90° from it; the other of which is located in the shock chamber about 4 inches from the forward shoulder.

Velocity is recorded using a break-screen chronograph system.

A standard 40-mm blowout disc is used to seal the two chambers from one another. This is shown in Figure 3. The disc on the left indicates the appearance before firing. It consists of a dished metal surface that has been grooved. At a pressure of about 12,000 to 15,000 psi the metal tears along the grooves forming four leaves that bend radially to the sides. The other two pictures show discs that have been fired, one in the 40-mm gun, the other under air pressure to measure the release pressure.

The gun chamber is sealed at the forward end using a shear or swage type of projectile.

IV. Experimental Results

In the 40-mm tests optimum performance was obtained with a mixture consisting of 8 parts helium, 3 parts hydrogen, and 1 part oxygen. This same mixture was therefore used in both chambers of the Shock Gun, the gun chamber being loaded to an initial pressure of 850 psi and the shock chamber to 8000 psi.

The first six shots gave velocities somewhat better than the 40-mm velocities. These tests indicated that the shock process was working but not as well as expected since the velocities were lower than the theory predicted.

These tests were hampered by instrumentation difficulties. The pressure gages used were too insensitive to show that the process was occurring as the theory predicted and it was impossible to tell if the gun chamber reaction was taking place.

The pressure gage was therefore redesigned to give higher sensitivity in the low-pressure range and some hangfire tests were made to study the gun chamber reaction. It was discovered that the standard 8:3:1 mixture at low initial pressures was marginal as to ignition and reaction. Consequently it was decided to adjust the gun chamber mixture so that a final pressure of 7500 psi was obtained with a reaction rate as fast as possible in order to minimize the cooling effect. The reaction rate can be raised by decreasing the helium concentration. This causes an increase in molecular weight which is, however, partly compensated for by an increase in temperature. One danger in this is the increased possibility of a detonation. A detonation in the gun chamber with its associated high-peak pressures nullifies the shock gun effect since the blowout discs open prematurely.

Figure 4 indicates a typical pressure trace obtained with one of the hangfire mixtures. The two horizontal

lines at the top represent the calibration and the sine curve is the timing cycle, peak-to-peak value representing one millisecond. The lower lines are the pressure trace, the horizontal one being the base line and represents the initial loading pressure (in this case about 1000 psi).

Notice the wave form superimposed on the pressure curve. It was reasoned that due to the method of ignition, namely, radially through the side wall, essentially point ignition was obtained. Thus a burning wave is propagated through the gun chamber reflected at the forward end back to the pressure gage. By knowing the length of the chamber it is therefore possible to measure the sound speed of the reacting gas in the chamber. The hangfire tests showed that the sound speed varied from 5600 to 7000 fps depending upon the mixture proportions used. The theoretical calculations are based upon a sound speed of 7000 fps. This would in part explain why the experimental velocities were lower than the theoretical ones.

These tests also indicated that the mixture was extremely temperature and pressure sensitive at low initial densities of loading. In general, the higher the loading pressure and temperature, the greater the possibility of a detonation. Figure 5 indicates the type of reaction that occurs in a

detonation. Here a peak pressure of over 20,000 psi was obtained with an initial loading pressure of about 1200 psi. This same mixture burns in a normal manner at a pressure of 1100 psi or lower. Furthermore, since our loading system is subject to the influence of outside air temperature, it was found that the mixture would not detonate at 1200 psi in cold weather.

Since the initial full scale shots previously mentioned, only a few firings have been made. A velocity of 12,400 fps has been obtained with a 2.1-gm missile. This represents an increase of 1500 fps over the standard NOL Gun velocity with an equivalent missile weight. This velocity is about 1000 fps lower than the theoretical velocity.

V. Conclusion

We have definite quantitative and qualitative information that the shock process is working although not as well as expected. Quantitatively, we have obtained velocities higher than the standard gun provides. Also full scale (both chambers loaded) hangfire shots indicate that the pressures obtained agree with the shock equation predictions.

Qualitatively, the gun chamber is considerably hotter than we have experienced in standard gun firings. This is particularly noticeable from the erosion observed.

[redacted]

Steps are being taken to try to improve the gun chamber hangfire reaction. It is hoped that more complete experimental data will be available in the next few months.

[redacted]

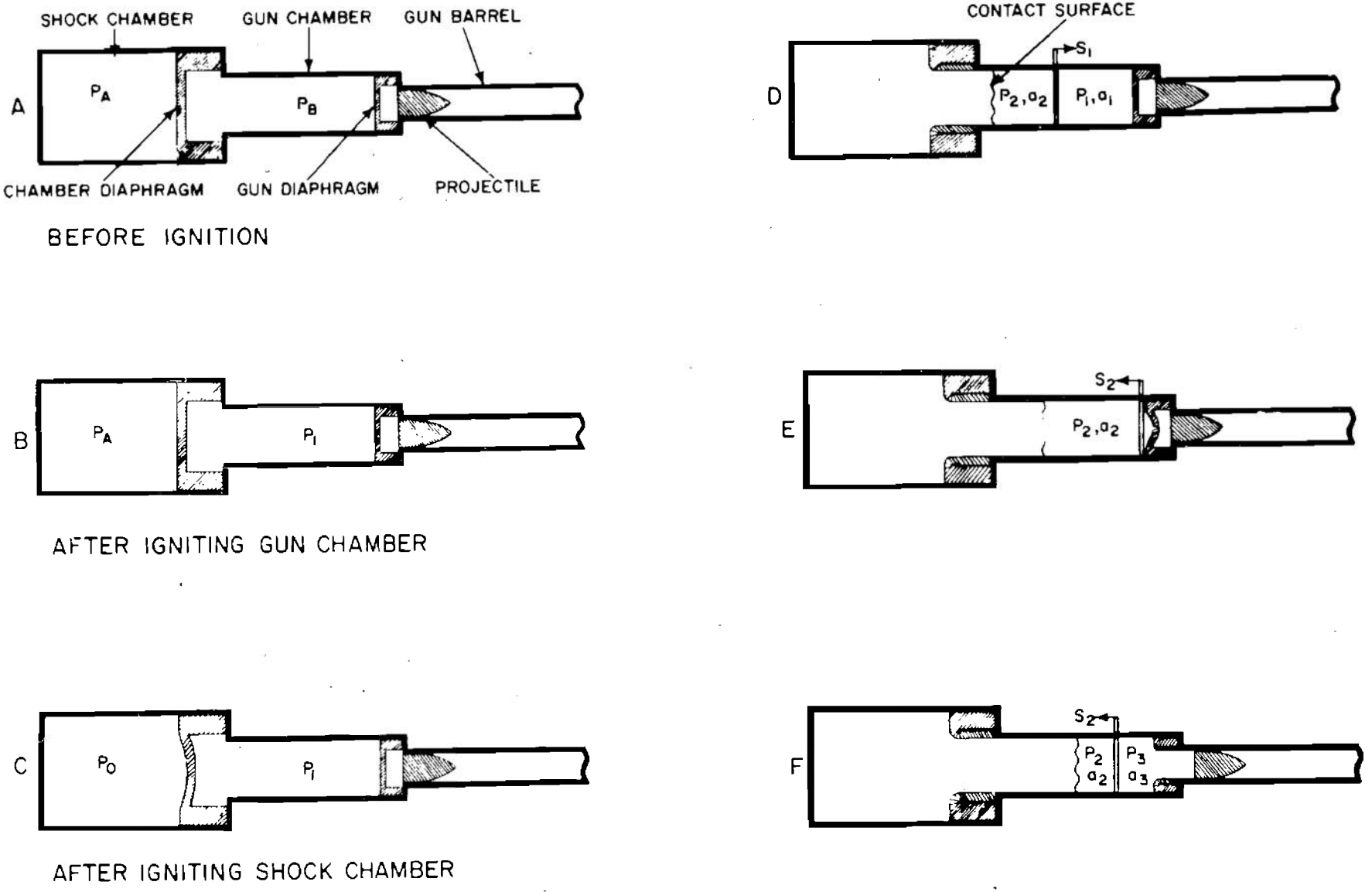

Fig. 1 Schematic diagram of shock gun operation

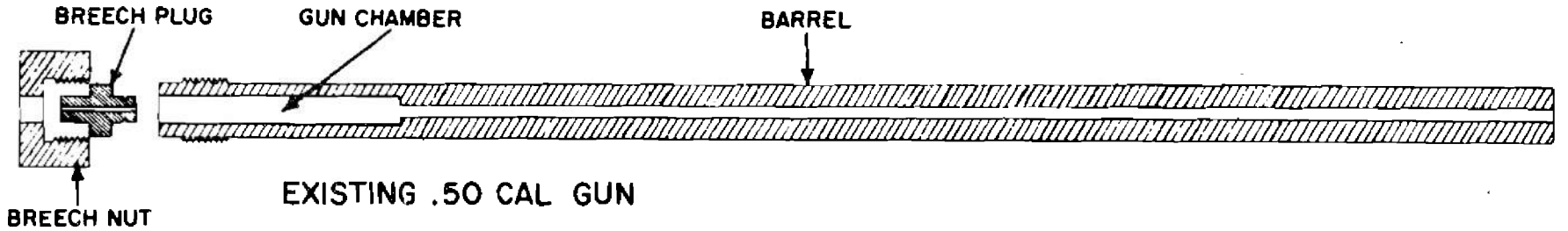

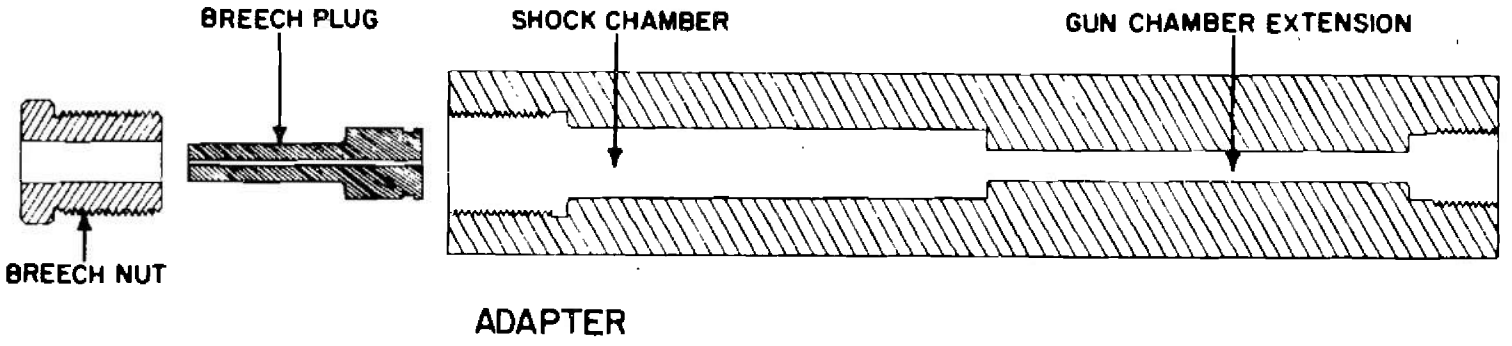

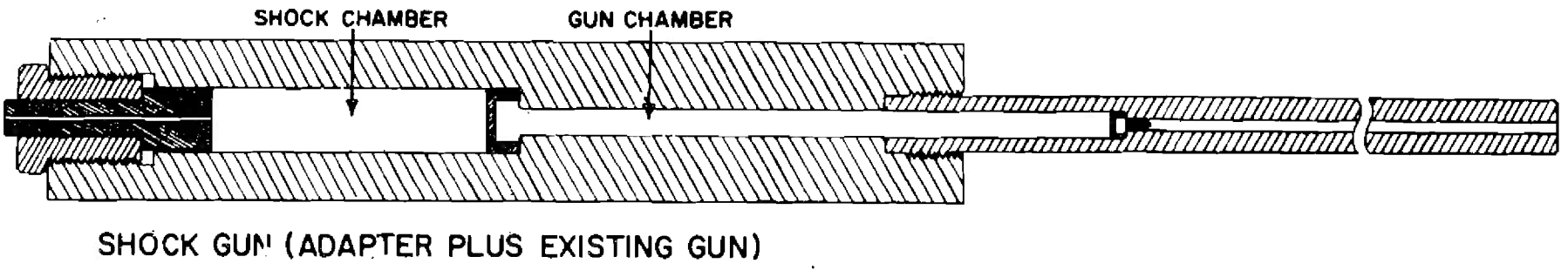

Fig. 2 0.50-caliber Shock Gun

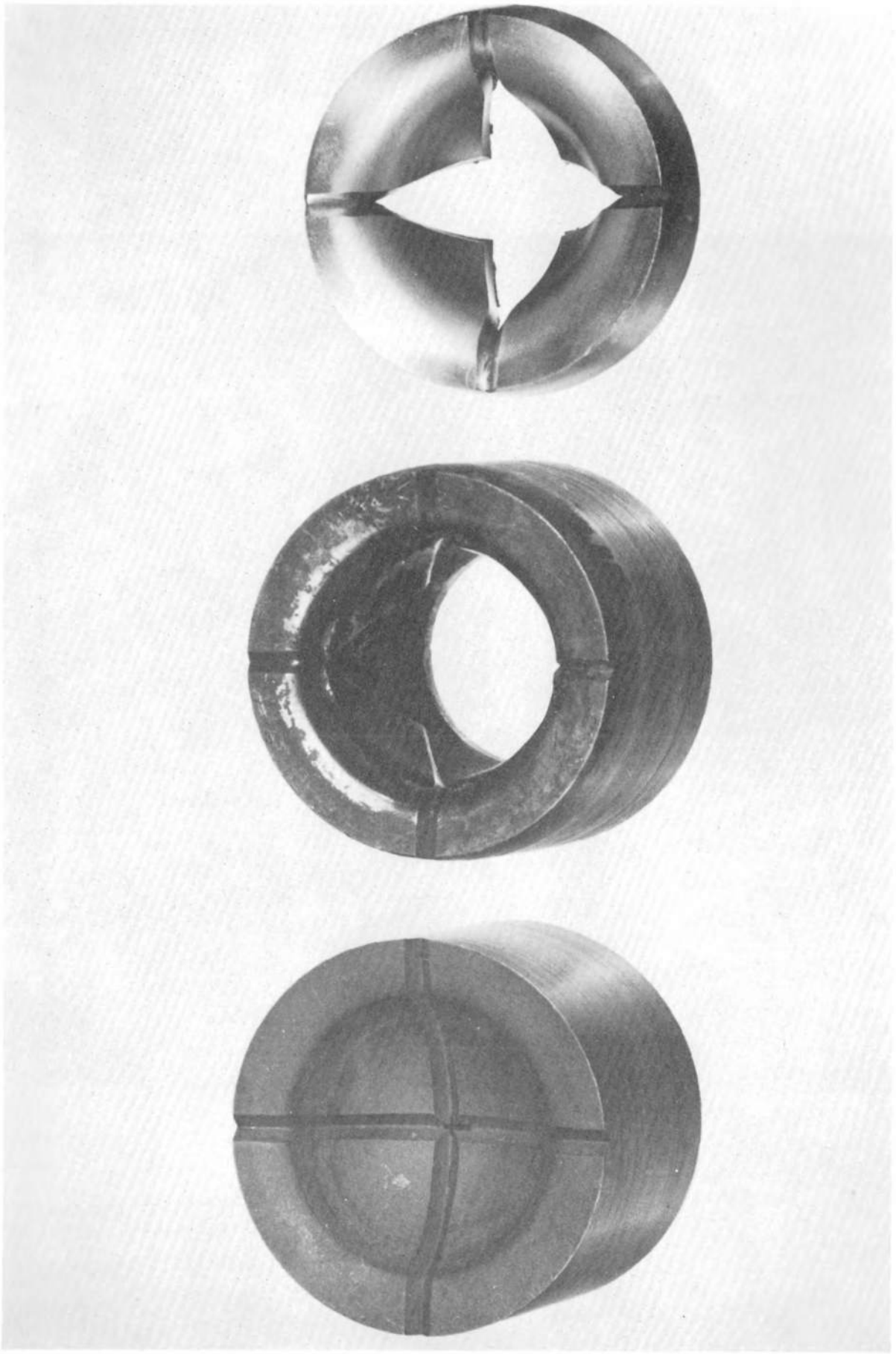

Fig. 3 40-mm blowout disc

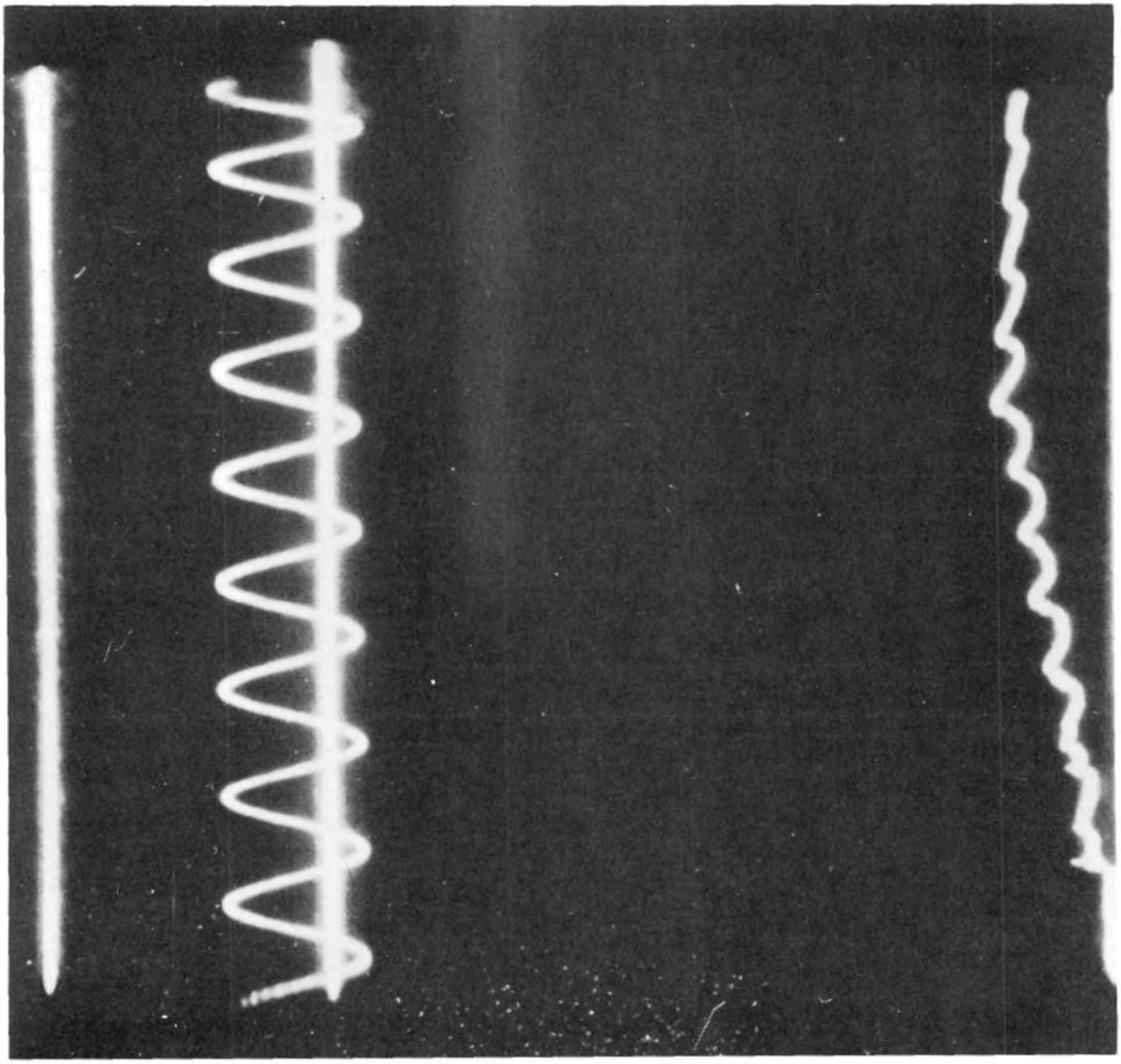

Fig. 4 Hangfire pressure trace (normal burning)

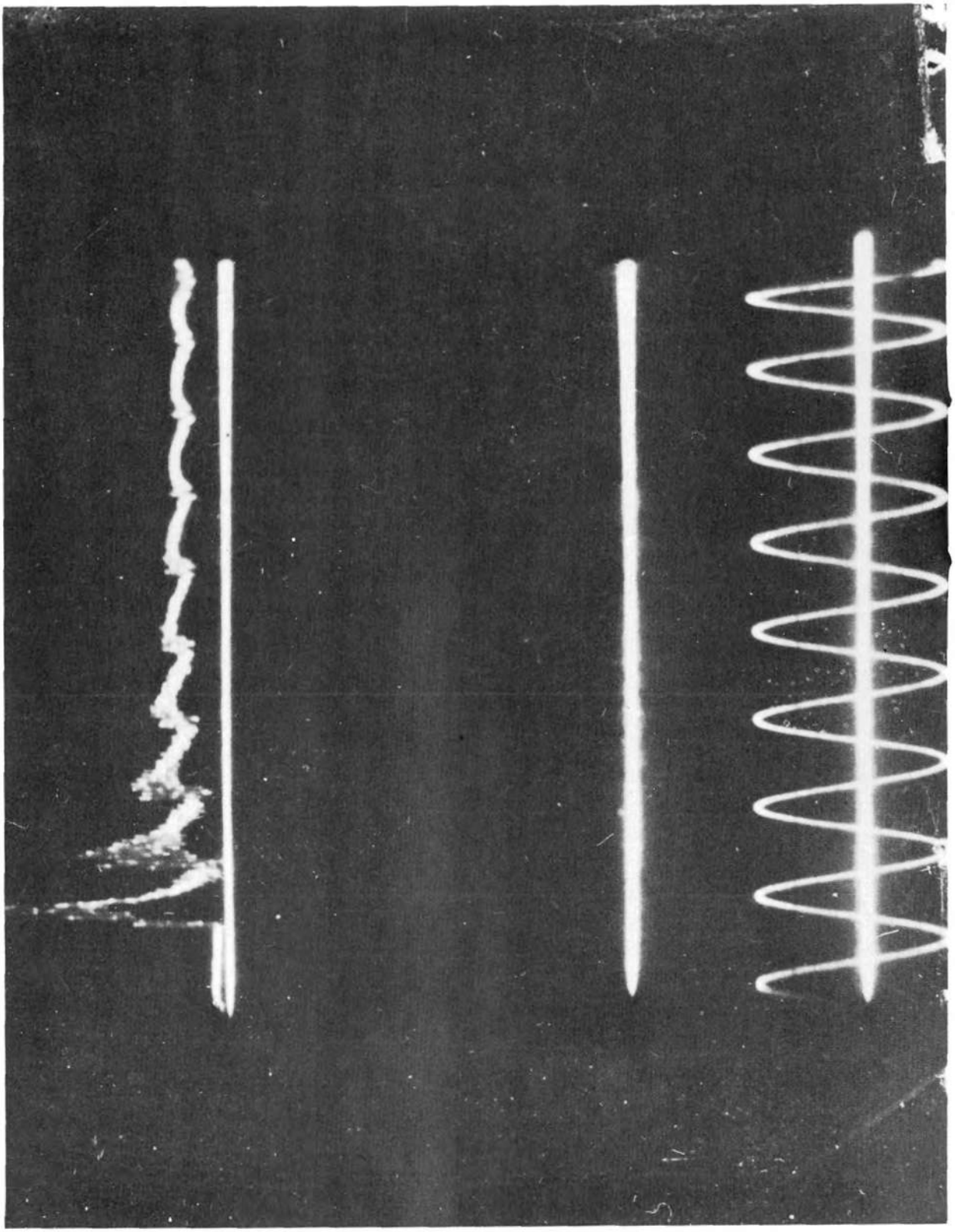

Fig. 5 Hangfire pressure trace (detonation)

INTENTIONALLY LEFT BLANK.

RESEARCH INVESTIGATIONS IN THE AMES SUPERSONIC FREE FLIGHT FACILITIES

Thomas N. Canning

National Advisory Committee for Aeronautics
Ames Aeronautical Laboratory
Moffett Field, California

INTENTIONALLY LEFT BLANK.

RESEARCH INVESTIGATIONS IN THE AMES SUPERSONIC FREE FLIGHT FACILITIES

by

Thomas N. Canning*

National Advisory Committee for Aeronautics
Ames Aeronautical Laboratory
Moffett Field, California

When early proposals for hypersonic wind tunnels were first considered at the Ames Laboratory, about 10 years ago, there was considerable uncertainty as to how high a Mach number could be realized with a conventional nozzle because of difficulties due to air condensation, variations in the nozzle throat height due to thermal expansion, and other difficulties. The shortcomings of conventional nozzles with respect to Reynolds numbers and temperature simulation were also evident. These considerations led Mr. H. J. Allen to propose, as a means for obtaining high test Mach numbers, that models be gun-launched upstream through the test section of a supersonic wind tunnel. The resulting facility, which has been described and discussed in NACA Rep. 1222 (ref. 1), is shown schematically in figure 1. The supersonic nozzle is at the left, and the model-launching gun is at the right. The wind-tunnel test section, in the center of the figure, is made relatively long and is instrumented with nine shadowgraph stations top and side. Thus, the facility may be viewed as a ballistic range operating within the test section of a supersonic wind tunnel.

The countercurrent air stream permits a large advance in test Mach number by adding the air velocity to that of the model; in addition, the air is cooled as it passes through the nozzle so that the speed of sound is greatly reduced. A muzzle velocity of 8600 feet per second, which is within the performance of guns used in this facility, gives a Mach number

*Aeronautical Research Engineer.

of 16 when the Mach number 3 nozzle is used. More completely, the Mach number - Reynolds number scope of the wind tunnel is summarized in figure 2. The upper speed limit for each region of operation is taken to be a muzzle-velocity limit of 8600 feet per second. The upper pressure limit is taken as the safe limit of the air supply. It is apparent that this facility provides test conditions covering a broad range of Mach numbers and Reynolds numbers, and perhaps most noteworthy is the fact that the maximum Reynolds number per inch obtainable increases with Mach number as is characteristic of ranges in general. For purposes of estimating total length, Reynolds number, it should be added that the models are usually from 3 to 6 inches long.

The disadvantages of the facility lie in its short length and small number of stations. In the case of drag measurement the short length is not too serious a limitation even though the models do not decelerate much in the test section. It is necessary, however, to measure distances within a few thousandths of an inch and times, to the order of a few hundredths of a microsecond. To attain this accuracy in time measurement, an instrument called the Ames circular-sweep interpolating oscilloscope has been developed. The scope display is shown in figure 3. In operation the electron beam of the tube is swept, in a circle about the tube axis, as the name implies, with a period of 2.5 microseconds. The intensity of the beam is too low to produce a visible image in the photograph except for a brief time while a spark fires. When the spark at station 1 fires, the beam is intensified by an electrical signal picked up at the spark and a line is produced as shown in figure 3. A few microseconds later the size of the sweep circle is reduced. The beam continues to rotate and after about 40 revolutions the next station fires and produces a second line. After all stations have produced lines on the scope a circle is automatically produced to locate the center of rotation. Electronic chronographs are used to count the number of complete revolutions of the electron beam in each interval, and the angular displacement between the leading edges of any two lines is used to determine the fraction of a revolution. This scheme gives an accuracy of about two

hundredths of a microsecond.

The main difficulty encountered with this facility is in the analysis of complex motions using only nine closely spaced stations. Even such a simple motion as sinusoidal pitching requires a minimum of four stations with no redundancy. Where additional degrees of freedom and nonlinear aerodynamic functions are considered the problems of data reduction can become formidable, and the accuracy of results suffers.

Perhaps the best means of illustrating the capabilities of this equipment is to show some photographs and shadowgraphs made during tests in the past. To assess the capabilities of range-type facilities for investigating the characteristics of airplane configurations we have tested several airplane-like models one of which is shown in figure 4. This model is about 4 inches long and was used to study discrepancies between results from a slotted-throat transonic wind tunnel and a large-scale free-flight test. Figure 5 shows a 6 inch-long model which is being tested to study techniques for obtaining static and dynamic derivatives. In these tests, the models are not roll stabilized and the motions can be quite complex. Thus far, reliable measured values of damping in pitch and yaw have been obtained only with models which did not roll too much in the length of the range. The complete motion of the model in the previous figure during one such test is shown in figure 6. A small, varying, rolling moment due to sideslip is shown to be present by the roll history. The rolling velocity was, however, small enough that the yaw and pitch planes remained essentially uncoupled, and the pitching and yawing motions were analyzed separately to obtain the data. The data for models which rolled significantly are being studied on an analog computer at present using more complete equations of motion.

Still another airplane configuration which is being studied in the free-flight wind tunnel is shown in figure 7. This airplane is being tested because it promises to have good stability and excellent heat-transfer and performance characteristics at Mach numbers up to 6 (ref. 2).

A shadowgraph of this model flying at Mach 6 and a Reyndlds number, based on length, of about 10 million is shown in figure 8. The possibility of getting extensive or complete laminar flow on this airplane is being pursued. The projection from the fuselage base is used for angle-of-attack measurements.

Another field of research, one step more basic than the airplane tests, was the investigation of skin friction of turbulent boundary layers in this facility at Mach numbers up to 7. These tests are reported in reference 3. The basic model for these tests was a 2-inch-long cylindrical sleeve having a sharp leading edge flown axially as shown in figure 9. Tare models, of identical leading-edge geometry and one-fourth the length were used to measure the pressure drag. The difference in drag was primarily skin friction. Optical distortion due to large density gradients makes the leading edge of the model appear very thick in this picture. This distortion is always present in varying degrees in shadowgraphs, particularly in the case of blunt models which will be discussed subsequently. The results of the skin-friction tests are summarized in figure 10. The ratio of skin-friction coefficient measured to that for incompressible flow with zero heat transfer is plotted as a function of Mach number. It is seen that as the rate of heat transfer to the model increases, (T_w/T_1 decreases) the skin friction increases. This test is believed to have been the first to show the strong dependence of the skin friction of turbulent boundary layers on heat-transfer rate in the high-speed range. The results of several rocket firings by the PARD group at the NACA, Langley Laboratory have confirmed this trend, which was also present in the theory of Van Driest.

Since the early days of flight it has been important to know the characteristics of turbulent boundary layers. Now that relatively steady flight at Mach numbers above 4 and short-duration flights at Mach numbers above 15 are contemplated, it is important to know with some accuracy where transition from laminar to turbulent flow will occur. Some aircraft may not even survive, much less perform efficiently, if transition occurs too far forward. This problem of predicting or delaying boundary-layer transition has occupied many researchers. The range facilities represented

at this symposium have made more contributions to this field than could be adequately treated here.

It will perhaps be of interest to discuss in some detail the evidences of turbulence which may be used by the researcher to locate transition using shadowgraphs. A few results of tests at Ames will be mentioned below. Figure 11 shows several evidences of transition. First the eddies in turbulent flow produce images in the shadowgraph which are usually visible. In this figure the most easily seen eddies are in the wakes, but they may also be seen along the lower side of the lower model.

The transition to turbulent flow results in a rapid increase in the rate of boundary-layer thickening. If the point of transition is moving downstream along the surface the apparent rate of growth just downstream is accentuated because the turbulent region has been growing in thickness from the time it first became turbulent while the laminar layer just ahead has been growing at the lower rate characteristic of laminar flow. This phemenon is called a burst of turbulence. These bursts frequently make themselves evident by producing weak, unsteady shock waves in the external flow; there are several such waves in the lower part of figure 11. Since the source of disturbance is moving downstream the angle of these waves is different from that of fixed disturbances.

A third evidence of the boundary-layer condition may be seen in the wake patterns of these models. If the flow leaving the base is fully laminar a clean line, which may extend for many boundary-layer thicknesses behind the base, may be seen as on the upper model of figure 11 as well as on the upper side of the other model in this figure. Where the boundary layer is turbulent, the mixing is more rapid and the line, if visible, is irregular and disappears quickly.

In some cases the boundary layer is so thin that no images of eddies are visible and the local flow is subsonic so that even bursts cannot produce shock waves. Such a situation exists on the face of the model in figure 12. In this case careful scrutiny of the original shadowgraph revealed a region where the edge of the model shadow appeared to be fuzzy. Tiny hairs

appeared to extend into the shadow in this region. This is taken to be evidence of turbulence since light passing through eddies is deflected erratically. In a few instances this hairiness has been detected where eddies were visible, but have never been noted where laminar flow was known to exist.

These evidences have been used to study transition on bodies ranging in fineness ratio from thirty to one quarter.

The first studies of this sort at Ames were for sharp nosed, high-fineness-ratio bodies of revolution, references 4 and 5, such as the one shown in figure 13. One of the most striking results from these studies is illustrated in figure 14. Here it may be seen that, even with fairly rough surfaces, long runs of laminar flow may be obtained provided the Mach number just outside the boundary layer is high enough. The tolerance to roughness increases rapidly as the Mach number is raised.

The most recent studies, reference 6, of transition have been made on low-fineness-ratio shapes for ICBM warheads. When these tests were first considered it was expected, at least by those doing the work, that it would be relatively easy to retain laminar flow up to the maximum Reynolds numbers attainable in this facility. It was felt, in particular, that a sphere should present no real difficulty, because of the favorable pressure gradients. In the early stages of these tests, rather discouraging results were obtained for configurations like the round-nosed, 60° included-angle cone in figure 15 and the hemisphere, figure 16. It now appears certain that these configurations will have early transition during the portion of flight where aerodynamic heating is severe. More recent tests by T. N. Canning and S. C. Sommer, as yet unreported, have indicated that shapes more nearly resembling right circular cylinders, figure 12 and 17, may be superior shapes for preserving laminar flow.

The capabilities of this equipment are being improved as time passes. Much emphasis at present is placed on increasing the Mach number range by use of better propellants than gun powder. The possibilities of getting data using other than photographic techniques are being pursued actively.

[redacted]

REFERENCES

1. Seiff, Alvin: The Ames Supersonic Free-Flight Wind Tunnel. NACA Rep. 1222, 1954.

2. Seiff, Alvin, and Allen H. Julian: Some Aspects of the Design of Hypersonic Boost-Glide Aircraft. NACA RM A55E26, 1955.

3. Sommer, Simon C., and Short, Barbara J.: Free-Flight Measurements of Skin Friction of Turbulent Boundary Layers With High Rates of Heat Transfer at High Supersonic Speeds. Jour. of the Inst. of the Aero. Sci., vol. 23, no. 6, June 1956.

4. Jedlicka, James R., Wilkins, Max E., and Seiff, Alvin: Experimental Determination of Boundary-Layer Transition on a Body of Revolution at M = 3.5. NACA TN 3342, 1954.

5. Carros, Robert J.: Effect of Mach Number on Boundary-Layer Transition in the Presence of Pressure Rise and Surface Roughness on Ogive-Cylinder Body With Cold Wall Conditions. NACA RM A56B15, 1956.

6. Seiff, Alvin, Sommer, Simon C., and Canning, Thomas N.: Some Experiments at High Supersonic Speeds on the Aerodynamic and Boundary-Layer Transition Characteristics of High-Drag Bodies of Revolution. NACA RM A56I05, 1957.

[redacted]

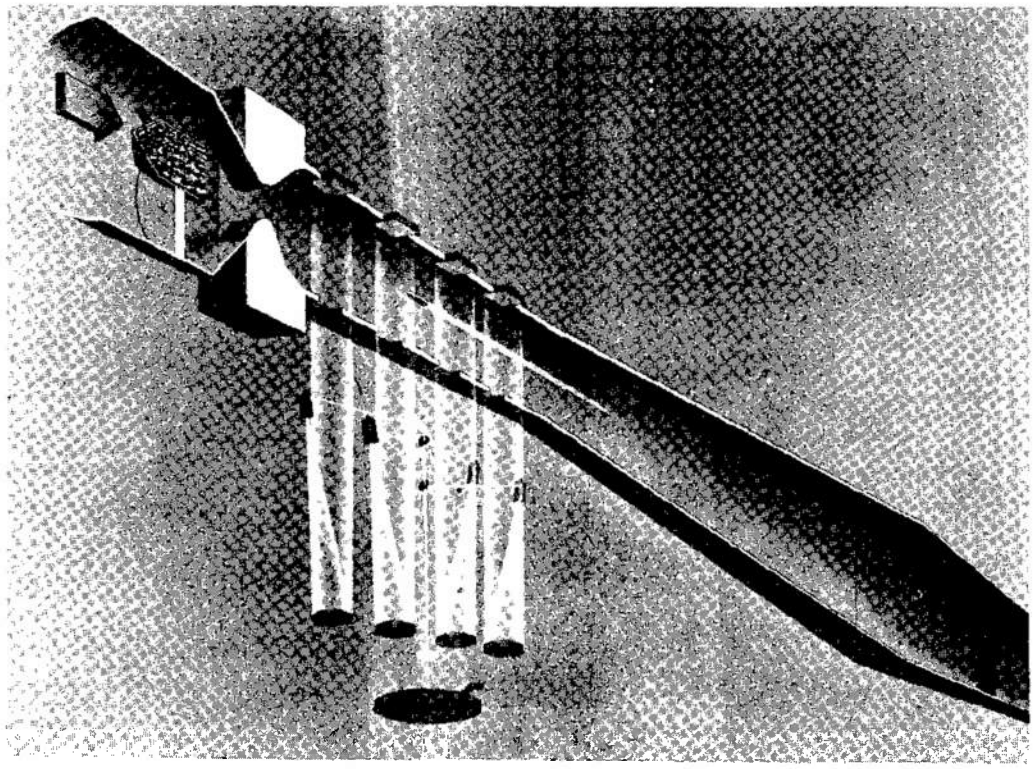

Figure 1.- Schematic diagram of Ames supersonic free-flight wind tunnel.

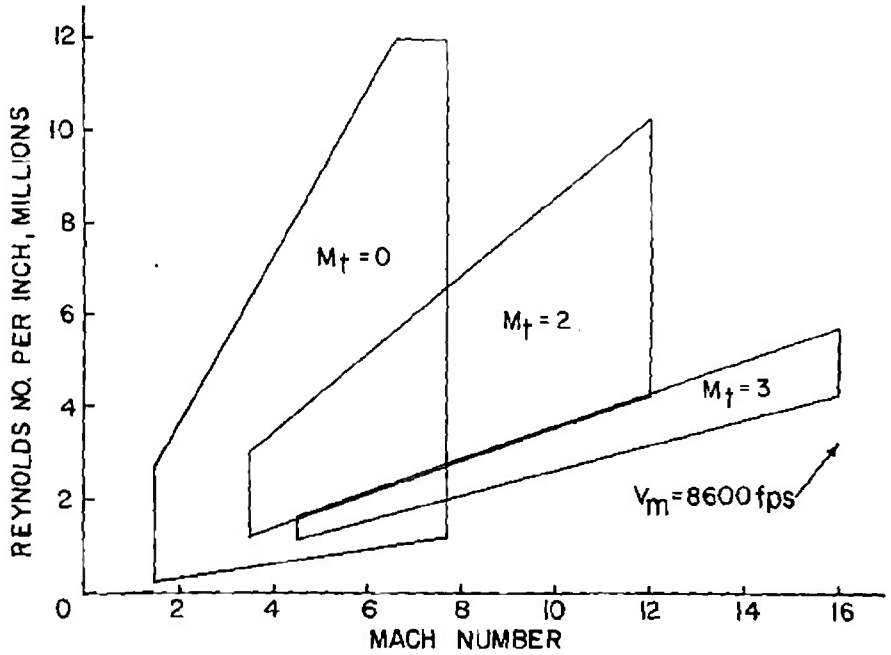

Figure 2.- Mach number - Reynolds number ranges for Ames supersonic free-flight wind tunnel.

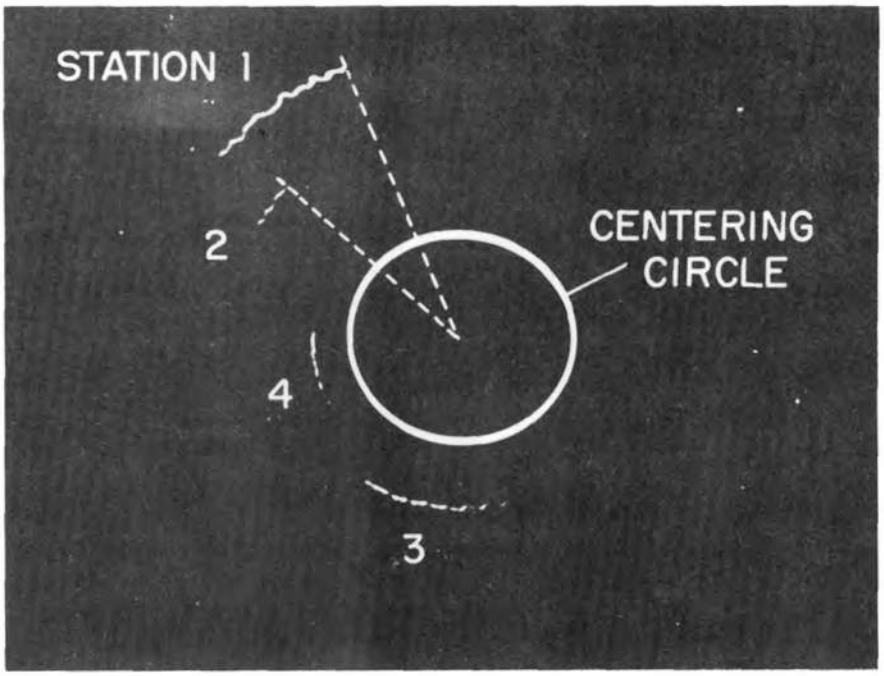

Figure 3.- Film from Ames circular-sweep interpolating oscilloscope.

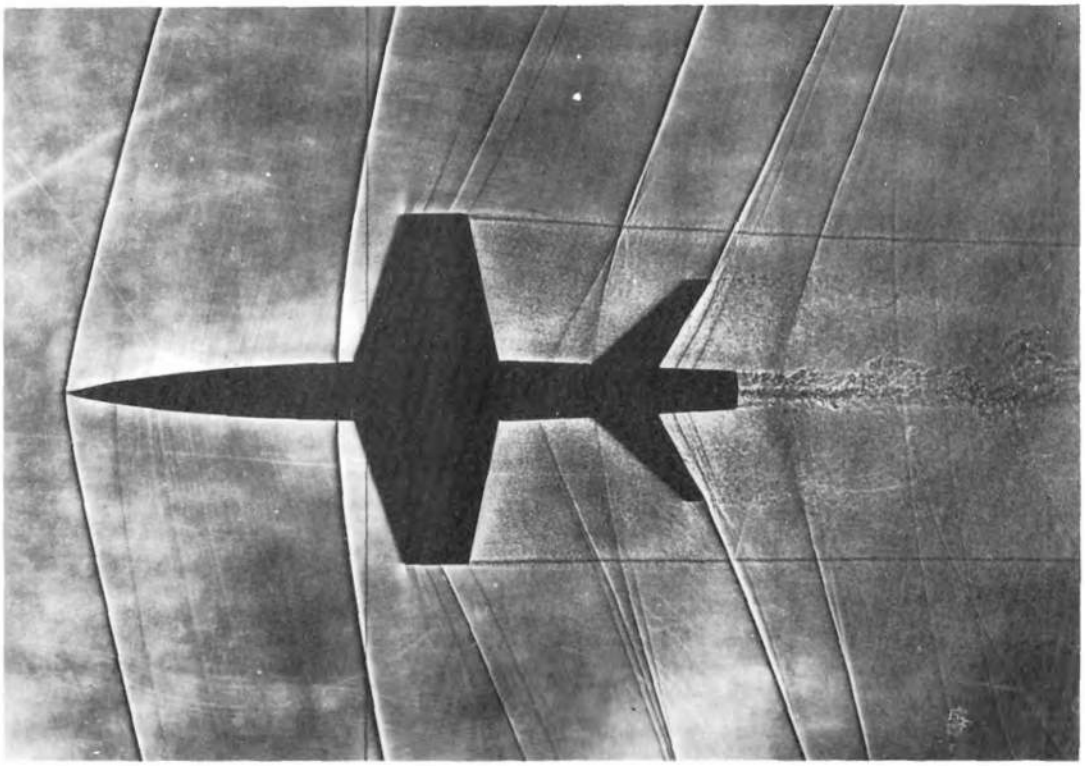

Figure 4. Transonic airplane model; M = 1.1.

TECHNICAL LIBRARY

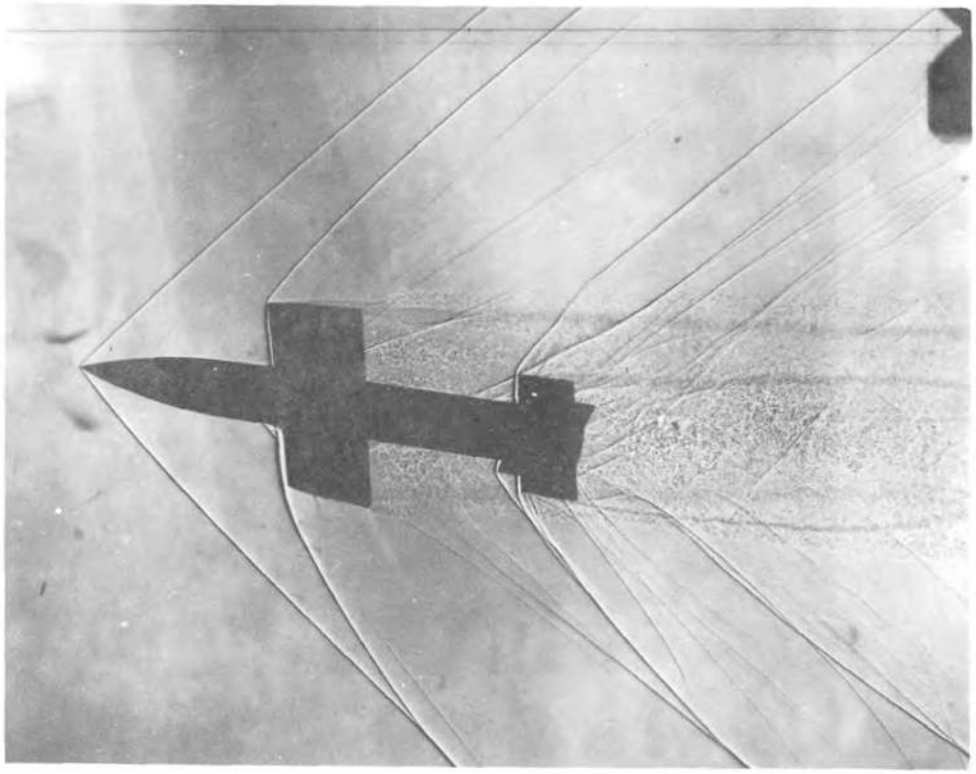

Figure 5.- Dynamic stability model; M = 1.3.

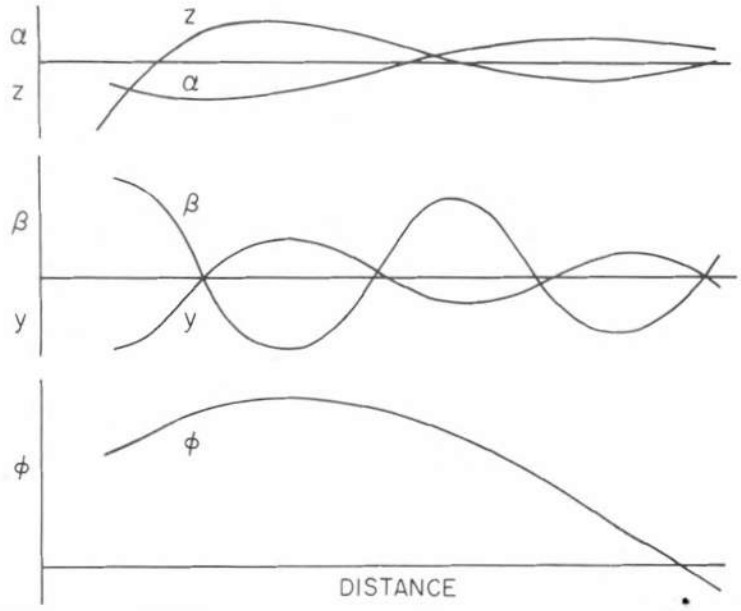

Figure 6.- Motion of an airplane model in free flight.

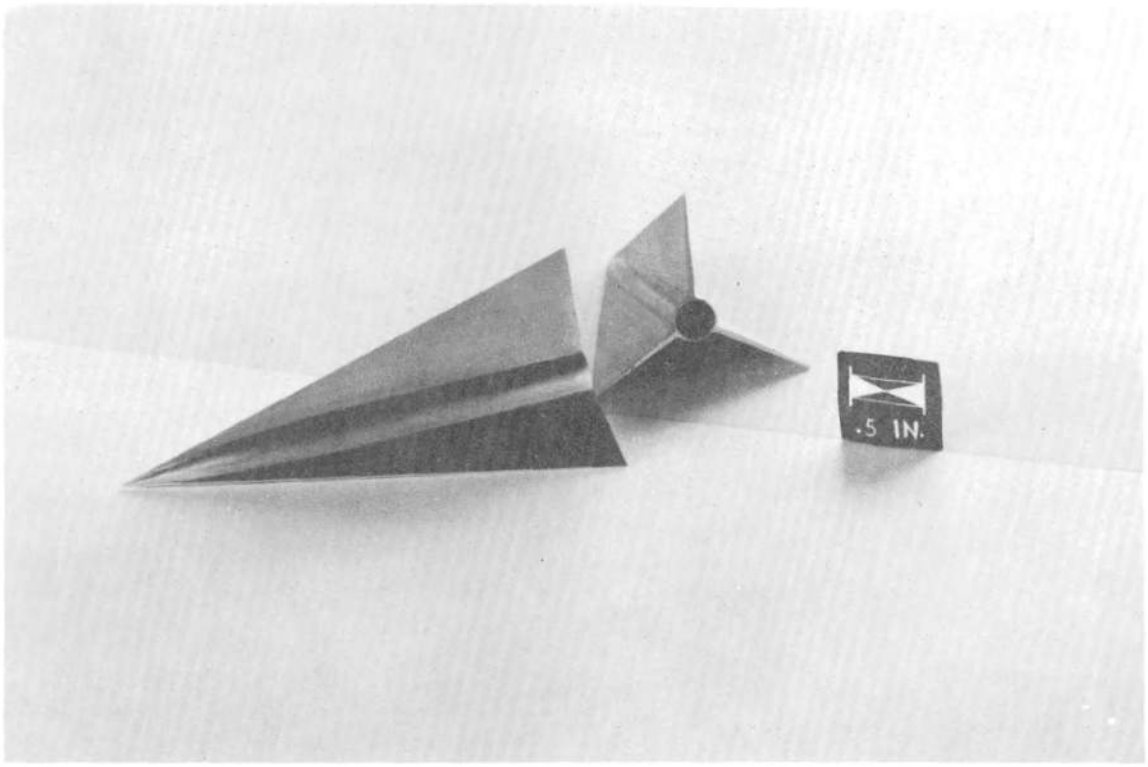

Figure 7.- Three-wing hypersonic airplane model.

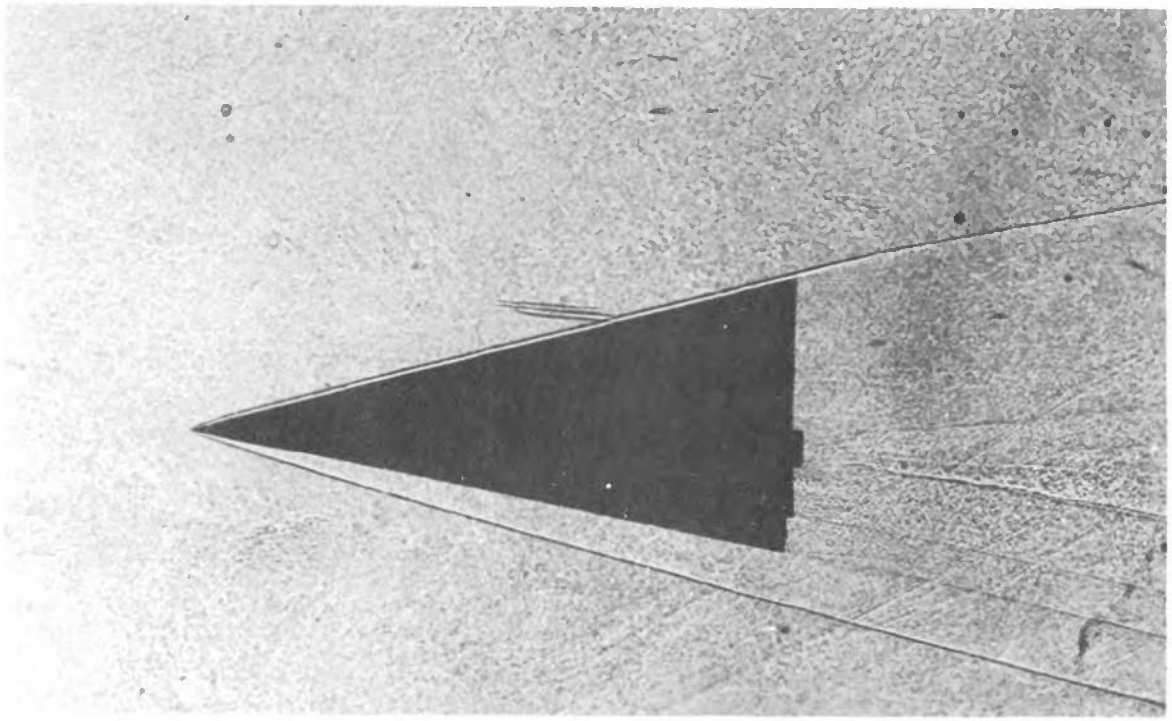

Figure 8.- Three-wing hypersonic airplane model; M = 6.

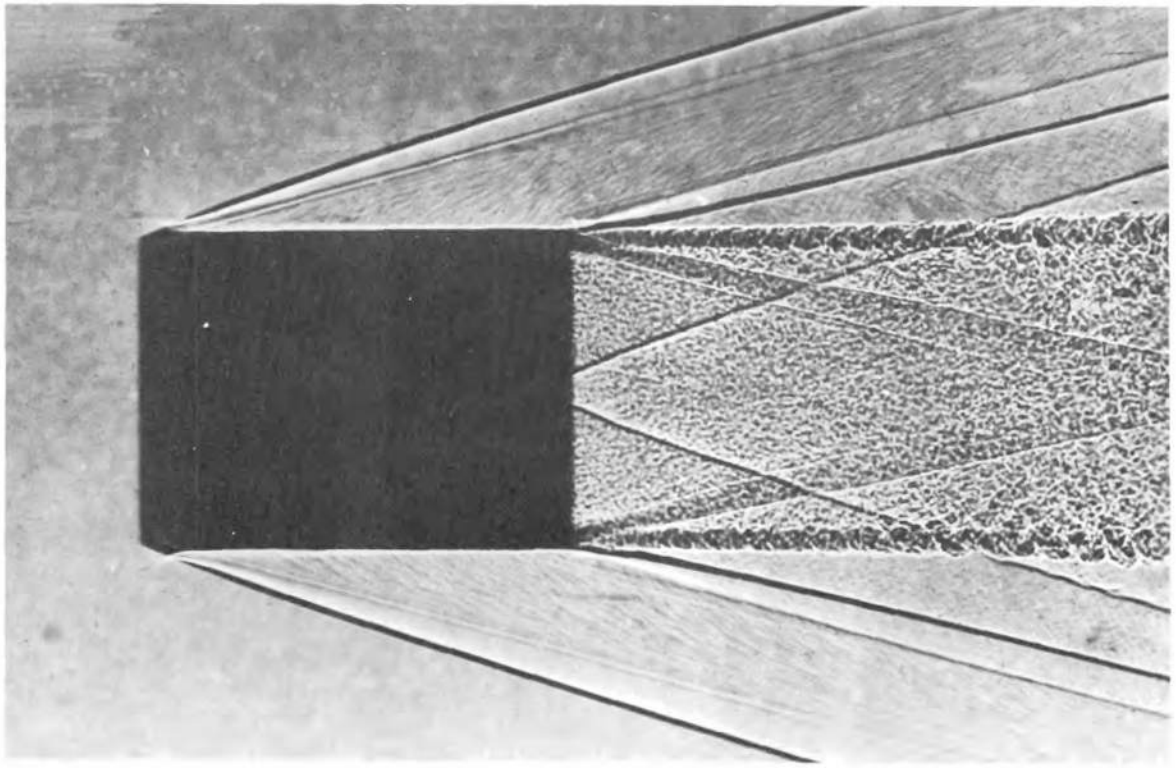

Figure 9.- Shadowgraph of test model with boundary-layer trip of 0.003-inch deep threads at M_o = 3.9.

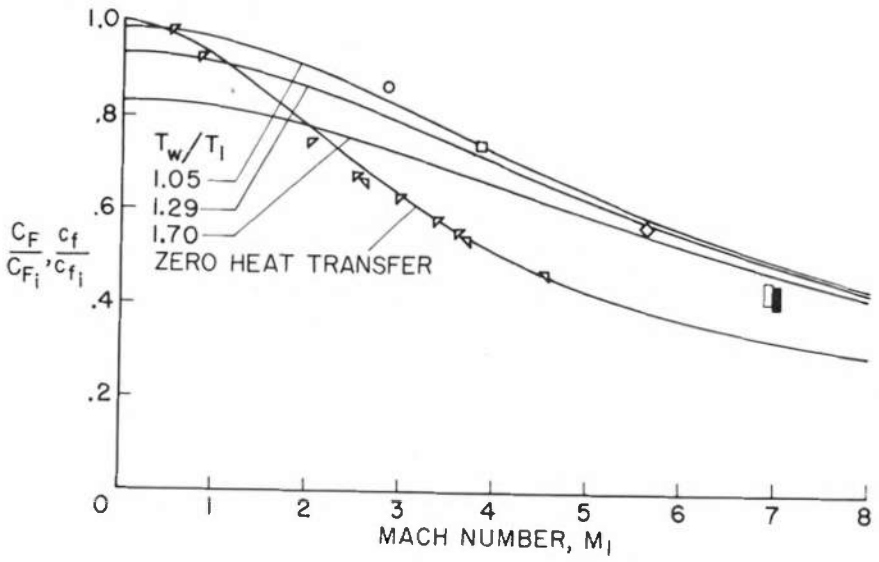

Figure 10.- Comparison of skin-friction ratio as determined by the use of the modified T' expression with experimental values.

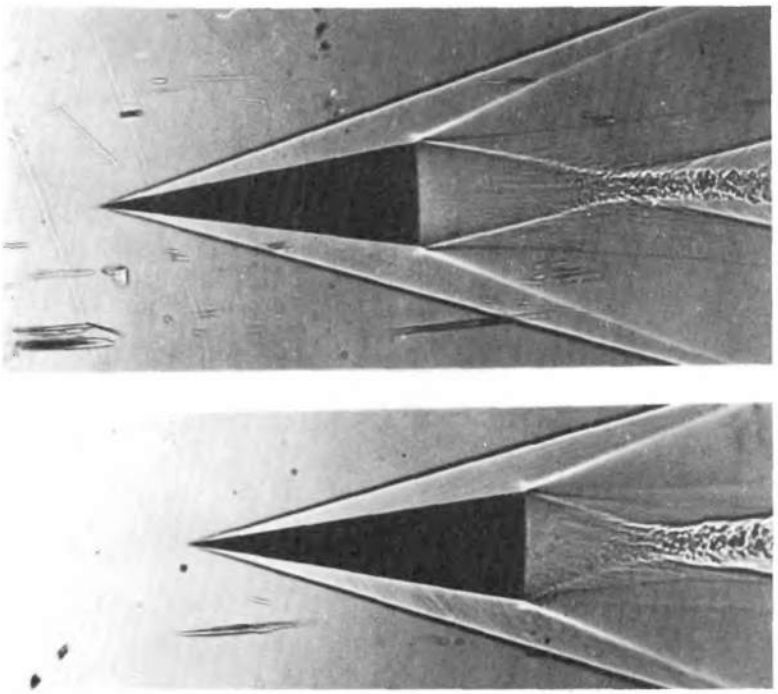

Figure 11.- Shadowgraph evidences of turbulence, eddies, bursts, and base-flow lines.

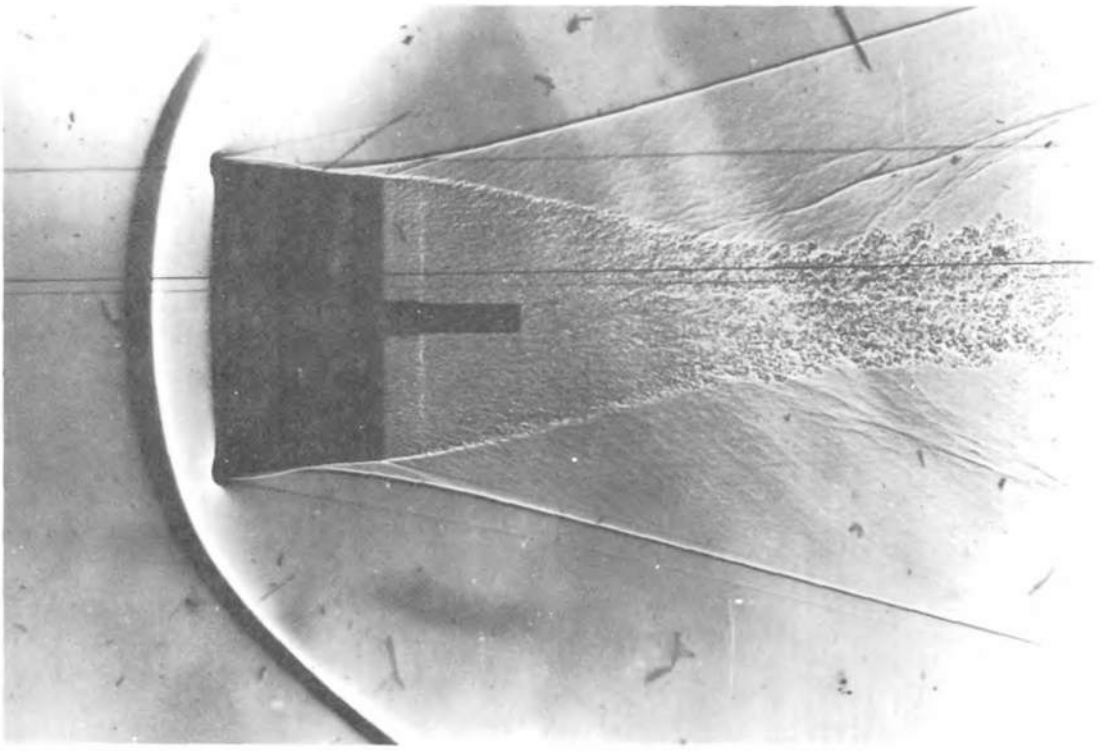

Figure 12.- Shadowgraph evidence of turbulence, "fuzzy" edge on face of model.

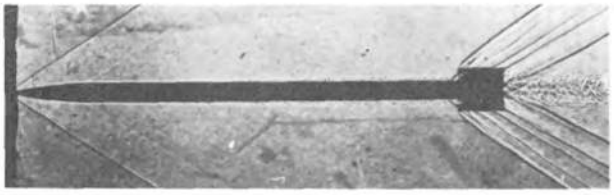

M=1.87, R_l =12.5x10^6

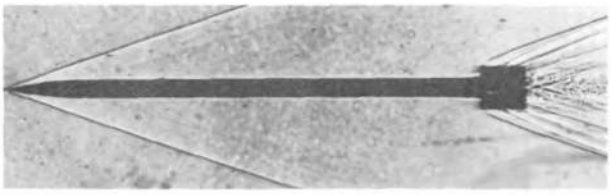

M=3.40, R_l =13.1x10^6

Figure 13.- Shadowgraphs of transition on a 0.0004-inch threaded surface.

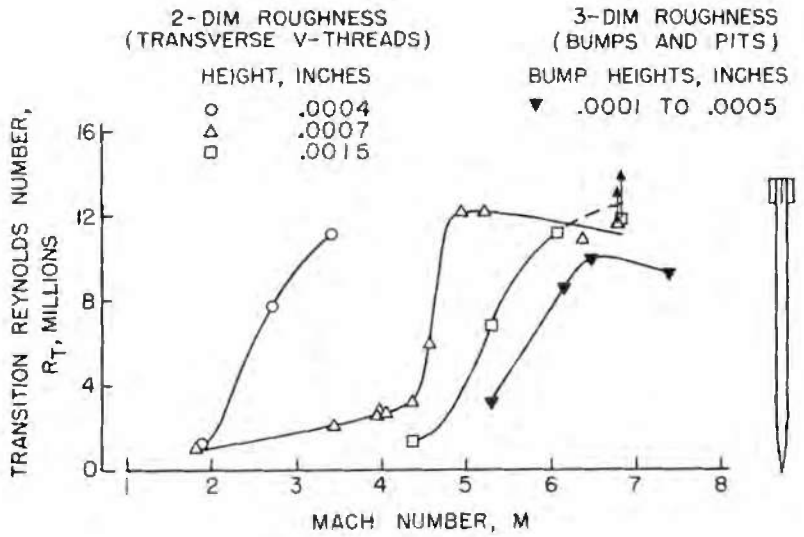

Figure 14.- Effect of Mach number on transition on a cold rough wall.

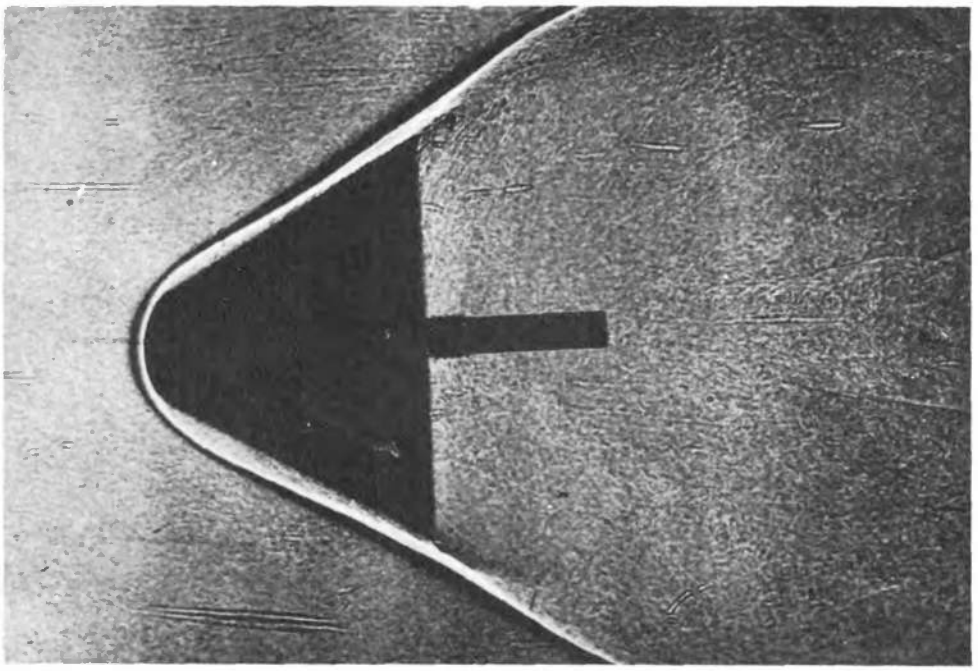

Figure 15.- Round-nosed 60° included-angle cone; M = 9.

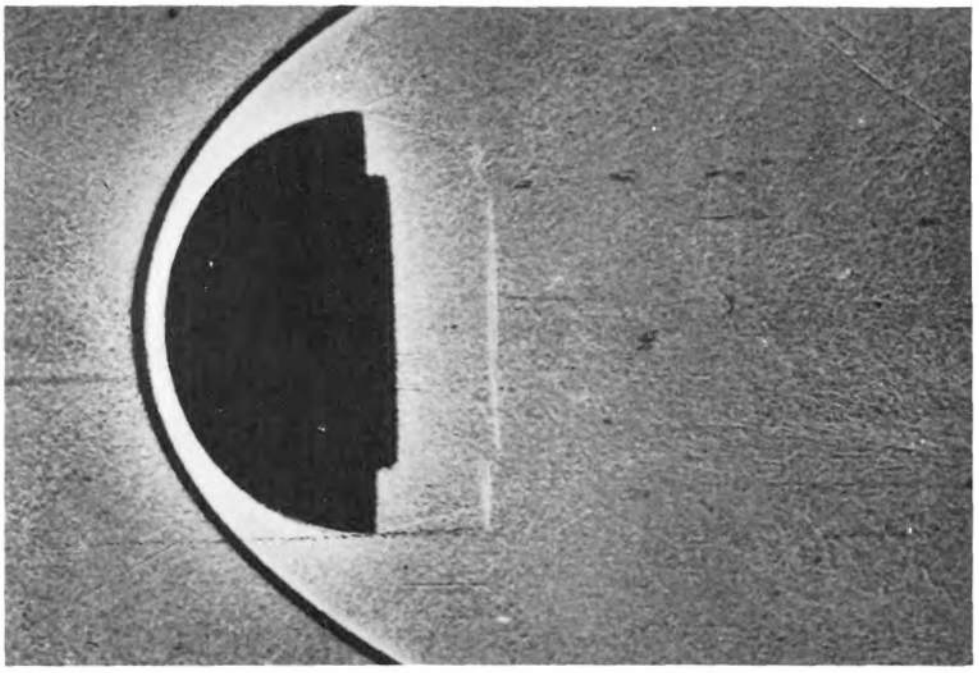

Figure 16.- Hemisphere; M = 9.

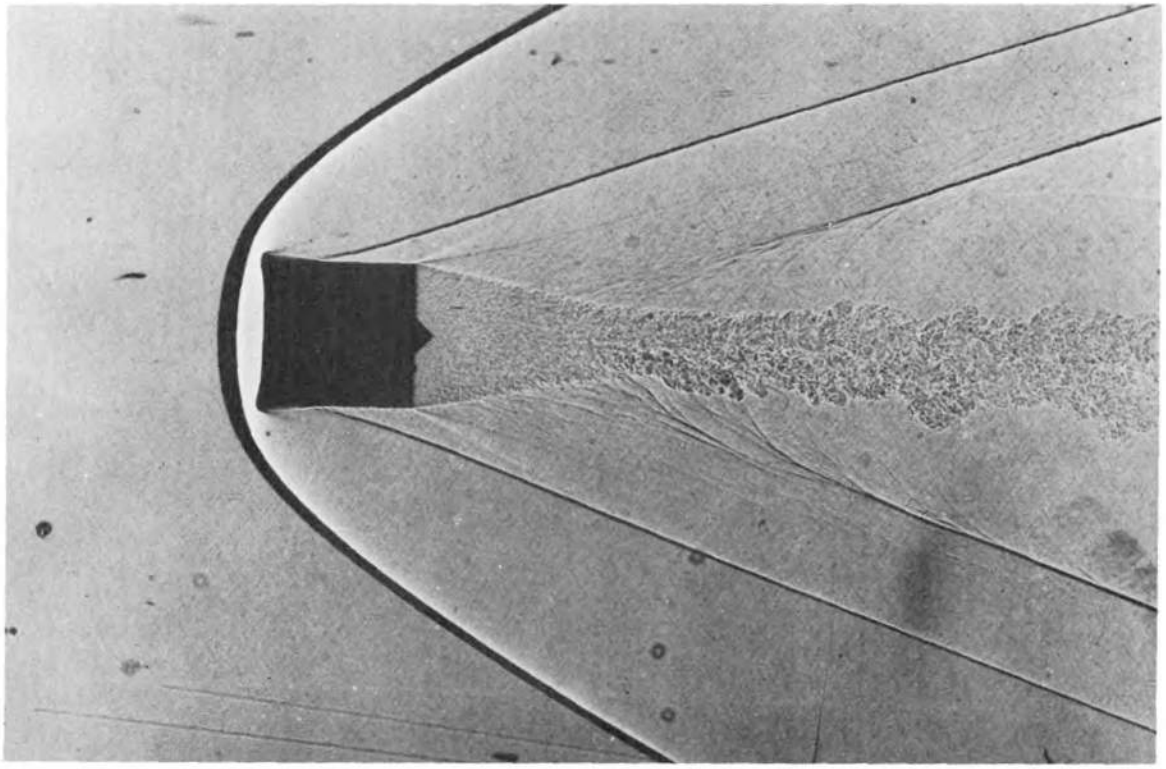

Figure 17.- Right circular cylinder; M = 4.

INTENTIONALLY LEFT BLANK.

AEROBALLISTICS RANGE MEASUREMENTS OF THE PERFORMANCE AND STABILITY OF A SUPERSONIC FIGHTER AIRCRAFT

H. R. Warren
The De Havilland Aircraft of Canada, Ltd.

R. J. Templin
National Aeronautical Establishment, Ottawa

B. Cheers
Canadian Armament Research and Development Establishment

INTENTIONALLY LEFT BLANK.

[redacted]

AEROBALLISTICS RANGE MEASUREMENTS OF THE PERFORMANCE AND STABILITY OF A SUPER-SONIC FIGHTER AIRCRAFT

1.0 INTRODUCTION

The technique of obtaining aerodynamic information from measurements of the cuts made in sheets of paper which have been punctured by a model in free flight has been used successfully at CARDE for several years for missiles and ballistic projectiles. The accuracy of the results obtained and the inherent simplicity of the method have led naturally to its use more recently with a wider variety of shapes. The work being done with delta wing tests has been described by Mr. Tidy in a previous paper.

In addition to these tests a number of successful firings have been made using small scale models of a supersonic delta wing aircraft and it is the purpose of this paper to give a report on the progress on this work. Although the program is not as yet complete, the results obtained so far are very encouraging and it is felt that a description of the work at its present state would be useful to others who may wish to carry out similar investigations.

A description of the method with particular reference to the differences encountered between missile tests and aircraft tests will be followed by a discussion of the type of results obtained and the methods of analysis which can be used on them, and before concluding, some of the limitations of the method will be discussed.

As a preface to details of the work however it would be in order to mention briefly the reasons for undertaking such a study.

[redacted]

The advantages of the aeroballistics range method include those of any free flight technique but with certain additional benefits. As long as the necessary measurements can be made externally, the elimination of the sting support used in the wind tunnel avoids the errors due to sting and support corrections. This is particularly important in the measurement of aircraft total drag. Tunnel wall corrections, which are difficult to allow for accurately especially in transonic wind tunnel tests are also eliminated. As the tests are done at sea level density with full scale Mach number, the Reynold's number is in general higher than with wind tunnel tests. For the CARDE tests the Reynolds number was 2.9 million.

The most obvious advantage of free flight tests is the ability to observe the complete three dimensional dynamic behaviour of the model with no more restrictions applied to it than those of the full scale aircraft, except that the controls are fixed. With the present trend in aircraft design to thin wings of large sweep back angles or of delta shape, there is an increasing need for knowledge of dynamic characteristics, particularly cross-coupling effects, at an early stage in design. It is because of this fact that the two main advantages of the range technique over other free flight methods are important. These are the simplicity of instrumentation and the small size and cheapness of the model itself. Because measurements are all made externally, the model carries no instrumentation, but requires only to be of the right shape and ballasted to a suitable centre of gravity position.

The basic instrumentation required in the range is no different to that used for missile and projectile testing and provides a much cheaper, more reliable and quicker means of obtaining dynamic information than by the use of airborne telemetry. This being the case, the type of test reported on here could be envisaged as forming a part of the preliminary testing on an aircraft design, complementary to the first wind-tunnel tests and at a sufficiently early stage in the aircraft's development that configurational changes specifically to improve the dynamic characteristics could still be made.

2.0 TEST METHODS & RESULTS

2.1 Description of Model & Test Methods

General views of the model used for these tests are shown in Figures 1 & 2. The model has a span of 5 inches, aspect ratio 2 and quarter chord sweep-back of 55°. An important factor in the feasibility of this type of testing is the accuracy and cheapness of manufacture of the models. In general the surface finish and accuracy of manufacture should be up to the standard of wind tunnel models, however with no method of recovering the models a large number of models may be required - depending on the scope of the test program. The body and wings of the CARDE models are machined from a single block of aluminum using a Deckel Pantograph Die-Sinker which scales the shape down from a master 1½ times the model size. Fin and rudder and ballast weights are added later. With this machine a surface finish of $\pm$ 0.002 can be maintained and the models can be produced at a rate of less than 100 man hours each, once the master and templates have been made. By way of comparison the typical cost of a wind tunnel model of similar scale is about $50,000, while for a large free flight model with full telemetry the cost could be as much as $120,000.

Models of the latter type would of course be able to supply a wider variety of information than could be obtained from the simple CARDE models. Alternative methods of investment castings using the lost wax process are also being considered although there is some doubt that tolerances on very thin wing sections could be maintained without some additional machining.

Also under consideration are methods of recovering the model. The relatively light damage sustained by the present models when they are fired into a sawdust butt suggests that with a large volume of liquid or some low density medium it would be possible to recover the model and fire it several times. Such a medium which is readily available in Canada is snow and it is hoped to use a snow butt on the next firing.

Prior to each shoot, model dimensions are measured very accurately for later use with yaw card measurements and the model's weight, centre of gravity position and principal moments and products of inertia are found. Centre of gravity location is found to the nearest 0.003 inch by using an accurate weigh scale, and moments of inertia are found by both torsion pendulum and compound pendulum methods.

The essential difference between firing an aircraft model and firing a missile in the aeroballistics range is that in the former case there is no trigonal symmetry, but the model is a complicated shape with merely mirror symmetry. This difference has its effect on the mounting of the model in its sabot, on the launch and flight of the model down the range and of course on the reading and analysis of the yaw cards. Considering these factors in turn, first the sabot design required some development because of the difficult problem of applying a large impulsive thrust load to the small irregular area at the base of the fuselage.

Some modifications to the base to increase the bearing area were made and the present sabot, shown in Figure 3, launches the model through a 12 inches escape hole at 40 ft. range with no difficulty. The clean separation of the petals is shown in Figure 4. This round was fired at BRL; the picture was taken using the smear technique with a Fastax camera.

The lack of symmetry makes it necessary to have some advance knowledge of the lift and pitching moment characteristics of the model in order that the controls can be preset to give a small trimmed lift coefficient. Otherwise, with too much lift on the wings, the model might diverge too far laterally before flying the full length of the range.

The method of measuring angles of incidence from the cuts made by the model in sheets of paper mounted at intervals down the range is fairly straightforward for missiles with fore and aft sets of cruciform wings. In the case of an aircraft however with only the one fin and wing surface protruding laterally to make a cut there were initially some doubts about the possibility of getting a card cut which could be read with sufficient accuracy. These doubts proved to be unfounded however when actual tests were made. In the case of the aircraft under test, the cut made by the jet intakes is clear enough that by measuring its relation to the position of the wing tip and fin tip cuts, the incidence angles α and β can be measured without difficulty to the nearest tenth of a degree. Figure 5 is a photograph taken of the actual hole made by the model in one of the yaw cards. For reference, a side elevation view of the model is shown above the cut.

It will be noted that the model is yawing to the left and is flying at a negative angle of attack, as indicated by the wing cut. Yaw angle is determined by measuring the distance the fin and rudder is displaced from being midway between the sides of the intake cut. Angle of attack is obtained by noting the height of the line joining the wing tips above a line drawn across the bottoms of the intakes. For $\alpha = 0$ this height is known from pre-flight measurements on the model, so the difference of the value measured on the card from the zero α value gives a direct indication of angle of attack. Roll angle is measured between the line joining the wing tips and the horizontal or vertical datum lines marked on the paper. As these datum lines can be surveyed in quite accurately, the lateral motion of the centre of gravity can be measured with equal accuracy.

One disturbing thing which will be noticed from this figure is the large area of paper which is missing from the centre. It appears that the intakes, which have quite sharp leading edges, are slicing out this piece of paper, but whether the intake subsequently swallows this paper or whether it is knocked aside around the outside of the model is not known yet. The photograph in Figure 6 was taken to try to answer this question. A break circuit of fine copper wire was used to trigger a microflash unit. As far as can be seen in this picture, the intakes are not picking up paper and carrying it with the model.

A total of 59 sheets of paper are used at present in the CARDE range, the first 39 at 5 foot intervals and the rest at 10 foot intervals. A general interior view of the range is shown in Figure 7, with the yaw cards themselves removed.

The wooden frames in the distance are to be replaced by the roller type shown in the middle distance. The latter incorporate a large roll of paper, facilitating rapid changing of the paper. By means of solenoid actuated pins, reference marks for the horizontal and vertical datum lines can be made in the paper quickly and accurately.

Velocity measurements are made by a system of light screens accurately surveyed in at 50 foot intervals and connected to Potter chronographs which measure the time of travel between light screens to the nearest microsec. The accuracy of this method of velocity measurement is approximately 0.3 ft/second in 1500 ft/sec. Drag values which are obtained by differencing the successive velocity readings are therefore subject to an error of about 2 per cent with the present light aluminum models.

2.2 Test Results

By suitable orientation of the model and sabot in the breech of the gun, the shadowgraph of the plan view of the model in Figure 8 was obtained. The amount of detail of shock wave and flow behaviour is equivalent to that obtainable with a wind tunnel schlieren system but with the advantage of showing the complete pattern with no interference from walls or stings. In Figure 9, showing the model's elevation, the fin and wing tip vortices, and build up of boundary layer along the fuselage can be seen.

Again with reference to the problem of yaw card interference at the model intakes, the shadowgraph pictures all show a flow pattern at the base of the model which indicates a clear passage of air through the ducts.

Furthermore a comparison of the shock wave pattern at the shock ramp and the lips of the intake with schlieren pictures taken during recent NACA tests of the same intake show a very close similarity suggesting that the intake and duct are functioning properly.

Plotted in Figure 10 versus distance down the range are the angles of incidence α and β in rolling co-ordinates, and the roll angle ϕ for a portion of the test record of a model with its centre of gravity at 8.7% MAC and flying at a supersonic Mach number. The points occur at the yaw card positions with intervals of 5 feet and at a sufficient frequency to give a good record of the shape of the β and ϕ curve. There is very little scatter of the points about these curves which is taken to be a further indication that the models are not unduly disturbed by their passage through the paper. Positive damping of all the records will be noted.

Figure 11 shows a similar plot for a model fired at the same Mach number but with the centre of gravity moved back to 19.2% MAC. The frequency of the oscillations in roll, pitch and yaw have decreased, while the damping has changed from positive to slightly negative.

3.0 ANALYSIS

3.1 Stability Derivatives

As seen from Figure 10 & 11 the models have a slow steady rate of roll on which is superimposed a dutch roll oscillation. The oscillation in yaw has the same frequency with a slight shift in phase and approximately the same rate of damping. The models also oscillated in pitch, but at a frequency substantially higher than that in dutch roll and with a much smaller amplitude.

Hence it can be concluded that no roll-pitch cross coupling occurred.

A second simplification is that in the records of the lateral co-ordinates of the model centre of gravity (which have not been included in the figures), there is no apparent ripple at the dutch roll frequency - although the method of measurement would have evidenced any such effect. Thus it may be assumed also that the model angle of yaw ψ is equal to $-\beta$ the sideslip angle. The implication of this assumption is that the aerodynamic side forces are negligible and therefore that in the equations of motion, the side force equation can be neglected, leaving only the two equations for yawing and rolling moments.

The method which has been used to deduce aerodynamic derivatives from these records is to subtract graphically the mean rate of roll from the total roll angle, leaving only the oscillations, and then to fit a damped sinusoidal oscillation to both roll and sideslip. Substituting these expressions into the equations of motion gives a set of algebraic equations from which several of the stability derivatives can be found.

The equations of motion, making use of the above simplifications are as follows:

$$\frac{d^2\phi}{dt^2} - \frac{I_{xz}}{I_x}\frac{d^2\psi}{dt^2} = \frac{\frac{1}{2}\rho V^2 Sb}{I_x}\left[C_{l_\beta}\beta + C_{l_p}\left(\frac{pb}{2V}\right) + C_{l_r}\left(\frac{rb}{2V}\right)\right] \cdot (1)$$

$$\frac{d^2\psi}{dt^2} - \frac{I_{xz}}{I_z}\frac{d^2\phi}{dt^2} = \frac{\frac{1}{2}\rho V^2 Sb}{I_z}\left[C_{n_\beta}\beta + C_{n_p}\left(\frac{pb}{2V}\right) + C_{n_r}\left(\frac{rb}{2V}\right)\right] \cdot (2)$$

On the basis of the character of the records a solution of the form shown below is assumed:

$$\psi = \psi_0 e^{-Kt} \sin \omega t \quad (3)$$

$$\phi = \phi_0 e^{-Kt} \sin (\omega t + \theta) \quad (4)$$

ωt is set equal to zero and alternatively equal to $\pi/2$ in equations (3) and (4) and in the corresponding equations for the first and second derivatives of ψ and ϕ . The two sets of values thus obtained are substituted into equations (1) and (2) resulting in four simple algebraic equations. When the appropriate values of amplitude ratio ϕ_o/ψ_o , frequency ω , damping factor K and phase angle ϵ are substituted into these four algebraic equations the only remaining unknowns are the six lateral stability derivatives C_{l_β} , C_{l_p}, C_{l_r} , C_{n_p} and C_{n_r} . With six unknowns in a set of four simultaneous equations we are thus faced with a choice of assuming two of the derivatives and solving for the remaining four. In our work it was considered preferrable to solve for C_{l_β} , C_{n_β} , and C_{l_p} as these three could most easily be verified from previous tests and of the remaining three it was decided to assume C_{l_r} and C_{n_r} on the grounds of numerical size of the terms involved and the accuracy with which estimates of their value could be made.

When the four stability derivatives were evaluated for the records shown surprisingly good agreement with wind tunnel values and estimates was found. The C_{n_β} value was almost identical with the wind tunnel value corrected to the same centre of gravity position, C_{l_p} was within a few per cent of estimates and C_{l_β} was close to the Langley wind tunnel value, although C_{n_p} came out rather higher than estimates for this aircraft.

In using this type of analysis for a test program in conjunction with preliminary wind tunnel tests, it would probably be more advisable to use the wind tunnel values of C_{n_β} and C_{l_β} as the assumed values in the equations and solve for the four rotary derivatives, as these are more difficult to evaluate from the wind tunnel.

With the test results so far obtained at CARDE, an analysis of only the lateral derivatives has been completed. Information gained from recent free-flight tests indicates that by altering the inclination of the principal axis, the dutch roll oscillation can be completely eliminated and by introducing an initial disturbance in pitch, a record will be obtained from which the longitudinal stability derivatives can be found using similar methods to those described above.

3.2 Lift & Drag

As a complete record of lateral centre of gravity movement is obtained as well as an angle of attack history, it should be possible to check points on the lift curve slope. This has not been done as yet with the present results. Drag values from the CARDE tests came out much higher than expected and, as explained previously the effect of the cards on the progress of the model was suspected. As a check on this, arrangements were made to have BRL fire one of our models at the same Mach number. Although further checks will be necessary to confirm this effect, the BRL results showed a total drag coefficient about 10% lower than the CARDE value, but still substantially higher than estimates.

4.0 LIMITATIONS

Before concluding, some of the limitations of the present technique should be mentioned. The model scale is necessarily limited to that of the barrel of the gun.

Although a large 14 inch gun is in the planning stages at CARDE, with the guns presently available in Canada and the United States this means a restriction of the wing span to 5 or 6 inches. At this scale, accurate simulation of intake conditions is difficult and manufacturing tolerances, as discussed earlier, have to be kept small. Because of the limited size of the range, advance knowledge of lift and pitching moment characteristics is required so that a suitable elevator setting can be chosen. For the same reason, there is a fairly low limit to the range of C_L's at which tests can be made.

5.0 CONCLUSIONS

A technique has been developed for launching a small scale model delta-winged aircraft at supersonic speed in the aeroballistics range. The yaw card technique is used to measure roll, pitch and yaw angles to the nearest tenth of a degree, and lateral centre of gravity position to the nearest twentieth of an inch. In addition, the model's velocity history is determined from a light screen system, while shock wave and flow visualization is obtained using 16" and 36" schlieren systems.

Efforts have been made to determine the effect of the cards on the model's behaviour, and although the matter is not as yet resolved, the indication is that a small rectangle of paper is being removed from each yaw card but that no blockage of the engine ducts occurs. The regularity of the pitch, yaw and roll records suggests that the model attitude is not disturbed by the cards while a comparison of drag values with and without cards in place indicate a maximum increase of total drag coefficient of about 10%.

Further work should enable a correction to be made to allow for this difference however.

The records obtained from the firings of the test aircraft show a strong dutch roll type oscillation in yaw and roll while the angle of attack record is of much higher frequency. Thus no roll-pitch cross-coupling effects are assumed, and on the further assumption, based on the records, that model side forces are small, a simple hand solution of the resulting equations of motion for two degrees of freedom has been carried out. From this solution, four of the lateral derivatives have been obtained, showing good agreement with previous wind tunnel tests and estimates.

By suitable adjustment of the inclination of the principal axis the dutch roll oscillation can be eliminated and a pitch disturbance introduced to obtain an angle of attack record from which similar information about the longitudinal stability derivatives can be deduced.

As explained earlier, this paper is merely a progress report on a program of work which is still underway and therefore the treatment, particularly of the analysis work, has not been as detailed and thorough as the authors would have wished. The results so far are very encouraging however and there is every indication that the method could have general application as a means of obtaining useful quantitative information about aircraft lateral and longitudinal stability and performance.

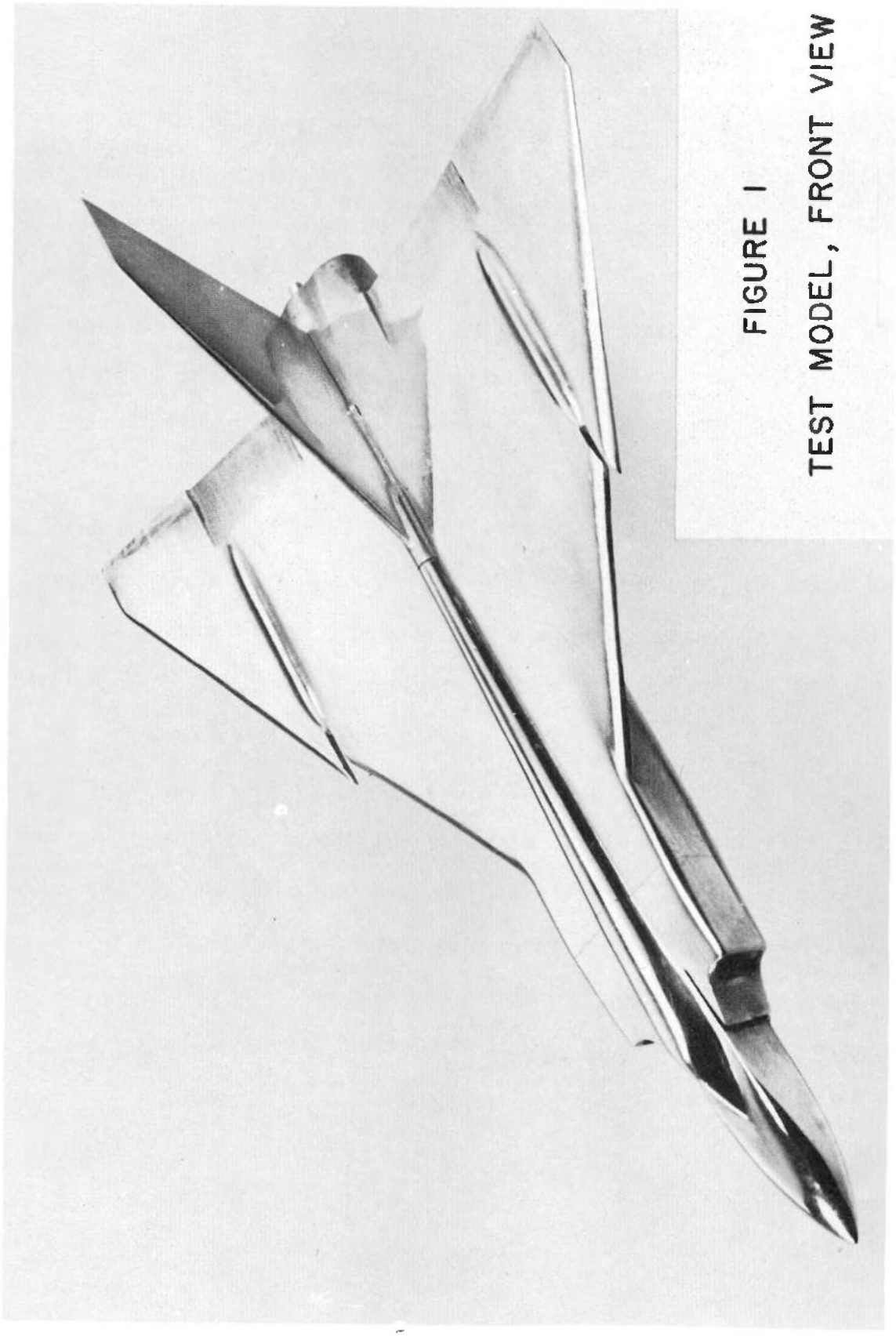

FIGURE 1

TEST MODEL, FRONT VIEW

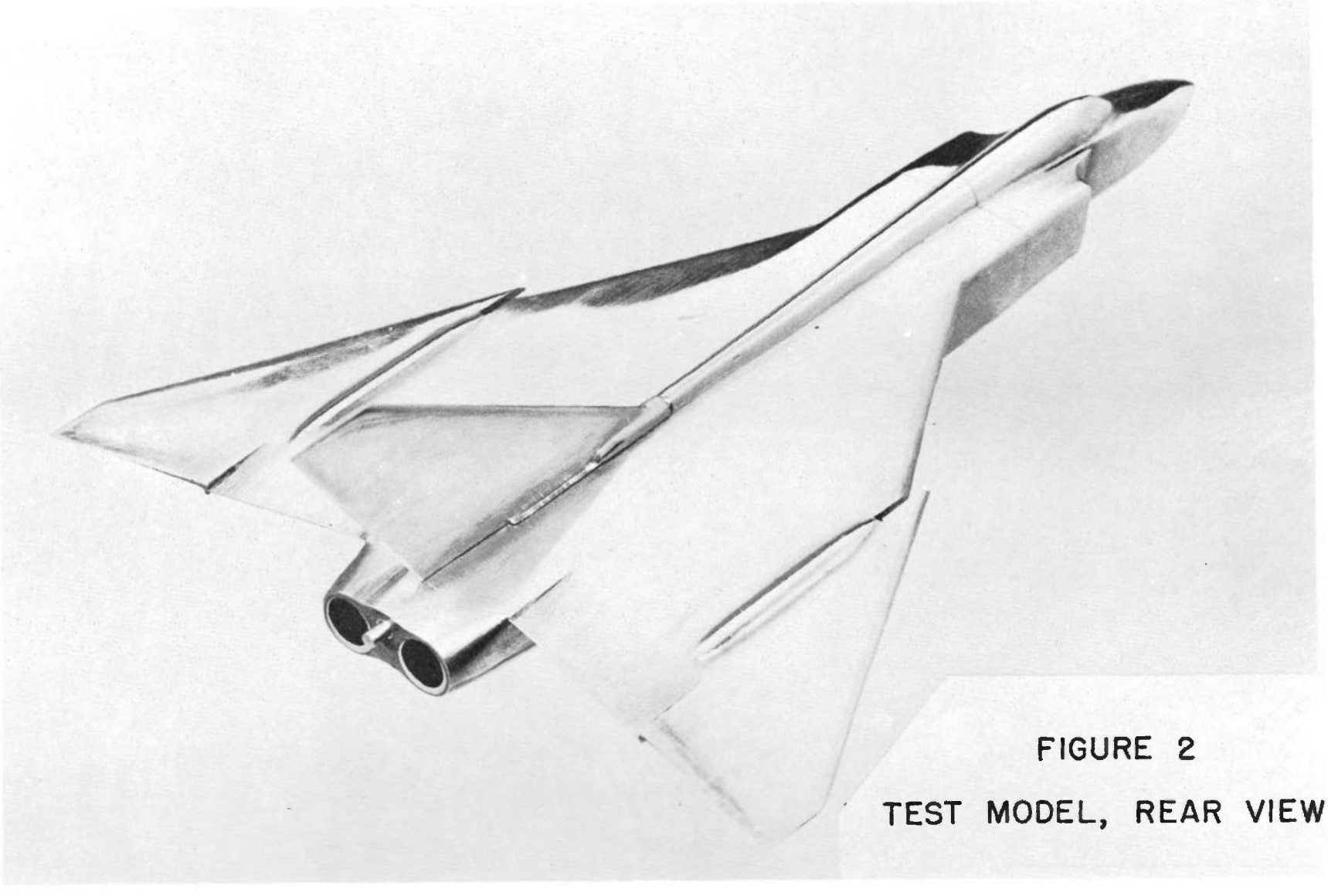

FIGURE 2

TEST MODEL, REAR VIEW

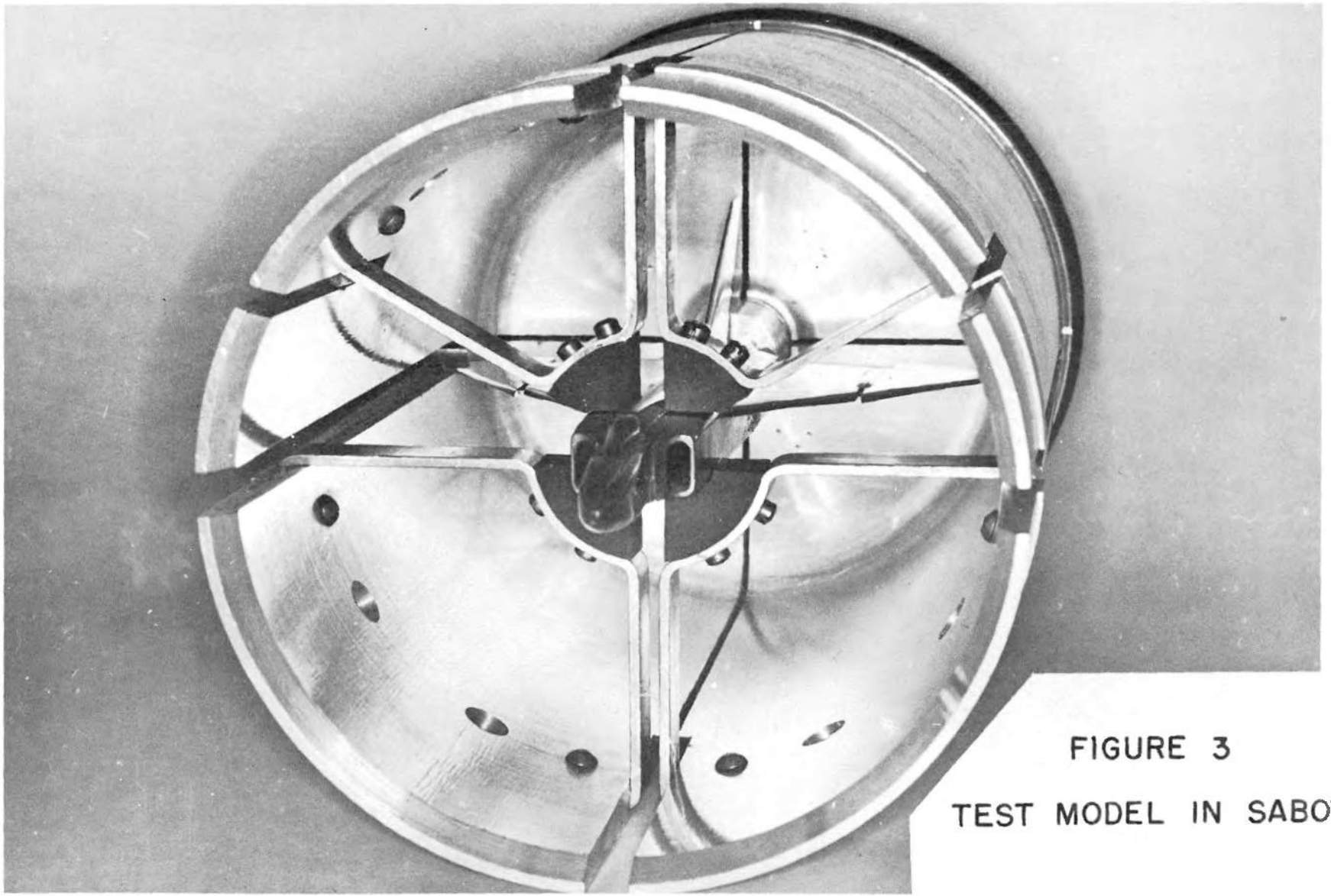

FIGURE 3

TEST MODEL IN SABOT

CONFIDENTIAL
UNCLASSIFIED

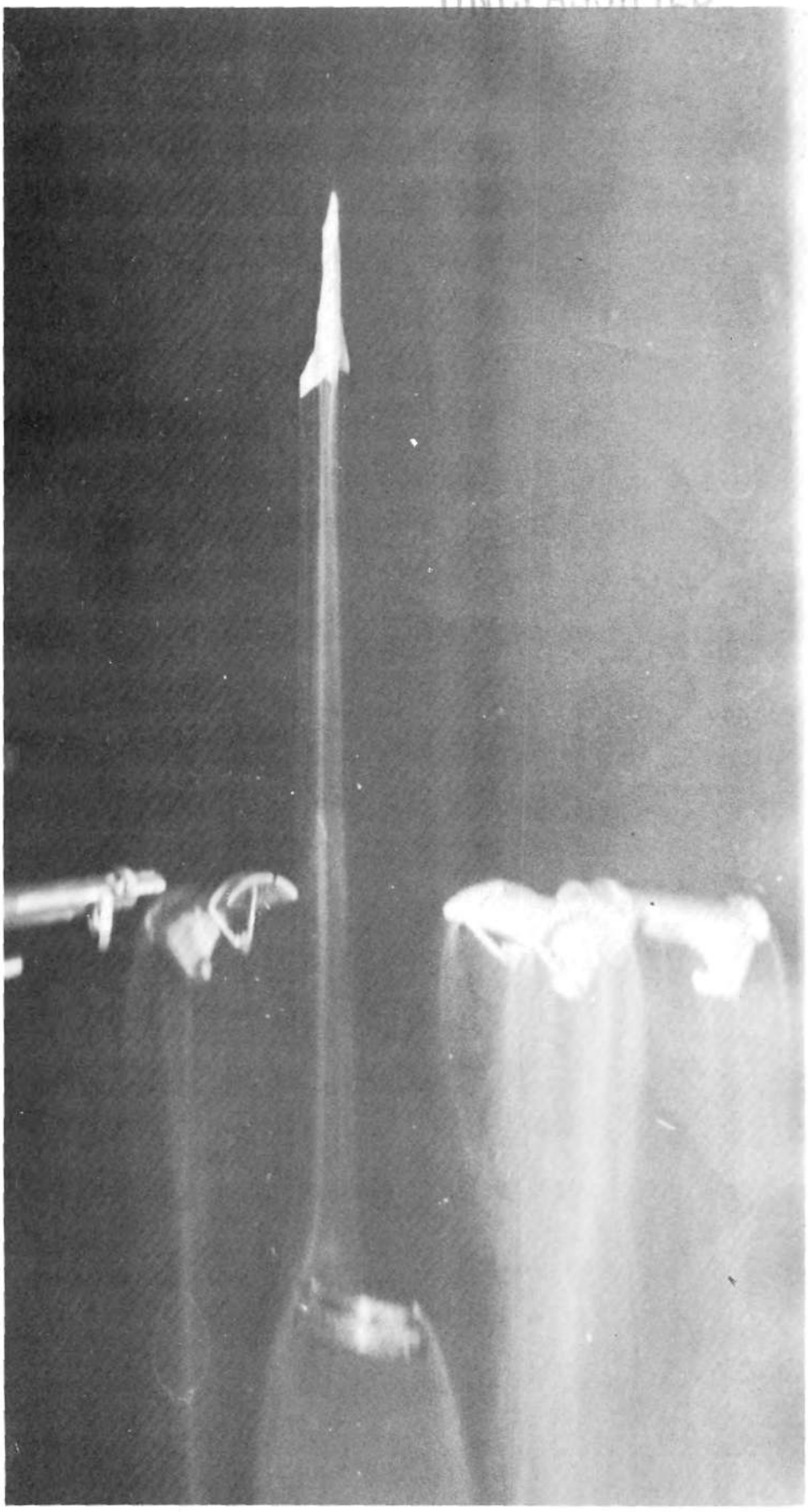

FIGURE 4

MODEL SEPARATING FROM SABOT

UNCLASSIFIED
CONFIDENTIAL

FIGURE 5

TYPICAL YAW CARD CUT

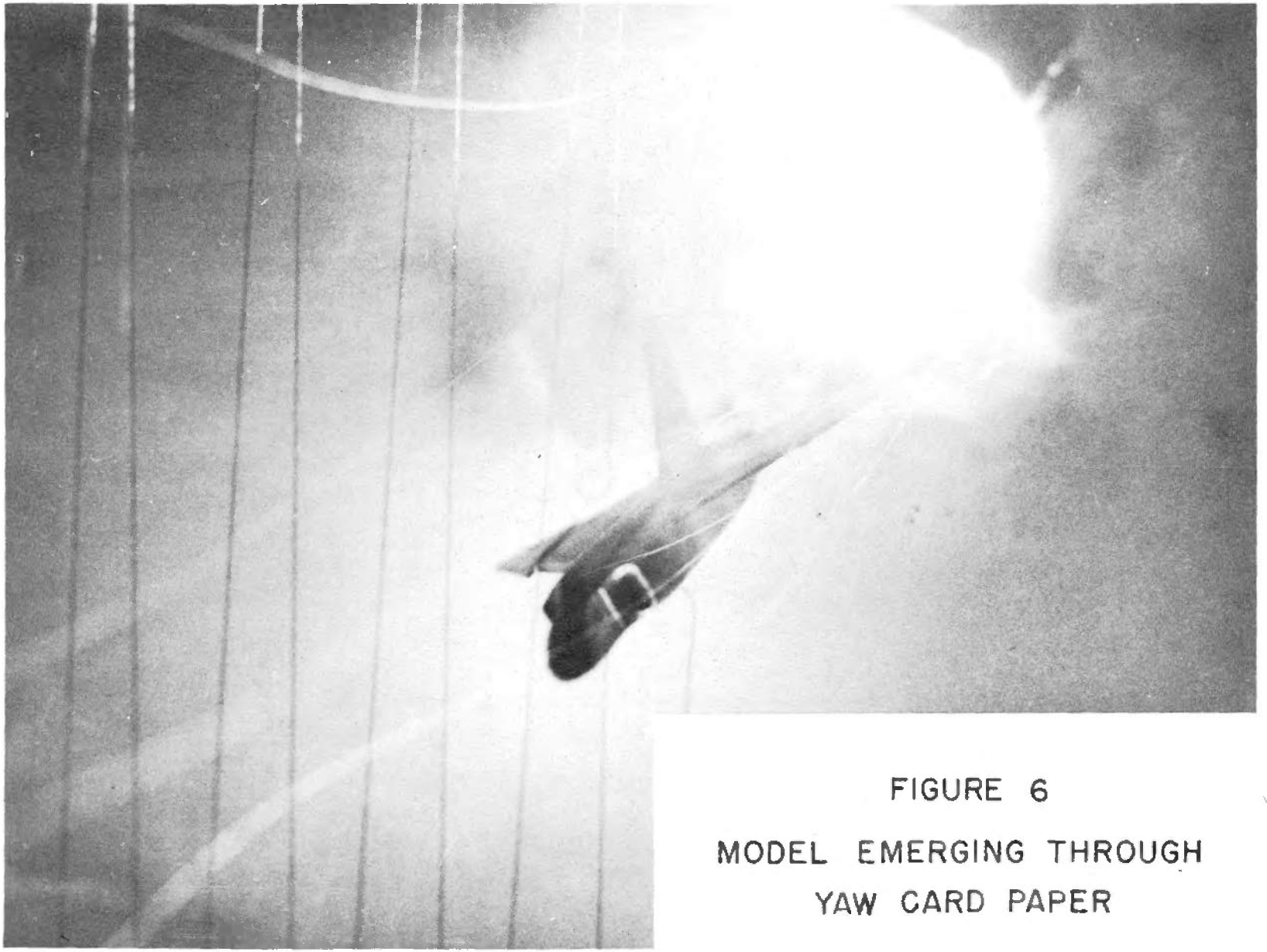

FIGURE 6

MODEL EMERGING THROUGH
YAW CARD PAPER

UNCLASSIFIED

UNCLASSIFIED

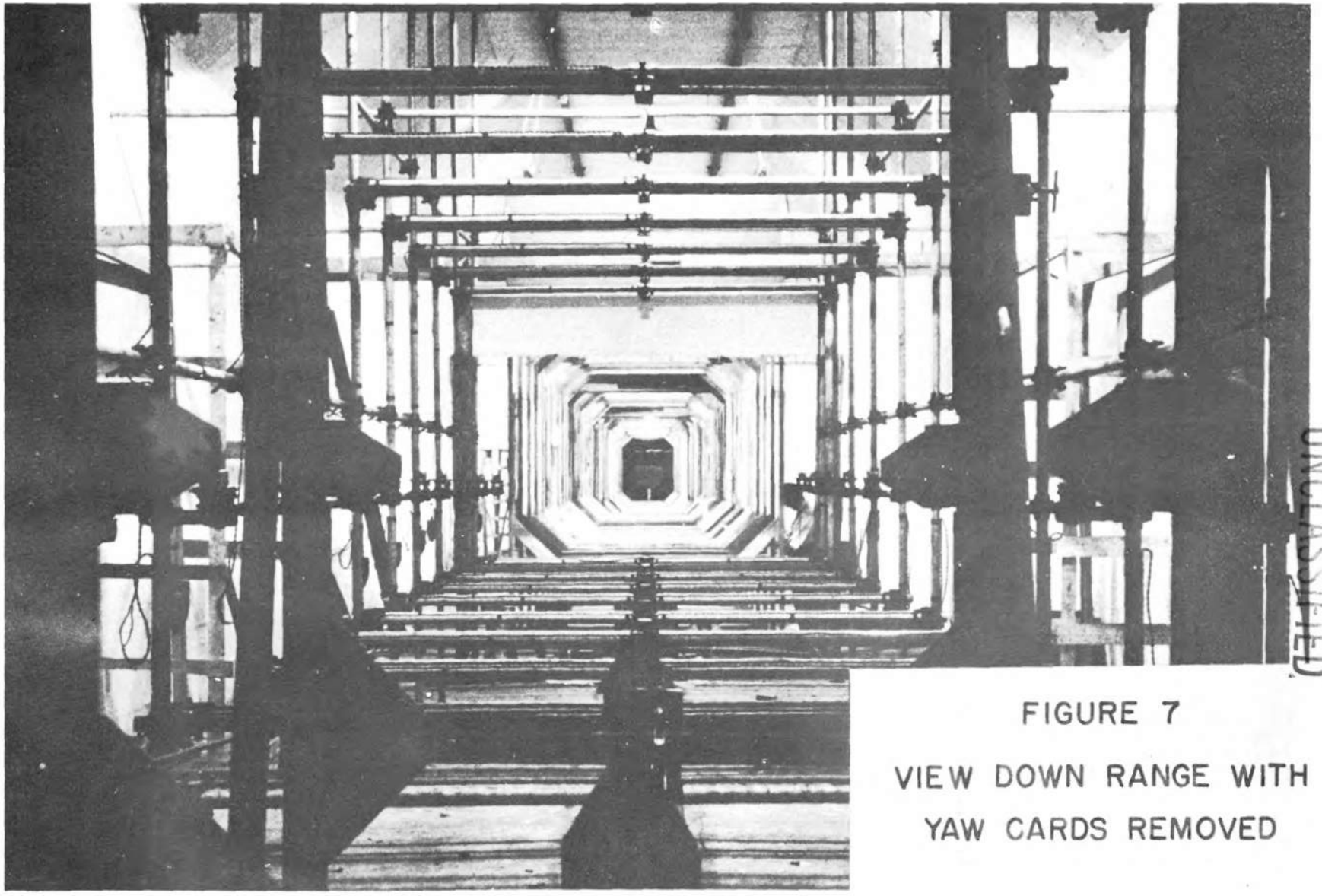

FIGURE 7

VIEW DOWN RANGE WITH
YAW CARDS REMOVED

UNCLASSIFIED
UNCLASSIFIED
CONFIDENTIAL

CONFIDENTIAL

UNCLASSIFIED

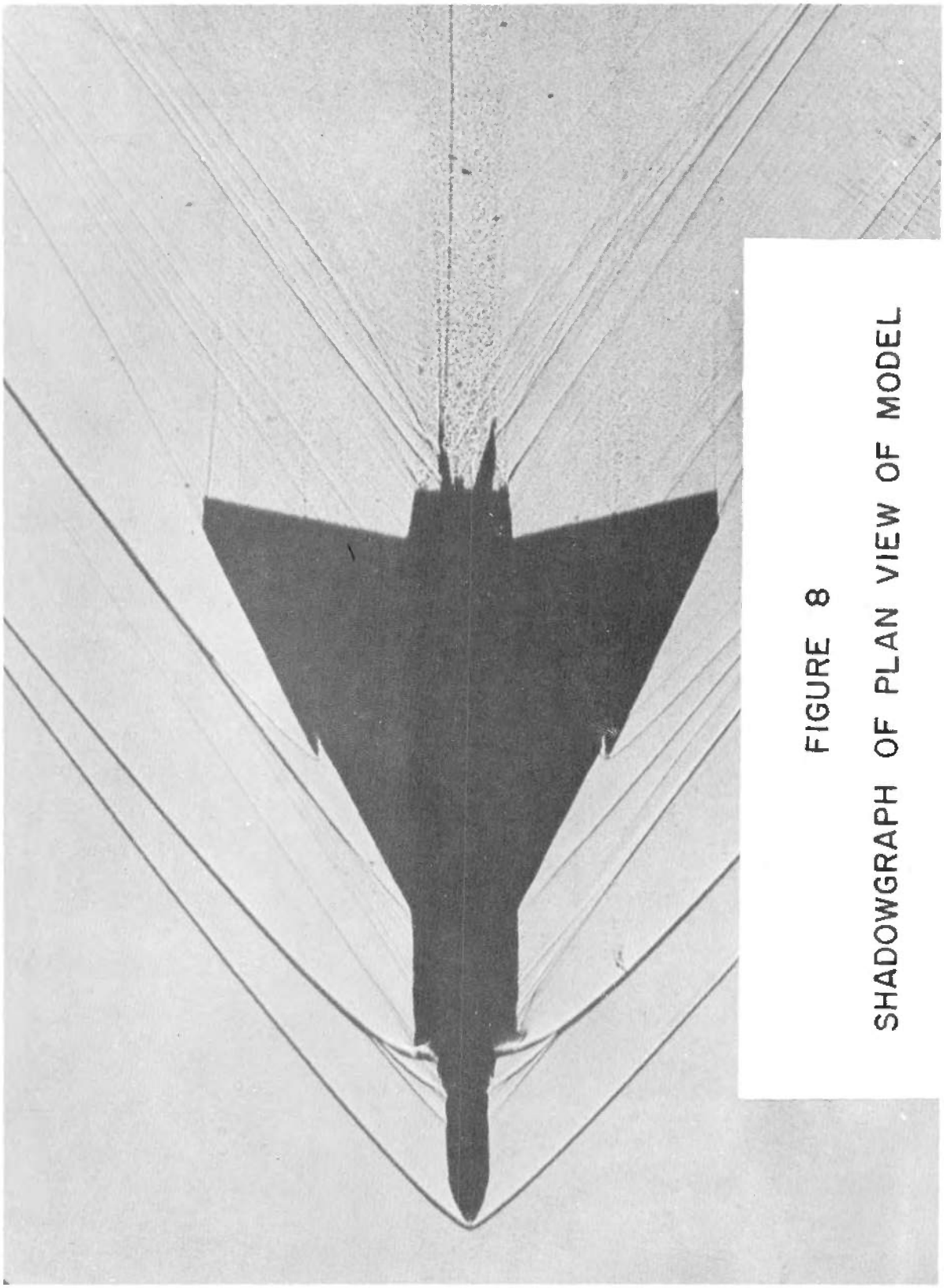

FIGURE 8

SHADOWGRAPH OF PLAN VIEW OF MODEL

UNCLASSIFIED

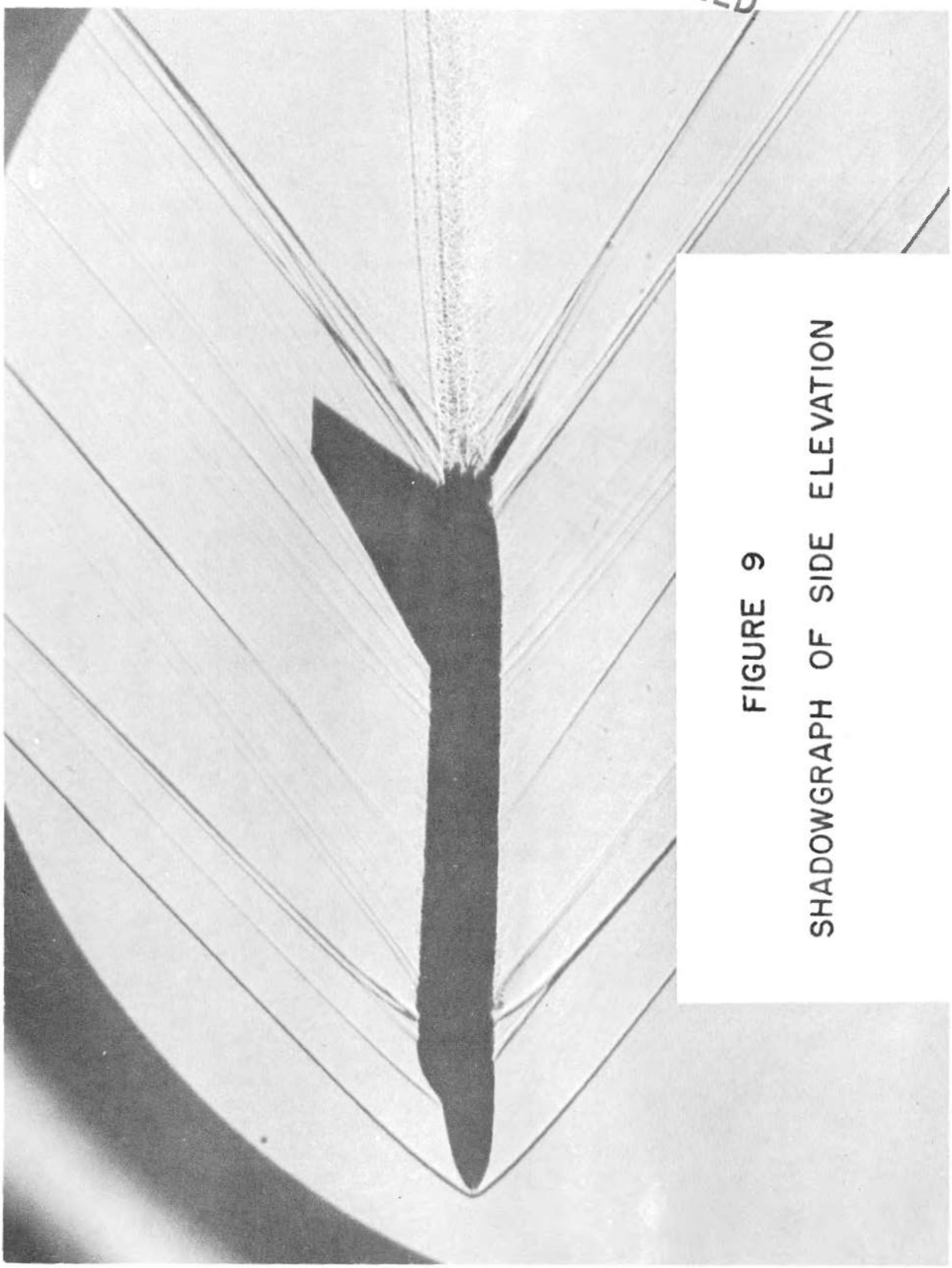

FIGURE 9

SHADOWGRAPH OF SIDE ELEVATION

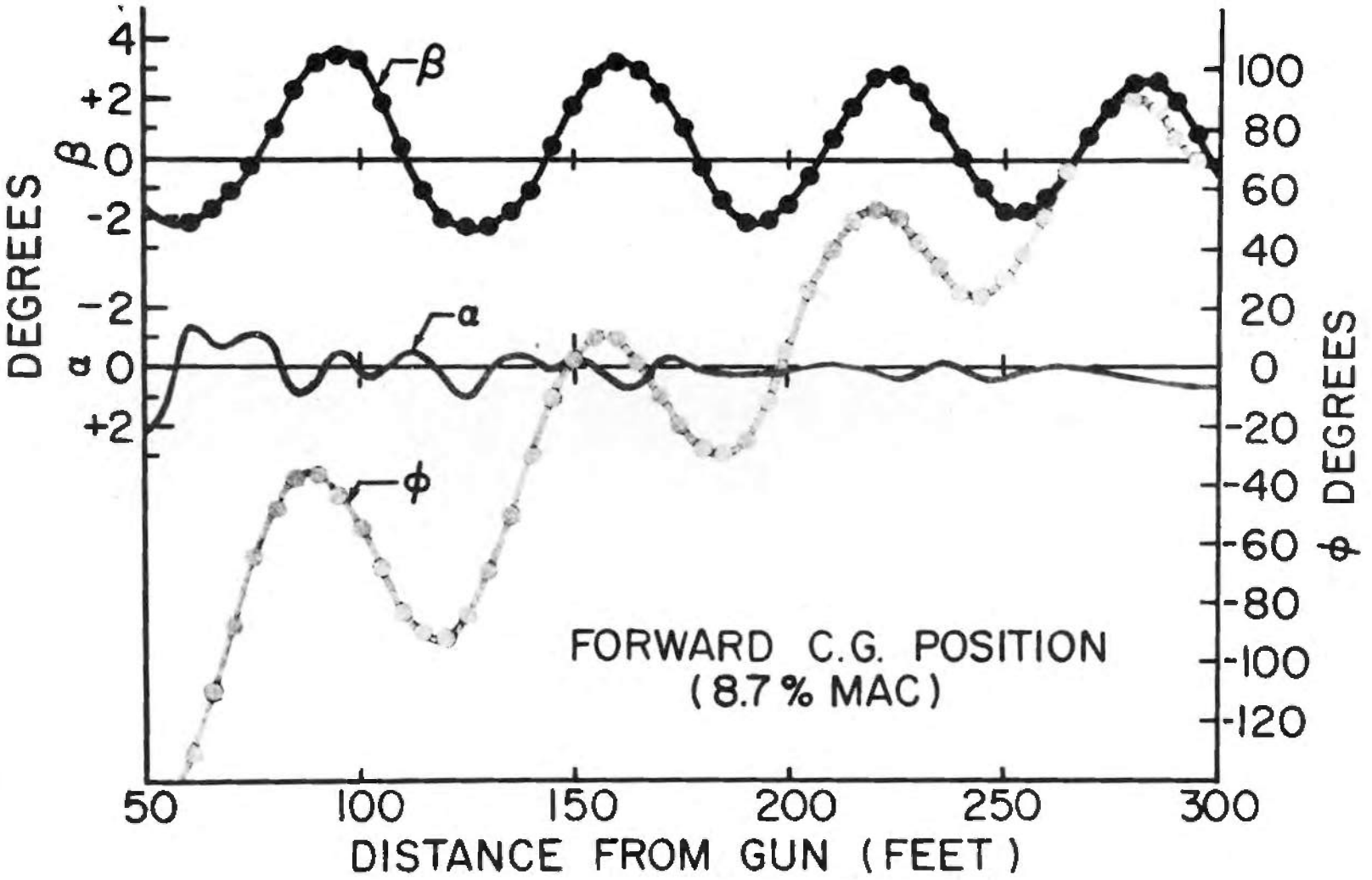

FIGURE 10

ATTITUDE AND ROLL HISTORY

UNCLASSIFIED

UNCLASSIFIED

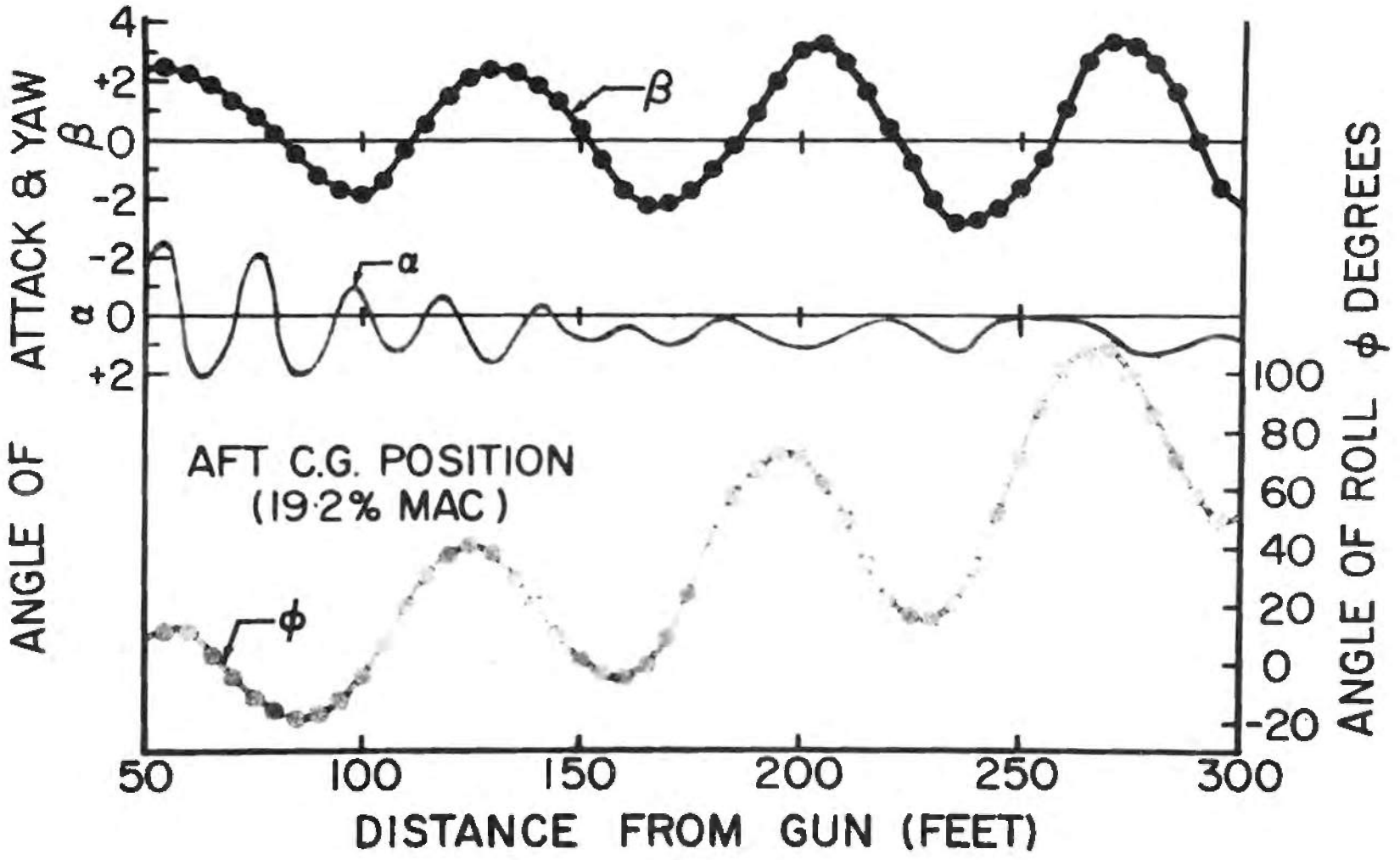

FIGURE 11

ATTITUDE AND ROLL HISTORY

UNCLASSIFIED

UNCLASSIFIED

[redacted]

APPENDIX UNCLASSIFIED

Part I

The following publications describe ranges presently in operation in North America.

1. Bull. G. V., "Some Aerodynamic Studies in the C.A.R.D.E. Aeroballistics Range", Canadian Aeronautical Journal, Vol. 2, No. 5. pp. 154-163, May 1956.

2. May, Albert and Williams, T. J., Free-Flight Ranges at the Naval Ordnance Laboratory, NAVORD Report 4063, July 1955.

3. Rogers, Walter K., Jr., The Transonic Free-Flight Range, BRL Report No. 849, Feb. 1953.

4. Seiff, Alvin, A Free-Flight Wind Tunnel for Aerodynamic Testing at Hypersonic Speeds, NACA Report 1222, May 1955.

5. Staff, Aeroballistics Laboratory, Dynamic Aeroballistic Evaluation, NOTS 1152, July 1955.

UNCLASSIFIED

[redacted]

Part II

Additional information on North American range facilities canbe obtained by writing to the following.

National Advisory Committee for Aeronautics
Ames Aeronautical Laboratory
Moffett Field, California
Attn: Mr. H. Julian Allen

Chief Superintendent
Canadian Armament Research and Development Establishment
P. O. Box 1427, Quebec, Province of Quebec, Canada
Attn: Dr. Gerald V. Bull

Commander
U. S. Naval Ordnance Test Station
China Lake, California
Attn: Dr. William Haseltine, Code 503

Commanding General
Aberdeen Proving Ground, Maryland
Attn: Dr. Boris G. Karpov, Ballistic Research Laboratories

Commander
U. S. Naval Ordnance Laboratory
White Oak, Silver Spring, Maryland
Attn: Dr. Albert May

ARMY-RARITAN ARSENAL (NMPC), METUCHEN, NJ-57-1013

[redacted]

UNCLASSIFIED

DISTRIBUTION LIST

No. of Copies	Organization
4	Chief of Ordnance Department of the Army Washington 25, D. C. Attn: ORDTB - Bal Sec ORDTU ORDTA ORDTX-AR
10	British Joint Services Mission 1800 K Street, N. W. Washington 6, D. C. Attn: Mr. John Izzard, Reports Officer A. E. Clarke N. K. Walker
10	Canadian Army Staff 2450 Massachusetts Ave. Washington 8, D. C. Of Interest to CARDE: G. V. Bull E. W. Greenwood G. H. Tidy D. A. G. Waldock D. W. Pounder H. R. Warren
3	Chief, Bureau of Ordnance Department of the Navy Washington 25, D. C. Attn: ReO
2	Superintendent Naval Postgraduate School Monterey, California Attn: Dr. Head
2	Commander Naval Air Missile Test Ctr. Point Mugu, California Attn: CT - 31 M. Fitzgerald
1	Commanding Officer Naval Air Rocket Test Stn. Dover, New Jersey
1	Commander Naval Air Development Ctr. Johnsville, Pennsylvania
7	Commander Naval Ordnance Test Station China Lake, California Attn: Tech. Library W. R. Haseltine (Code 503) H. L. Newkirk (Code 503) E. B. Mayfield (Code 5015) W. H. Allan E. L. Dunn I. Highburg
2	Commander Naval Proving Ground Dahlgren, Virginia
2	Commander Naval Research Laboratory Washington 25, D. C. Attn: W. W. Atkins R. H. Fuller
13	Commander Naval Ordnance Laboratory White Oak Silver Spring, Maryland Attn: J. J. Brady V. C. Dawson J. N. Fedenia A. Greenwald R. K. Lobb H. H. Kurzweg J. E. Long A. May Z. I. Slawsky P. A. Thurston E. Winkler W. R. Witt F. De Merritt

UNCLASSIFIED

[redacted]

DISTRIBUTION LIST

No. of Copies	Organization
1	Chief of Naval Research Code 438 Washington 25, D. C. Attn: F. S. Sherman
5	Commander Wright Air Development Ctr. Wright-Patterson Air Force Base Ohio Attn: WCLSW - F. J. Huber WCLCO - M. Shorr WCLSS - Tung-Sheng Liu WCRR WCLSW-5
1	Commander USAF Fighter Weapons School Nellis Air Force Base, Nevada
5	Commander Air Force Armament Center Eglin Air Force Base, Florida Attn: ACOTT ACB - C. M. Halton ACB - R. Jacobs ACB - J. E. Stevens ACB - A. S. Galbraith
4	Commander Air Research & Development Command P. O. Box 1395 Baltimore 3, Maryland Attn: Deputy for Development
2	Commander Air Force Missile Test Center (MTE) Patrick Air Force Base, Florida
2	U. S. Atomic Energy Commission Sandia Corporation P. O. Box 5400 Albuquerque, New Mexico Attn: H. R. Vaughn, Div. 5141 W. K. Cox
2	National Advisory Committee for Aeronautics 1512 H Street, N. W. Washington 25, D. C. Attn: I. H. Abbott R. E. May
2	National Advisory Committee for Aeronautics Lewis Flight Propulsion Lab. 21000 Brookpark Road Cleveland 11, Ohio Attn: E. Reshotko F. K. Moore
4	National Advisory Committee for Aeronautics Ames Aeronautical Lab. Moffett Field, California Attn: H. J. Allen T. Canning L. Neice A. C. Charters
6	National Advisory Committee for Aeronautics Langley Aeronautical Lab. Langley Field, Virginia Attn: J. D. Bird R. Hopko P. Huber A. Sabol C. E. Brown A. Busemann
10	Director Armed Services Technical Information Agency Documents Service Center Knott Building Dayton 2, Ohio Attn: DSC-SD
1	Assistant Secretary of Defense (R&D) The Pentagon, Room 3E116 Washington 25, D. C. Attn: I. Nestigen

[redacted]

DISTRIBUTION LIST

No. of Copies	Organization
4	Director, JPL Ord Corps Installation Department of the Army 4800 Oak Grove Drive Pasadena 3, California Attn: M. Eimer H. R. Schurmier P. P. Wegener I. E. Newlan, Reports Group
3	Assistant Secretary of Defense (R&D) Washington 25, D. C. Attn: Committee on Guided Missiles Committee on Ord. Committee on Aeronautics
1	Commanding General Army Ballistic Missile Agency Huntsville, Alabama Attn: T. G. Reed
2	Commanding Officer Diamond Ordnance Fuze Labs. Building 92 Washington 25, D. C.
1	Commanding Officer Watertown Arsenal Watertown 72, Massachusetts Attn: R. Muldoon
1	Commanding General Arnold Engineering Development Center Tullahoma, Tennessee Attn: Deputy Chief of Staff, R&D
1	Commanding Officer and Director David W. Taylor Model Basin Washington 7, D. C. Attn: Aerodynamics Lab.
1	Commanding Officer Chemical Corps Chemical and Radiological Labs. Army Chemical Center, Maryland
3	Commanding Officer Picatinny Arsenal Dover, New Jersey Attn: Samuel Feltman Ammunition Labs.
2	Commanding General Frankford Arsenal Bridge and Tacony Streets Philadelphia 37, Pennsylvania
5	Commanding General Redstone Arsenal Huntsville, Alabama Attn: Technical Library W. D. Murphree D. H. Newby C. L. Northrop N. M. Shapiro
1	Johns Hopkins University Operations Research Office Department of the Army 7100 Connecticut Avenue Chevy Chase, Maryland Washington 15, D. C.
2	AVCO Manufacturing Company Advanced Development Corp. 20 South Union Street Lawrence, Massachusetts Attn: T. R. Munson W. B. Stephenson
	THRU: District Chief Boston Ordnance Dist. Boston Army Base Boston 10, Mass.

[redacted]

DISTRIBUTION LIST

No. of Copies	Organization
1	Armour Research Foundation of the Illinois Institute of Tech. Technology Center Chicago 16, Illinois Attn: Mr. W. Casier THRU: District Chief Chicago Ordnance Dist. 209 W. Jackson Blvd. Chicago, Illinois
4	Applied Physics Laboratory Johns Hopkins University 8621 Georgia Avenue Silver Spring, Maryland Attn: Mr. G. L. Seielstad R. H. Cramer L. L. Cronvich H. A. Wallskog THRU: Naval Inspector of Ord. Applied Physics Lab. Johns Hopkins University 8621 Georgia Avenue Silver Spring, Maryland
2	Aerophysics Development Corp. P. O. Box 657 Pacific Palisades, Calif. Attn: Dr. W. Bollay D. Bitonda THRU: District Chief Los Angeles Ordnance Dist. 55 South Grand Avenue Pasadena, California
1	Adalia Limited 1410 Stanley Street Montreal 2, P. Q., Canada Attn: J. B. Reid THRU: Canadian Army Staff 2450 Mass. Ave., N. W. Washington 8, D. C.
1	Aircraft Armaments, Inc. Cockeysville, Maryland Attn: N. J. La Costa THRU: Deputy Dist. Chief Baltimore Regional Office Philadelphia Ord. Dist. Main Post Office Baltimore 1, Maryland
2	ARO, Inc. Gas Dynamic Facility Tullahoma, Tennessee Attn: M. K. Kingery A. J. Zazzi THRU: District Chief Cincinnati Ord. Dist. Swift Bldg. 230 E. 9th Street Cincinnati 2, Ohio
3	Bell Aircraft Corporation P. O. Box 1 Buffalo 5, New York Attn: K. Pearce N. F. Meullen R. J. Whalen THRU: Air Force Plant Rep. Bell Aircraft Corp. Niagara Falls, New York
1	Boeing Airplane Company Bomber Weapons Unit (Mail Stop 18-54) Physical Research Staff Box 3707 Seattle 24, Washington Attn: D. Martin THRU: Air Force Plant Rep. Boeing Airplane Company Seattle, Washington

[redacted]

DISTRIBUTION LIST

No. of Copies	Organization
1	Boeing Airplane Company Wichita, Kansas Attn: R. E. Wallace THRU: Air Force Plant Rep. Boeing Airplane Co. Wichita, Kansas
1	Boeing Airplane Company Plant 2 Seattle 14, Washington Attn: R. E. Bateman THRU: Air Force Plant Rep. Boeing Airplane Co. Seattle, Washington
1	Budd Company Red Lion Plant Philadelphia 15, Pennsylvania THRU: Deputy Dist. Chief Philadelphia Ord. Dist. 128 N. Broad Street Philadelphia 2, Pa.
4	CONVAIR Div. of General Dynamics Corp. San Diego, California Attn: C. W. Frick E. Katz M. F. Romig S. V. Starr THRU: Bureau of Aero. Rep. CONVAIR San Diego, California
1	Cornell Aero. Laboratory, Inc. 4455 Genesee Street Buffalo 21, New York Attn: Miss E. T. Evans, Library THRU: Bureau of Aero. Rep. Cornell Aero. Lab., Inc. P. O. Box 235 Buffalo 21, New York
1	Chicago Midway Laboratories 6220 S. Drexel Avenue Chicago 37, Illinois Attn: M. F. Malis THRU: District Chief Chicago Ord. Dist. 209 W. Jackson Blvd. Chicago 6, Illinois
3	Computing Devices of Canada, Ltd. P. O. Box 508 Ottawa, Ontario, Canada Attn: J. L. Howland C. B. Jeffery J. E. Smith THRU: Canadian Army Staff 2450 Mass. Avenue Washington 8, D. C.
1	Chance-Vought Aircraft, Inc. P. O. Box 5907 Dallas, Texas THRU: Bureau of Aero. Rep. Naval Industrial Reserve Plant Aeronautical P. O. Box 5907 Dallas, Texas
1	CONVAIR Division of General Dynamics Corp. Pomona Division P. O. Box 1011 Pomona, California THRU: Naval Inspector of Ord. 1675 West 5th Street Pomona, California
1	Cornell University Graduate School of Aero. Engrg. Ithaca, New York Attn: Dr. W. R. Sears THRU: Bureau of Aero. Rep. P. O. Box 235 Buffalo 21, New York

[redacted]

[redacted]

UNCLASSIFIED

DISTRIBUTION LIST

No. of Copies	Organization
1	CONVAIR Div. of General Dynamics Corp. Fort Worth 1, Texas Attn: Mr. L. W. Bonnell THRU: Air Force Plant Rep. CONVAIR Fort Worth 1, Texas
3	CONVAIR Div. of General Dynamics Corp. Ord. Aerophysics Laboratory Daingerfield, Texas Attn: J. E. Arnold R. J. Volluz K. L. Goin THRU: Assistant Inspector of Naval Material Ord. Aerophysics Lab. Daingerfield, Texas
2	Canadair, Pl. Y P. O. Box 6087 Montreal, P. Q., Canada Attn: D. A. Jackman H. J. Luckert THRU: Canadian Army Staff 2450 Mass. Avenue, N. W. Washington 8, D. C.
1	Canadian Westinghouse Co. Electronic Division Longwood Road Hamilton, Ontario, Canada Attn: J. N. Leavitt THRU: Canadian Army Staff 2450 Mass. Ave., N. W. Washington 8, D. C.
1	Chamberlain Corp. Waterloo, Iowa Attn: E. R. Caponi THRU: Dist. Chief Chicago Ord. Dist. 209 W. Jackson Blvd. Chicago 6, Illinois
1	Defense Research Board Room 4735 "A" Building Ottawa, Ontario, Canada Attn: J. L. Oatway THRU: Canadian Army Staff 2450 Mass. Ave., N. W. Washington 8, D. C.
1	Directorate of Armament Dev. Army Headquarters Ottawa, Ontario, Canada Attn: W. B. Snarr THRU: Canadian Army Staff 2450 Mass. Avenue, N. W. Washington 8, D. C.
1	Douglas Aircraft Co., Inc. El Sequndo Division 827 Lapham Street El Sequndo, California Attn: F. C. Newton THRU: Air Force Plant Rep. Douglas Aircraft Corp. 3855 Lakewood Blvd. P. O. Box 200 Long Beach 1, Calif.
3	Douglas Aircraft Co., Inc. Engineering Department 3000 Ocean Park Blvd. Santa Monica, California Attn: R. M. Wood, Library W. S. Cohen H. Klein THRU: District Chief Los Angeles Ord. Dist. 55 South Grand Ave. Pasadena 2, Calif.

UNCLASSIFIED

[redacted]

[redacted]

DISTRIBUTION LIST

No. of Copies	Organization
1	Emerson Electric Manufacturing Company 8100 W. Florissant Avenue St. Louis 21, Missouri Attn: Mr. G. Hauser THRU: St. Louis Air Procurement District Oklahoma City Air Materiel Area 1114 Market Street St. Louis, Missouri
1	Firestone Tire and Rubber Co. Defense Research Division 1200 Firestone Parkway Akron 17, Ohio Attn: V. E. Lucas THRU: District Chief Cleveland Ord. Dist. Lincoln Bldg. 1367 E. 6th St. Cleveland 14, Ohio
6	General Electric Company 3198 Chestnut Street Philadelphia 4, Pennsylvania Attn: V. Kebely R. F. Peck J. Powers A. M. Smith W. R. Warren Y. A. Yoler THRU: Philadelphia Air Procurement Dist. 1411 Walnut Street Philadelphia 2, Penna.
1	General Electric Company Schenectady, New York Attn: Mr. F. V. Johnson, A&OE THRU: Rochester Ord. Dist. Branch Office General Electric Co. Bldg. 23, Room 232 Schenectady, New York Attn: Lt. Col. Davies
2	General Mills, Inc. Engineering Research and Dev. 2003 E. Hennepin Avenue Minneapolis 13, Minnesota Attn: R. I. Hakomaki R. C. Huntington, Mech. Div. THRU: Milwaukee Air Procurement District 770 N. Plankinton Ave. Milwaukee, Wisconsin
3	Grumman Aircraft Engrg. Corp. Engineering Plant No. 5 Bethpage, New York Attn: R. L. Gustafson A. E. Munier R. A. Scheuing THRU: Bureau of Aero. Rep. Grumman Aircraft Engrg. Corp. Bethpage, L.I., New York
2	Hughes Aircraft Company Aerodynamics Department Florence Avenue at Teal St. Culver City, California Attn: I. Naiman W. L. Phillips THRU: Air Force Plant Rep.,WEAPD Hughes Aircraft Co. Florence Ave. at Teal St. Culver City, California

UNCLASSIFIED

[redacted]

[redacted]

DISTRIBUTION LIST

No. of Copies	Organization
1	M. W. Kellogg Company Foot of Danforth Avenue Jersey City 3, New Jersey Attn: Miss E. M. Hedley THRU: Inspector of Naval Material Naval Industrial Reserve Shipyard Bldg. 13, Port Newark Newark 5, New Jersey
3	Lockheed Aircraft Corp. Missile Systems Division Van Nuys, California Attn: E. Bershaded E. T. Cannon R. S. Swanson THRU: Air Force Plant Rep.,WEAD Lockheed Aircraft Corp. Factory "A", P.O. Box 551 Burbank, California
1	Lockheed Aircraft Corp. Factory "A" P. O. Box 551 Burbank, Calif. Attn: Mr. Ed Baldwin THRU: Air Force Plant Rep., WEAPD Lockheed Aircraft Corp. Factory "A", P.O. Box 551 Burbank, California
4	Glenn L. Martin Company Baltimore, Maryland Attn: J. M. Bidwell M. L. Coon L. L. Jackson T. Reisert THRU: Bureau of Aero. Rep. Glenn L. Martin Co. Baltimore 3, Maryland
1	Mass. Institute of Tech. Naval Supersonic Lab. 80-208 560 Memorial Drive Cambridge, Massachusetts Attn: F. H. Durgin THRU: Inspector of Naval Material Dev. Contract Dept. Mass. Inst. of Tech. Cambridge 39, Mass.
1	Massachusetts Institute of Tech. Instrumentation Laboratory Cambridge 39, Massachusetts Attn: L.E. Wilkie (41-203 THRU: Inspector of Naval Material Dev. Contract Dept. Mass. Inst. of Tech. Cambridge 39, Mass.
2	McDonnell Aircraft Corporation P. O. Box 516 St. Louis 3, Missouri Attn: R. M. Flesh R. E. Rohtert THRU: Bureau of Aero. Rep. McDonnell Aircraft Corp. P. O. Box 516 St. Louis 3, Missouri
1	National Research Council of Canada Defense Research Board Ottawa, Ontario, Canada THRU: Canadian Army Staff 2450 Mass. Avenue Washington 8, D. C.
1	North American Aviation, Inc. Columbus, Ohio Attn: W. Simon THRU: Air Force Plant Rep. North American Aviation,Inc. Columbus Plant Columbus, Ohio

[redacted]

[redacted]

DISTRIBUTION LIST

UNCLASSIFIED

No. of Copies	Organization
4	North American Aviation, Inc. Missile Development Division 12214 Lakewood Blvd. Downey, California Attn: E. Briggs J. K. Dew R. B. Oliver J. Elms THRU: Air Force Plant Rep. North American Aviation, Inc. Los Angeles International Airport Los Angeles 45, Calif.
1	North American Aviation, Inc. Los Angeles International Airport Los Angeles, California Attn: J. Covert G. Bussiere THRU: Air Force Plant Rep.,WEAPD North American Aviation, Inc. Los Angeles International Airport Los Angeles, California
1	North Carolina State College Raleigh, North Carolina Attn: Prof. J. W. Cell THRU: District Chief Philadelphia Ord. Dist. 128 North Broad St. Philadelphia 2, Pa.
1	Northrop Aircraft, Inc. Dept. 3483 Ogden Air Material Area Hawthorne, California Attn: D. C. Olmore THRU: Air Force Plant Rep.,WEAPD Northrop Aircraft, Inc. Hawthorne, California

No. of Copies	Organization
1	Princeton University Head, Gas Dynamics Laboratory James Forrestal Research Center Princeton, New Jersey Attn: Prof. S. M. Bogdonoff THRU: Office of Naval Research 246 Broadway New York 13, New York
2	The Ramo-Woolridge Corporation 5730 Arbor Vitae Street Los Angeles 45, California Attn: A. Ambrosio W. D. Hayes THRU: District Chief Los Angeles Ord. Dist. 55 S. Grand Avenue Pasadena, California
3	Republic Aviation Corporation Scientific Staff Farmingdale, New York Attn: W. McIlroy C. Rennemann R. Sanator THRU: Air Force Officer-In-Charge Republic Aviation Corp. Farmingdale,L.I., New York
1	Republic Aviation Corporation Guided Missiles Division 233 Jericho Turnpike Mineola, New York Attn: R. M. Kennedy THRU: Air Force Officer-In-Charge Republic Aviation Corp. Farmingdale,L.I., New York
2	A. V. Roe Canada, Ltd. Aircraft Division Malton, Ontario, Canada Attn: J. A. Chamberlin W. Taylor THRU: Canadian Army Staff 2450 Mass. Ave., N. W. Washington 8, D. C.

UNCLASSIFIED

[redacted]

[redacted]

DISTRIBUTION LIST

UNCLASSIFIED

No. of Copies	Organization
1	Sperry Gyroscope Company Div. of The Sperry Corp. Great Neck, L.I., New York Attn: J. J. Gallaghan, Federal Dept. THRU: Assistant Inspector of Naval Material c/o Sperry Gyroscope Co. Div. of Sperry Corp. Great Neck, L.I., N. Y.
1	University of Michigan Aero. Research Center Willow Run Airport Ypsilanti, Michigan Attn: J. E. Corey THRU: Commander Central Air Proc. Dist. W. Warren & Lonyo Aves. Detroit 32, Michigan
3	University of Minnesota Rosemount Aero. Laboratories Rosemount, Minnesota Attn: R. V. Deleo R. Herman F. A. Moynihan THRU: Milwaukee Air Proc. Dist. 770 N. Plankinton Ave. Milwaukee, Wisconsin
1	University of Southern Calif. Engineering Center 3518 University Avenue Los Angeles 7, California Attn: H. R. Saffell, Director THRU: Office of Naval Research Branch Office 1030 E. Green Street Pasadena, California
1	University of Texas Military Physics Research Lab. 500 East 24th Street Austin, Texas THRU: Office of Naval Research Box 7786, University Stn. Austin 12, Texas
1	United Aircraft Corporation Research Department East Hartford 8, Connecticut THRU: Bureau of Aero. Rep. Pratt and Whitney Aircraft Division United Aircraft Corp. East Hartford 8, Conn.
1	Wright Aeronautical Division Curtiss-Wright Corporation Wood-Ridge, New Jersey Attn: Sales Dept. (Gov't) THRU: Air Force Plant Rep. Wright Aero. Division Curtiss-Wright Corp. Wood-Ridge, N. J.
1	Westinghouse Electric Corporation Air Arm Division Friendship International Airport Baltimore, Maryland THRU: Bureau of Aero. Rep. Glenn L. Martin Co. Baltimore 3, Maryland
1	Professor George Carrier Division of Applied Science Harvard University Cambridge 38, Massachusetts

UNCLASSIFIED

[redacted]

[redacted]

DISTRIBUTION LIST UNCLASSIFIED

No. of Copies	Organization
1	Captain W. S. Diehl, USN, Ret. 4501 Lowell Street, N. W. Washington 16, D. C. THRU: National Advisory Committee for Aeronautics Subcommittee on Stability and Control 1512 H Street, N. W. Washington 25, D. C.
1	Professor C. B. Millikan Guggenheim Aeronautical Laboratory California Institute of Technology Pasadena 4, California
1	Dr. A. E. Puckett Hughes Aircraft Company Culver City, California
1	Dr. L. H. Thomas Watson Scientific Computing Laboratory 612 West 116th Street New York 27, New York

UNCLASSIFIED

All

[redacted]

DISTRIBUTION LIST

To Receive UNCLASSIFIED Part Only

No. of Copies	Organization
1	California Institute of Technology Pasadena, California Attn: Library
1	Guggenheim Aeronautical Laboratory California Institute of Technology Pasadena, California Attn: Prof. H. W. Liepman
1	Professor Francis H. Clauser, Jr. Department of Aeronautics Johns Hopkins University Baltimore 18, Maryland
1	Institute of the Aeronautical Sciences, Inc. 2 E. 64th Street New York 21, New York Attn: John J. Glennon, Librarian
1	Professor J. B. Eades Engineering Department Virginia Polytechnic Institute Blacksburg, Virginia
1	Professor R. Truitt Engineering Department Virginia Polytechnic Institute Blacksburg, Virginia